SEMMELWEIS EGYETEM
DOKTORI ISKOLA

Ph.D. értekezések

3217.

TYLER TEADORA

Neuromorfológia és sejtbiológia
című program

Programvezető: Dr. Alpár Alán, egyetemi tanár
Témavezető: Dr. Adorján István, tudományos főmunkatárs

Multi-scale investigation of cellular and molecular patterns in schizophrenia

PhD thesis

Teadora Tyler

Semmelweis University Doctoral School

Szentágothai János Neurosciences Division

Supervisor: István Adorján, MD, PhD

Official reviewers: Zsófia Maglóczky, PhD, DSc

Karolina Pircs, PhD

Head of the Complex Examination Committee:

Alán Alpár, MD, PhD, DSc

Members of the Complex Examination Committee:

Árpád Dobolyi, PhD, DSc

Ádám Dénes, PhD, DSc

Budapest

2025

Table of Contents

List of Abbreviations

°C – degree Celsius

2D, 3D – 2-dimension, 3-dimension

ABI3BP – gene encoding ABI family member 3 binding protein

ADARB2 – gene encoding RNA-specific B2 adenosine deaminase

AMP1–3 – amplification reagent 1–3

ARHGAP1 – gene encoding Rho GTPase activating protein 1

ATP – adenosine triphosphate

Ba – Brodmann area

BG – basal ganglia

BP – biological process

BSA – bovine serum albumine

C5orf17 – long intergenic non-protein coding RNA 2899

C5orf63 – chromosome 5 open reading frame 63

CALB1 – gene encoding calbindin 28-Dk

CALB2 – gene encoding calretinin

CB – calbindin 28-Dk protein

CCK – gene encoding prepro-cholecystokinin

CCK – cholecystokinin protein

CDH9 – gene encoding cadherin 9

cDNA – copy DNA

CGE – caudal ganglionic eminence

CHAT – gene encoding choline o-acetyltransferase

CHRFAM7A – CHRNA7 (exons 5-10) and FAM7A (exons A-E) Fusion

CHST9 – gene encoding carbohydrate sulfotransferase 9

CN – caudate nucleus

CNTN4 – gene encoding contactin 4

COL15A1 – gene encoding collagen type XV alpha 1 chain

CR – calretinin protein

CRH – gene encoding corticotropin-releasing hormone

CRYAB – gene encoding crystallin alpha B

CTR – control

CUX2 – gene encoding cut-like homeobox 2

D1R – dopamine receptor D1 protein

D2R – dopamine receptor D2 protein

DAPI – 4′,6-diamidino-2-phenylindole (enables nuclear staining)

DEG – differentially expressed gene

DLPFC – dorsolateral prefrontal cortex

dMSN – direct pathway medium spiny neuron

DNA – deoxyribonucleic acid

DRD2 – gene encoding dopamine receptor D2

E/I – excitatory/inhibitory

EEG – electroencephalography

EGR1 – gene encoding early growth response protein 1

EYA4 – gene encoding EYA transcriptional coactivator and phosphatase 4

EX – excitatory

FANS – fluorescent-activated nucleus sorting

FEZF2 – gene encoding FEZ family zinc finger 2

FF – fresh frozen

FFPE – formalin-fixed, paraffin-embedded

FOS – gene encoding Fos proto-oncogene, AP-1 transcription factor subunit

FREM3 – gene encoding FRAS1-related extracellular matrix protein 3

fMRI – functional magnetic resonance imaging

GABA – gamma-aminobutyric acid

GABRA1 – gene encoding gamma-aminobutyric acid type A receptor subunit alpha1

GABRB2 – gene encoding gamma-aminobutyric acid type B receptor subunit beta2

GAD1 – gene encoding glutamate decarboxylase 1

GEMs – gel beads in emulsion

GLM – general linear model

GO – Gene Ontology

GP – globus pallidus

GPe – globus pallidus externa

GPi – globus pallidus interna

GPM6A – gene encoding glycoprotein M6A

GRIK3, *GRIK4* – gene encoding glutamate ionotropic receptor kainate type subunit 3/4

GRIN2A – gene encoding glutamate ionotropic receptor NMDA type subunit 2A

GWAS – genome-wide association study

H1FX – gene encoding H1.10 linker histone

H_2O_2 – hydrogen peroxide

HBTB – Human Brain Tissue Bank

HES4 – gene encoding HES family bHLH transcription factor 4

HRP – horseradish peroxidase

HSP1A – gene encoding heat shock protein family a (HSP70) member 1A

HSPB1 – gene encoding heat shock protein family B (small) member 1

HT – high throughput

HTR2C – gene encoding 5-hydroxytryptamine (serotonin) receptor 2C

HTR3A – gene encoding 5-hydroxytryptamine (serotonin) receptor 3A

Iba1 – ionized calcium-binding adapter molecule 1 protein

iPSC – induced pluripotent stem cells

ID – identifier

ID2 – gene encoding "inhibitor of DNA binding 2" transcriptional regulator

IHC – immunohistochemistry

iMSN – indirect pathway medium spiny neuron

IN – inhibitory

INs – interneurons

KCL – King's College London Neurodegenerative Diseases Brain Bank

KNN – k-nearest-neighbour clustering

L1–L6 – cortical layers I – VI

LAMP5 – gene encoding lysosomal-associated membrane protein family member 5

LHX6 – gene encoding LIM homeobox 6

LMM – linear mixed model

MAP2 – gene encoding microtubule-associated protein 2

MB-COMT – gene encoding membrane-bound catechol-O-methyltransferase

MEPE – gene encoding matrix extracellular phosphoglycoprotein

MGE – medial ganglionic eminence

MIA – gene encoding MIA SH3 domain-containing protein

MMP16 – gene encoding matrix metallopeptidase 16

mRNA – messenger RNA

MSN – cammedium spiny neuron

NBB – Netherlands Brain Bank

NBTR – Newcastle Brain Tissue Resource

NCKAP5 – NCK associated protein 5

NeuN – neuronal nuclei antigen protein

NGS – new-generation sequencing

NMDA – N-methyl D-aspartate

NOS1 – gene encoding nitric oxide synthase 1

NOS1 – nitric oxide synthase 1 protein

NPY – gene encoding neuropeptide Y

NPY – neuropeptide Y protein

NRXN3 – gene encoding neurexin 3

OBB – Oxford Brain Bank

OXTR – gene encoding oxytocin receptor

PAX6 – gene encoding paired-box protein 6

PET – positron emission tomography

PFC – prefrontal cortex

PMI – post-mortem interval

PNs – pyramidal neurons

PRSS12 – gene encoding serine protease 12

PSD95 – postsynaptic density protein 95

PTHLH – parathyroid hormone-like hormone protein

PTHLH – gene encoding parathyroid hormone-like hormone

Put – putamen

PV – parvalbumin protein

PVALB – gene encoding parvalbumin

qPCR – quantitative PCR

RELN – gene encoding reelin

RNA – ribonucleic acid

ROI – region of interest

RORB – gene encoding RAR-related orphan receptor B

SATB2 – gene encoding SATB homeobox 2

SCH – schizophrenia

SCHLAP1 – gene for SWI/SNF complex antagonist associated with prostate cancer 1

scRNAseq – single cell RNA sequencing

SEMA3A–E: genes encoding semaphorin 3A–E

SHANK2 – gene encoding SH3 and multiple ankyrin repeat domains 2

SLC6A4 – gene encoding solute carrier family 6 member 4

SMI-311 – anti-neurofilament antibody

SN – substantia nigra

SNpc – substantia nigra pars compacta

SNpr – substantia nigra pars reticulata

snRNAseq – single nucleus RNA sequencing

SST – gene encoding somatostatin

SST – somatostatin protein

SSTR1 – gene encoding somatostatin receptor 1

STN – subthalamic nucleus

TAC3 – gene encoding tachykinin 3

TBST – Tris-buffered saline with TritonTMX-100

TCF4 – gene encoding transcription factor 4

TH – tyrosine hydroxylase protein

TH – gene encoding tyrosine hydroxylase

Thal – thalamus

THEMIS – gene encoding thymocyte selection associated protein

THS7DA – gene encoding thrombospondin type 1 domain-containing 7A

TLE4 – gene encoding TLE family member 4, transcriptional corepressor

TMEM119 – transmembrane protein 119

TRPC3 – gene for transient receptor potential cation channel subfamily C member 3

TUBA4A – gene encoding tubulin alpha 4a

TYR – gene encoding tyrosinase

UMAP – Uniform Manifold Approximation and Projection for Dimension Reduction

UMI – unique molecular identifier

VGLUT-1 – vesicular glutamate transporter 1

VIP – gene encoding vasoactive intestinal peptide

VTA – ventral tegmental area

WB – wash buffer

WM – working memory

1. Introduction

1.1. Schizophrenia

Schizophrenia (SCH) is a complex neuropsychiatric disorder that continues to challenge both clinicians and researchers. Although its prevalence is relatively low (estimated ~ 0.5 – 1% globally), it profoundly impacts the affected patients, their families, and society [1, 2]. It is highly heritable (60–80% [3]); however, understanding its genetic background proved challenging. Hundreds of risk loci have been identified, many of which only contribute with small effect sizes [4], and many are also implicated in other psychiatric and neurodevelopmental disorders [5], further complicating the genetic landscape. SCH manifests through a wide range of symptoms affecting perception, emotion, and cognition, traditionally classified into three symptom domains [6]. "Positive" symptoms include hallucinations and delusions, and can be accompanied by abnormal psychomotor behaviours, such as rigid movements and disorganized behaviour. "Negative" symptoms involve social withdrawal, avolition (decreased or lacking interest in goal-directed behaviour), alogia (poverty of speech), and anhedonia (inability to enjoy normally enjoyable activities). The third symptom domain is characterized by cognitive deficits, primarily affecting memory, attention, executive functioning, and processing speed [5, 7, 8]. Although positive symptoms are what usually bring patients to medical attention, cognitive symptoms are recognized as central features of SCH [9, 10] and even the best predictors of long-term disease outcome [11].

Today, SCH is thought to be caused by complex interactions of various genetic and environmental factors (such as *in utero* adverse effects [4]), which disturb neurodevelopment and ultimately give rise to abnormal brain connectivity, thereby increasing the risk of developing the disorder [12]. Symptoms generally emerge in late adolescence and early adulthood, coinciding with a critical period of brain maturation [13] involving neuronal and circuit maturation, myelination, synapse elimination, and the maturation of neurotransmitter systems [14, 15]. Currently, SCH lacks objective biomarkers, has no cure, does not have a fully representative animal model, and its etiology remains elusive [16, 17, 18]. It is important to emphasize that there is no evidence of SCH being one single well-defined disease; instead, it is considered a group or spectrum of conditions [19, 20]. The fact that SCH remains so enigmatic despite extensive

clinical and laboratory research suggests that our current understanding is limited by fragmented approaches and most likely requires a rethinking of how we conceptualize and study this condition.

1.1.1. Theories of schizophrenia etiology

SCH symptomatology is thought to be associated with disrupted frontal cortical activity, dopamine dysfunction, and excitatory–inhibitory (E/I) imbalance [21–25]. In the 1950s, clinicians observed that high doses of the tranquilizer Largactil (chlorpromazine) reduced psychotic symptoms in patients [26] by blocking dopamine D2 receptors (D2R) [27–29]. These discoveries led to the "dopamine receptor hypothesis" of SCH, which linked positive symptoms to excess dopaminergic neurotransmission [30, 31]. This was further refined after discovering low dopamine levels in the neocortex in SCH [32], where dopaminergic neurotransmission is primarily mediated by D1-type dopamine receptors (D1R) [33]. Based on pioneering experiments exploring connectivity in rodents [34, 35], it was proposed that the observed excess striatal dopaminergic activity may be a direct consequence of cortical dysfunction [36–39]. Meyer-Lindenberg and colleagues [40] tested this hypothesis in patients with SCH using positron emission tomography (PET) to measure regional cerebral blood flow and striatal dopaminergic activity during the Wisconsin Card Sorting Test, an abstract reasoning–working memory task commonly used to investigate cortical function [41]. Their findings confirmed a strong inverse correlation between prefrontal cortex (PFC) activity and striatal dopaminergic function, with PET scans pinpointing the locus of cortical hypoactivation in the dorsolateral PFC. The current version of the dopamine hypothesis [42] proposes dopamine imbalance (subcortical hyperactivity with cortical hypoactivity [43]), and acknowledges that the etiology of SCH is more complicated than previously thought, with disturbances in almost all major systems across the brain [44–47]. In addition, a line of post-mortem [48] and patient-derived induced pluripotent stem cell studies [49] have linked abnormal microglia activation and excess synaptic pruning to compromised synaptic plasticity, neuroinflammation, and early cognitive impairment in SCH [50, 51]. In fact, aberrant synaptic pruning during critical developmental periods has been proposed as the root cause of cortical E/I imbalance and disrupted connectivity in SCH [52].

E/I dysfunction has also been extensively studied in SCH (for review, see [53] and Chapter 1.4.1). Many elements crucial for the production, transport, and metabolism of the major inhibitory neurotransmitter gamma-aminobutyric acid (GABA) have been repeatedly found disrupted in SCH [54–56]. This led to the "GABA theory" of SCH, which proposes disrupted GABAergic function and, thus, compromised cortical inhibition as a key mechanism underlying SCH symptoms [57]. However, this theory is less well-established and may not be specific to SCH alone, as similar patterns have been observed in other neuropsychiatric conditions, such as major depression and autism spectrum disorder [44]. In addition, glutamatergic dysfunction has also been noted in SCH, particularly involving hypofunctionality of N-methyl-D-aspartate (NMDA) glutamate receptors [58]. Because E/I activity is widely modulated by dopamine and other monoaminergic neurotransmitters, it is unclear and challenging to prove whether E/I imbalance may be directly caused by neurodevelopmental disturbances associated with SCH, disrupting the development and connectivity of excitatory and inhibitory circuits [59, 60], or indirectly by the imbalance of other, interconnected signalling pathways [61].

Although excess striatal dopaminergic neurotransmission has long been recognized as a central feature of SCH symptomatology and directly linked to cortical dysfunction, the striatum remains underrepresented in histological and transcriptomic investigations of SCH [53]. It is important to emphasize that executive functioning, voluntary action control, emotional control, and working memory cannot be comprehensively interpreted without the context of fronto–striatal circuitry.

1.2. Fronto-striatal circuitry

Cognition and behaviour are mediated by functionally segregated, dynamically interacting cortico–basal ganglio–cortical circuits collectively called “fronto–striatal networks” [Figure 1/A; 62]. These pathways encompass distinct limbic, motor, and cognitive/associative networks, which have been extensively mapped in non-human primates in a series of pioneering experiments [63–65] and validated in humans through functional magnetic resonance imaging (fMRI) studies [66, 67]. The supplementary motor areas, the putamen (PUT), and the substantia nigra (SN) are highly involved in motor function; the dorsolateral prefrontal cortex (DLPFC) and the caudate nucleus (CN) account for cognitive/associative information flow, while the ventromedial prefrontal cortical areas, the ventral striatum, and the ventral tegmental area (VTA) account for

limbic information flow [68, 69]. These functional subregions do not have clear anatomical borders but manifest as gradients – mirrored by the distribution, density, and gene expression profile of the neurons creating it [70, 71]. Therefore, the basal ganglia (BG), comprising the CN, PUT, globus pallidus (GP), and – from a functional aspect – the subthalamic nucleus (STN) and SN, participate in crucial functions such as motor control, learning, and value-based decision making [72–75]. Although comparative neuroanatomical studies found the structure and neurochemical organization of the basal ganglia highly conserved across vertebrates [76], striking differences have been elucidated recently regarding its cellular composition and cell type-specific properties, suggesting it may also nurture unexpected hubs for evolutional innovation [71, 77].

Within the basal ganglia circuitry, glutamatergic cortical input is received by the striatum, which consists of the CN and the PUT. From the striatum, GABAergic output is transmitted through two parallel, functionally complementary pathways: the direct and indirect pathways [78]. The direct pathway promotes movement by inhibiting the substantia nigra pars reticulata (SNpr) and globus pallidus internus (GPi). This leads to the disinhibition of thalamo–cortical projections, ultimately promoting motor activity (Figure 1/B). In contrast, the indirect pathway inhibits the globus pallidus externus (GPe), thus allowing the STN to excite the GPi and SNpr, which consequently inhibit thalamo-cortical projections and thereby inhibit motor activity [79] (Figure 1/C). The delicate balance between these pathways allows for precise initiation and suppression of actions. The significance of the fronto–striatal pathways is underscored by the profound impact their disruption can have on normal motor and cognitive functioning. For example, in Parkinson's disease, the progressive loss of dopaminergic neurons in the substantia nigra pars compacta (SNpc) leads to reduced dopaminergic input to the striatum, disrupting the activity of both the direct and indirect pathways, resulting in the characteristic motor symptoms [80]. Imbalance of dopamine neurotransmission has also been associated with schizophrenia, autism spectrum disorder, attention deficit hyperactivity disorders, and drug abuse [81–85, respectively].

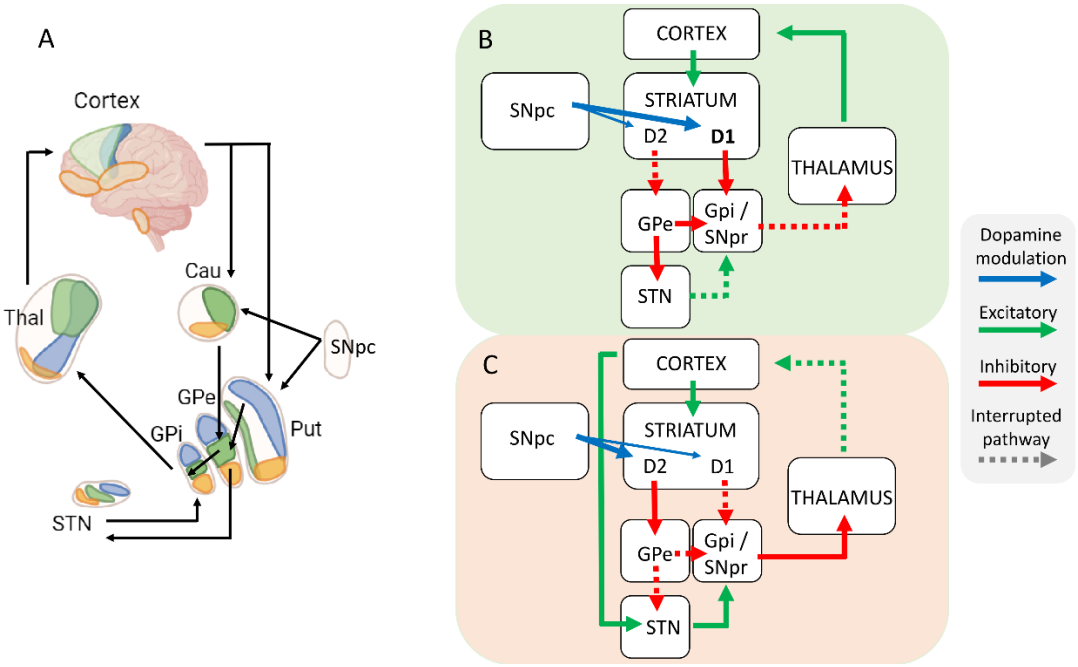

Figure 1. Schematic representation of fronto–striatal circuitry. ***A)*** *Schematic representation of the connectivity within the basal ganglia circuitry. Blue: motor domains; green: associative domains; orange: limbic domains.* ***B)*** *Schematic representation of the direct pathway.* ***C)*** *Schematic representation of the indirect pathway.* ***Blue*** *arrows represent dopaminergic modulation.* ***Green arrows*** *represent excitatory drive.* ***Red*** *arrows represent inhibitory drive.* ***Dashed arrows*** *represent suppressed pathways.* ***Abbreviations****: Cau – caudate nucleus; Put – putamen; SNpc – substantia nigra pars compacta; SNpi – substantia nigra pars reticulata; GPe – globus pallidus externa; GPi – globus pallidus interna; STN – subthalamic nucleus; Thal – thalamus. Created with Biorender based on [69] and [79].*

Basal ganglia function is strongly regulated by dopamine, a critical neurotransmitter involved in motor control, motivation, reward, and learning [79]. Dopamine primarily originates from two sources: the VTA and the SNpc. The VTA gives rise to the mesocortical and mesolimbic pathways, which are involved in executive functioning and reward-related behaviour, respectively [86, 87]. Meanwhile, the dopaminergic neurons of the SNpc project to the striatum via the nigrostriatal pathway, where dopamine acts on direct and indirect striatal projection neurons to ensure appropriate execution of motor and cognitive functions [88] (Figure 1/B–C). In addition to dopamine, other neurotransmitters such as acetylcholine and enkephalin also significantly influence striatal activity, contributing to the complex regulation of BG functions [79]. For example, cortico–striatal projection neurons also innervate striatal cholinergic

interneurons, which in turn modulate dopamine neurons via nicotinic receptors, thereby exerting cortically regulated control on striatal dopamine release [89].

Although beyond the scope of this dissertation, it is important to note that neuroimaging-based research has been providing valuable insights into schizophrenia [90, 91], revealing intriguing structural dysconnectivity in the condition [92] and indicating that SCH may be deeply associated with abnormal dynamic functional connectivity [93]. Yoon and colleagues demonstrated abnormal functional PFC–BG connectivity in SCH with an event-related fMRI experiment and found that nigrostriatal connectivity predicts the severity of psychosis symptoms [94]. The authors proposed that the disrupted PFC–BG connectivity disinhibits the substantia nigra, causing excessive dopaminergic activity in the striatum. These results underscore the involvement of fronto–striatal pathways in SCH and highlight the importance of understanding these circuits and the cell types creating them in relation to the disorder's symptomatology.

1.3. Striatum: topology, structure, and function

As the primary input structure of the fronto–striatal circuitry, the striatum receives, selects, and relays information from cortical areas, and is, therefore, crucial for motor control and cognitive function. Within the striatum, incoming cortical information is processed and relayed by GABAergic medium spiny projection neurons (MSNs), which account for ~90% of striatal neurons in humans (~ 95% in rodents) [95, 96, 77] and form the direct and indirect pathways. Direct (dMSNs) express D1R and substance P, while indirect MSNs (iMSNs) can be distinguished based on the expression D2R and enkephalin [97]. However, a subset of MSNs co-express both receptors [98], and recent transcriptomic studies in both mice [99] and primates [100] revealed further heterogeneity within the MSN population. Striatal GABAergic local inhibitory neurons (~5% in the rodent, ~10-15% in the nonhuman primate and human striatum; [95, 101–104]) are essential modulators of striatal activity and output. They consist of the rare but widely arborizing large cholinergic neurons marked by the expression of choline acetyltransferase (CHAT, encoded by *CHAT*) and a diverse population of local interneurons traditionally identified based on the expression of parvalbumin (PV, encoded by *PVALB*), calretinin (CR, encoded by *CALB2*), calbindin (CB, encoded by *CALB1*), somatostatin (SST, encoded by *SST*), neuropeptide Y (NPY, encoded by *NPY*),

nitric oxide synthase 1 (NOS1, encoded by *NOS1*), tyrosine hydroxylase (TH, encoded by *TH*), or NADPH-diaphorase [71, 77, 105, 106]. Recently, transcriptomic studies began to describe comprehensive striatal cell type composition in rodents, nonhuman primates, and humans [71, 77, 107], revealing intriguing interspecific differences – a topic of pivotal importance for drug development and translational medicine. In mice, seven interneuron subtypes were described based on mRNA expression patterns: *Sst–Npy, Npy–Mia* (MIA SH3 domain-containing)*, Cck–Vip* (vasoactive intestinal peptide), *Cck*, *Chat*, *Th*, and parathyroid hormone like-hormone (*Pthlh*), the latter group including *Pvalb*-expressing neurons [105]. In the human striatum, however, Garma and colleagues established eight interneuron types: *SST–GRIK3* (glutamate ionotropic receptor kainate type subunit 3); *SST–NPY; CCK–VIP; CCK* without *VIP; PVALB; PTHLH; CHAT;* and *TAC3,* a population which includes the majority of *CALB2*-expressing neurons. In this study, the interneurons accounted for 10.67% of the total neuronal cells, confirming previous histological estimates [101–104].

To our knowledge, the most abundant human striatal interneurons belong to the *TAC3* and the *PTHLH*-expressing types [71]. The *PTHLH* subtype was only recently described (rodent: [105]; human: [71]) and thus requires further research, as does the elusive CCK population [71]. Striatal CR-expressing interneurons have been described early in rodents [108], nonhuman primates [95], and humans as well [109, 110]; however, their functional, electrophysiological, and molecular properties are still poorly understood [106]. Morphologically, we can distinguish small (approx. 6–15 μm), medium (approx. 15–25 μm), and large (approx. 25–60 μm) CR subtypes in the human striatum [101, 111, 112], the latter largely overlapping with large cholinergic neurons [109, 113]. There is some confusion regarding the extent of this overlap: Cichetti and colleagues report that about 50% of CHAT-positive neurons also express CR, while Holt and colleagues report that "virtually all of the large, multipolar calretinin-positive cells of the human striatum are also immunoreactive for CHAT". The molecular and functional traits of small and medium CR neurons are largely unknown. In primates, secretagogin has been reported to mark a rostrally biased subtype of CR interneurons, and although the presence of this subtype in humans has not been confirmed yet [103], it does corroborate the spatial heterogeneity of the cellular and molecular landscape of the striatum (described comprehensively in mice in [70]).

Notably, transcriptomics revealed that *CALB2* is expressed by the *CCK–VIP,* the *CHAT,* the *MOXD1*-expressing *PTHLH*, and the *TAC3* cell types [71], suggesting that what previous histological studies refer to as "CR interneurons" belong to these transcriptomically diverse cell types. This could potentially explain their heterogenous morphology; however, it is currently unknown whether small and medium CR neurons strictly correspond to certain transcriptomic cell types.

The *TAC3* population has been recently described by Krienen and colleagues as a primate-specific, evolutionarily "novel" striatal interneuron subtype in marmosets and humans [77]. Further exploring this topic, they identified the *Tac2*-expressing homologues of this cell type in the mouse striatum [107], confirming previous observations [71]. While these neurons are rare in mice, the *TAC3* population makes up 30% of striatal interneurons in primates, which is a significant expansion [107]. Together, these data suggest that non-cholinergic CR interneurons may have been "upgraded" during primate brain evolution to provide more refined control necessary for more complex behaviours, and therefore represent an evolutionally "interesting" cell type with potential relevance to human behaviour and striatum–related disorders as well. These data further underline the importance of comparative studies, and of characterizing the neurochemical, developmental, and functional properties of human interneurons.

The origin and development of striatal interneurons has been thoroughly characterized in mice [114], but not in humans – largely due to the limited technologies available to study human brain development and the scarcity of high-quality developmental human brain tissue. In rodents, most striatal interneurons are known to migrate tangentially from the medial ganglionic eminence (MGE) or the preoptic/entopeduncular areas, marked by the expression of the transcription factor NK2 homeobox 1 (*NKX2.1*) [114]. Recent transcriptomic studies involving adult human striatal samples revealed that most human striatal interneuron types also express MGE-associated transcription factor profiles (such as *NKX2.1,* and LIM homeobox 6 (*LHX6)*; [71]), except for CCK neurons, which selectively express adenosine deaminase RNA specific B2 (*ADARB2*; [71]); see Figure 2 based on [77]. *ADARB2* expression has been previously associated with caudal ganglionic eminence (CGE)-origin in both rodent and human cortical interneurons [115]. Interestingly, Garma and colleagues [71] found that several types of human striatal interneurons also express serotonin receptor 3A (*HTR3A*), a marker of CGE-origin in the

rodent cortex [115] – which might suggest shared developmental origins of these subtypes.

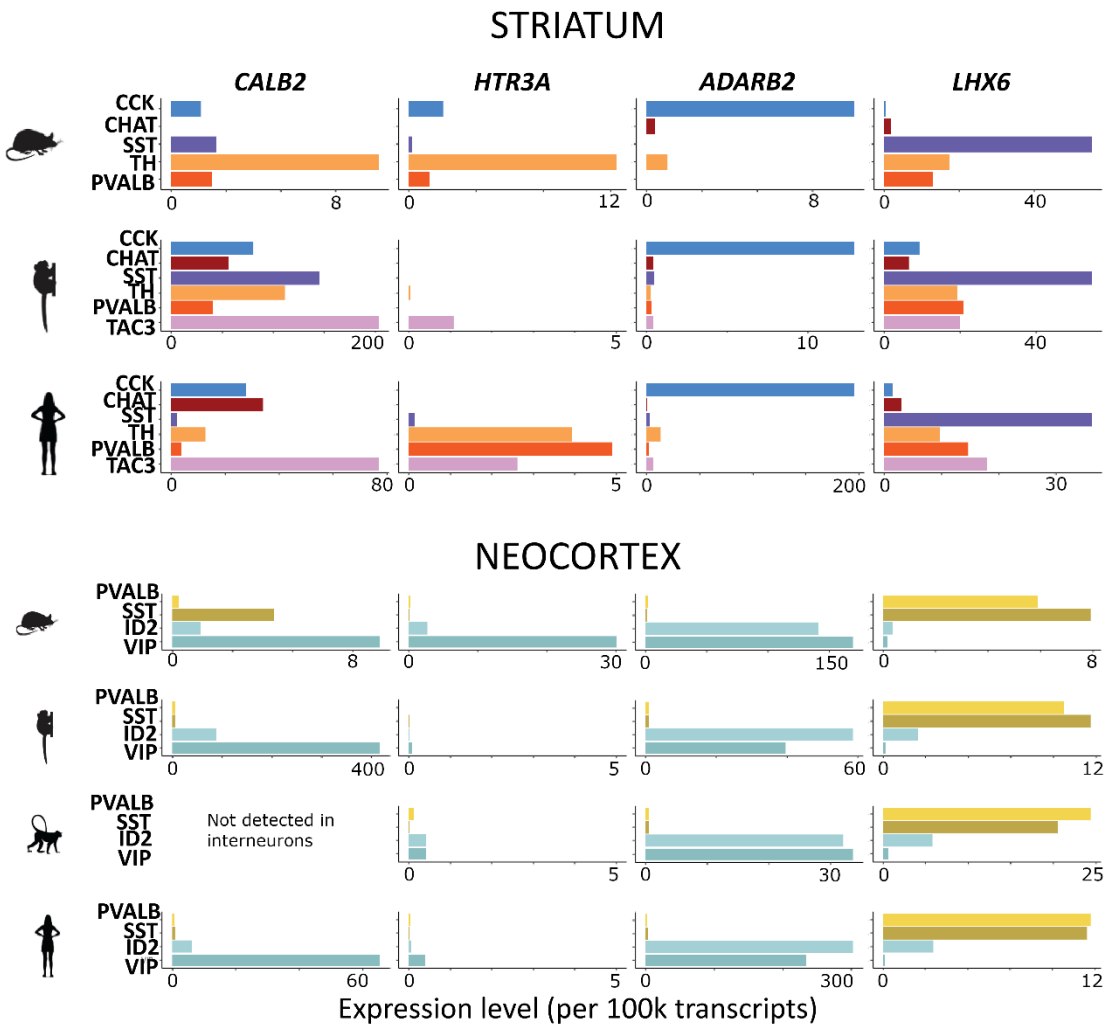

Figure 2. Plots depicting the expression of developmentally informative genes in the interneuron populations of striatum and neocortex of mice, nonhuman primates, and humans based on the data published by Krienen and colleagues [77]. *Pictograms indicate the species the data originated from (**striatum**: mouse, marmoset – new world monkey, human; **cortex**: mouse, marmoset – new world monkey, macaque – old world monkey, human). Cell type marker genes: cholecystokinin (**CCK**), choline acetyltransferase (**CHAT**), somatostatin (**SST**), tyrosine hydroxylase (**TH**), parvalbumin (**PVALB**), tachykinin 3 (**TAC3**), inhibitor of DNA binding 2 (**ID2**), vasoactive intestinal peptide (**VIP**). ADARB2 expression represents caudal ganglionic eminence-origin (CGE; expressed by **ID2** and **VIP**/**CR** subtypes in neocortex), while LHX6 indicates medial ganglionic eminence-origin (MGE; expressed by **PVALB** and **SST** cell types in the neocortex). In the striatum, only **CCK** neurons express ADARB2, while every other interneuron subtype expresses LHX6. This pattern seems conserved across species. In contrast, serotonin receptor 3A (HTR3A), also an indicator of CGE origin in rodents, is expressed quite differently across species in both brain regions. Images generated with the open, interactive browser established by Krienen and colleagues, available at http://interneuron.mccarrolllab.org/ [77].*

However, this does not provide direct evidence because cortical and striatal interneurons have been shown to differ in their developmentally relevant transcription factor expression patterns [116]. These results also suggest substantial interspecies differences: while *HTR3A* is highly expressed in mice cortical CGE-derived interneurons, it seems almost absent from that population in humans (see Figure 2 based on [77]). Together, these data highlight that there is still much to explore and understand about the origin, development, and function of human striatal interneurons.

1.3.1. The striatum in schizophrenia

Although the associative striatum has been pinpointed as a hub of dopaminergic hyperactivity in SCH [117] and is therefore a prominent region of interest in SCH research [118], literature regarding its cellular and molecular patterns in SCH remains scarce. One workgroup reported reduced density of large cholinergic neurons in SCH [113, 119]. Several types of structural changes (such as ventricular enlargement, basal ganglia enlargement, and total grey matter loss [120, 121] have been detected in patients with SCH, however, results are rather mixed [122, 123]. No comprehensive in situ hybridization or single cell transcriptomics study has been conducted yet on the striatum in SCH. However, applying bulk RNA-seq revealed the selective downregulation of the short isoform of dopamine receptor D2 mRNA (*DRD2*) in SCH, and highlighted important gene expression changes associated with long-term antipsychotic medication [124].

Notably, a recent study reported the generation of patient-derived ventral forebrain organoids to recapitulate potential developmental disturbances [60]. “Striatal” GABAergic neurons (including immature medium spiny neurons and *CALB2*-expressing neurons) in these SCH organoids demonstrated accelerated maturation compared to control-derived organoids, indicating early developmental dysfunction affecting striatal neurons. Timing is a crucial aspect of neuronal maturation; its disturbance could contribute to E/I imbalance in the mature neuronal network.

1.4. Dorsolateral prefrontal cortex: topology, structure, and function

The neocortex is a 2–4.5 mm thick sheet of tissue enveloping the majority of the hemispheres of the human brain. The prefrontal cortex and its circuitry are strongly associated with cognitive control, perception, and executive function [125], making it a

primary interest in psychiatry. The dorsolateral prefrontal cortex can be localized to the middle frontal gyrus, occupying the lateral part of the Brodmann areas 9, 10, and 46 [126, 127], although it is an area defined functionally, rather than anatomically. The DLPFC plays a crucial role in cognitive control and flexibility, working memory, planning, and goal-directed behaviour [128, 129]. Because it is particularly enlarged in non-human primates and humans, it has been proposed to contribute to the enhanced cognitive abilities characteristic of these species [130].

The grey matter of the DLPFC consists of 6 cortical layers (L1–L6), which are vertically organized into functional units referred to as 'minicolumns' [131, 132]. The layers are populated with diverse, specialized subtypes of neuronal and non-neuronal cells. Cell types can be classified based on many characteristics, such as morphology, electrophysiological properties, postsynaptic target, expression of specific proteins, and gene expression profile. Pyramidal projection neurons (PNs) release the excitatory neurotransmitter glutamate, and can be broadly classified as cortico-cortical or cortico-fugal based on whether their axonal projections target other cortical areas or subcortical structures, respectively [133]. Cortico-cortical PNs encompass diverse subgroups of neurons across L2–L6, while cortico-fugal PNs are more confined to lower layers [largely based on rodent data; 133]. In contrast, local inhibitory interneurons (INs) release GABA and project locally*, with the primary aim of regulating the excitability of PNs and other INs [134, 135]. The non-neuronal compartment contains diverse astroglial populations, oligodendrocytes and oligodendrocyte precursor cells, microglia, and vascular elements (such as endothelial cells, smooth muscle cells, and pericytes). Oligodendrocytes produce myelin and create myelin sheets around neuronal axons, thereby insulating them and enabling efficient electrical signalling [136]. Astroglia are essential for maintaining the blood brain barrier, keeping homeostasis, recycling glutamate, and providing metabolic and structural support for neurons; however, they also participate in signalling [136]. Microglia are specialized immune cells residing in the brain, accounting for housekeeping, early synaptic pruning [137], immune reactions, and protecting against pathogens [138]. Vascular elements form the blood-brain barrier and have a crucial role in maintaining a healthy blood-CNS interface [139]. Although my dissertation is primarily focused on the neuronal elements, it is important to keep in mind that these

* Exceptions exist, for example the SST-NPY long-range projecting interneurons [135].

compartments function together, and investigating one without the others will always give incomplete results.

Cortical PNs are characterized by an apical dendrite that usually extends upwards to the pial surface and arborizes extensively in cortical layer 1. These cells distinguish and integrate inputs in real-time, establishing dynamic cortical activity and adaptability [140]. Recent work applying single cell RNA sequencing to uncover the detailed composition of the human neocortex identified many intermingled PN subtypes based on gene expression profiles [142]. For example, micro-dissecting and sequencing each layer of the middle temporal gyrus, Hodge and colleagues found 24 excitatory neuron types [143]. These results highlight that there is still much to discover about the human neocortex, let alone other, less well-known brain regions.

INs comprise 20-25% of the total neocortical neuronal population in both monkey and humans [144, 145], a ratio generally supported by transcriptomics studies as well [142, 143]. Their striking diversity – only recently beginning to be elucidated– suggests that human synaptic inhibition is highly specialized, presumably to optimize the efficacy and efficiency of computation in cortical circuits [146]. Importantly, much of what we know about the function and electrophysiology of interneurons is still based on rodent and non-human primate experiments [146]; for review, see [147]. Cortical interneurons are traditionally classified based on the expression of specific calcium-binding proteins and neuropeptides, such as PV, CR, calbindin (CB), SST, and "inhibitor of DNA binding 2" (ID2) [148, 149].

PV interneurons have two main morphological subtypes. PV basket cells are present with highest density in deep L3 and L4 [144]. Their axons arborize widely and form perisomatic 'baskets' around numerous nearby PN somata, providing strong inhibitory control of cortical activity [150], while they are in turn heavily targeted by the local axon collaterals of L3 PNs [151]. PV chandelier cells are less abundant, and present with vertically arrayed sets of axon terminals ("cartridges") which terminate on the axon initial segment of PNs [152], thus potently controlling their firing [153]. Intriguingly, some evidence suggests that this input can also exert depolarizing effects [154], depending on the current state of the cortical circuit [155]. Converging evidence [156, 157] suggests a pivotal role for PV neurons in the generation of gamma oscillations associated with working memory [158], particularly for basket cells [159]. Recent transcriptomic studies

[143, 160, 161] also identified these main types of PV interneurons, with further putative subtypes suggesting potential functional specialization.

A second large group of cortical interneurons express **CR**, which often co-express VIP [162]**.** These mostly reside in cortical L2-3, manifest with double bouquet, bipolar or multipolar morphology, and target not only pyramidal neurons, but also other interneurons (extensively studied in rodents, while human data is still scarce [163, 164], capable of exerting a disinhibitory effect on PNs [165] and fine-tuning cortical activity. In the monkey prefrontal cortex, Gabbott and Bacon found that CR-immunoreactive axons frequently contact the somata and proximal dendrites of CB and PV interneurons [166]. In contrast, the one study addressing directly this topic in the human temporal cortex identified many pyramidal cell bodies, but relatively fewer non-pyramidal GABAergic neurons targeted by CR terminals [164]. Whether this result may be limited by technical factors, or whether it reveals intriguing species-specific differences, remains unresolved to this day. Transcriptomic studies revealed unexpected heterogeneity within the CR–VIP cell type [143, 160], however, many putative subtypes have not been confirmed with histological methods yet.

PV and CR belong to the family of EF-hand calcium-binding proteins [167], which, by regulating intracellular calcium homeostasis, also shape synaptic responses and modulate cellular excitability of neurons [168] – for example, the loss of CR impaired long-term potentiation in the dentate gyrus of CR-knockout mice [169].

A third major group of INs expresses **somatostatin** (SST), which primarily target the distal dendrites of PNs [170]. Morphologically, they can be classified as Martinotti or non-Martinotti cells [171, 172]. Martinotti cells distinctively send their axons into L1 where they arborize widely and terminate on the apical dendrites of PNs [148, 173]. Some non-Martinotti cells in L4 have been shown to inhibit PV interneurons in the mouse sensory cortex [174]. Studies about the distribution of human cortical SST cells so far yielded mixed results [175, 176], in part perhaps due to the inconsistent levels of cellular SST protein content across the cortex, which makes reproducible visual evaluation and quantification challenging [173]. Combining immunofluorescence and in situ RNA hybridization, Banovac and colleagues concluded that SST neurons represent about 7% of the total cortical neuron population and are present uniformly across layers 2-6 and the superficial white matter [173]. Furthermore, the authors revealed that almost all

supragranular SST neuron co-expresses calbindin (CB), while almost all infragranular SST neuron co-express neuronal nitric oxide synthase (nNOS1) – the latter identified in rodent as long-range interneurons [135]. The authors defined 5 SST subtypes based on location, immunoreactivity, and morphology. Recent transcriptomic findings also revealed several subtypes within the human SST neuronal population, but the correlation between morphological and transcriptomic subtypes has not been characterized yet [142, 143].

In addition to the main IN groups described above, there remains an additional population of GABAergic interneurons expressing **inhibitor of DNA binding 2** (*ID2*), reelin *(RELN)*, and lysosomal-associated membrane protein family member 5 (*LAMP5*) [177], which encompasses diverse interneurons (including rosehip neurons [178], neurogliaform cells [179], and cholecystokinin basket cells [177, 180]. Neurogliaform cells are intriguing, but relatively poorly characterized in the human cortex. In rodents, they have been shown to have an extremely high degree of output connectivity (to both PNs and other INs) suggesting a pivotal role in information processing [181]. CCK basket cells represent an elusive subtype which has been shown to target a high variety of both PNs and other IN types in mice; however, they have not been deeply characterized in the human PFC [182].

The recent renaissance of cell type discovery, driven by the emergence of high-throughput single cell techniques, enabled researchers to discover (e.g., rosehip neurons [178]) and rediscover cell types with unprecedented detail and resolution [143]. Based on transcriptomic profiles, there may be up to 25 excitatory, and 20 inhibitory neuronal subtypes in the prefrontal cortex [142, 143, 160]. Today, the aim is the comprehensive mapping of the cellular and molecular composition of the human brain, and relating transcriptomically defined cell types to morpho-electrophysical properties (as seen, for mice, in [147]). Challenges of this multi-omic quest include handling and visualizing extremely large amounts of data, redefining the concept of "cell type" in light of "cell states" [183], and achieving meaningful integration and interpretation of data derived from different modalities.

1.4.1. The DLPFC in schizophrenia

Pioneering psychiatrist Emil Kraepelin postulated that "the mind in dementia praecox is like an orchestra without a conductor" [21]. He suggested that the observed deficits may

be linked to impaired frontal lobe function – paving the way for a line of studies linking impaired executive function to prefrontal cortical dysfunction in SCH. One of the core features of SCH is working memory (WM) impairment, making the DLPFC, a critical WM hub, a primary region of interest in SCH [184]. Numerous in vivo structural neuroimaging studies have reported gross macroscopic abnormalities of the DLPFC in SCH (for review, see [185]), such as thinner grey matter (which may be associated with antipsychotic treatment; [186, 187]), and lower connectivity between the DLPFC and other areas [188]. Functional neuroimaging studies repeatedly showed lower frontal cerebral blood flow in patients with SCH compared to neurotypical controls during WM tests such as the Wisconsin Card Sort Task and the N-Back Task [189–192]. Electroencephalography (EEG) allowed researchers to reveal that high frequency (gamma; ~30–80 Hz) neuronal oscillations are strongly associated with working memory and cognitive control-related tasks [193, 194]. SCH patients generally demonstrated lower gamma oscillatory power compared to neurotypical controls during WM-related tasks [159]. As gamma oscillations are thought to be directly dependent on synaptic inhibition [195], cognitive dysfunction in SCH has been suggested to be a consequence of cortical cellular dysfunction, particularly of disrupted GABA-mediated inhibition [57]. Which brings us to another line of studies directly measuring the density, mRNA content, and physiological properties of cortical INs (mostly conducted between 1990 and 2015; [196–199]). Benes and colleagues reported lower density of small, nonpyramidal neurons in the PFC in SCH [200], suggesting putative interneuron loss or dysfunction. PV neurons received a lot of attention from early on because of the obvious functional connection to WM [159]. While indeed several studies reported lower cortical PV neuron density in cortical areas, unaltered or even higher PV neuron densities were also reported (for review, see [199]). To date, the most robust framework has been presented recently by Dienel and colleagues [201], where the authors showed that PV and SST mRNA levels are markedly lower without the loss of the respective cells (relying on cell type-specific markers thought to be independent of SCH).

To my knowledge, 9 studies focused on CR interneurons in the DLPFC in SCH, none of which reported significant differences in their density, *CALB2* gene expression level, or the excitatory input converging on CR neurons [202–211], until a recent study published with our contribution, where a subset of SCH cases was highlighted with significantly

lower L2 CR interneuron density in this brain region [160]. These studies differ in technical and statistical methodology, the post-mortem confounding effects are not always accounted for, and naturally occurring individual heterogeneity further complicates results, making the interpretation of the results challenging [201]. However, the mixture of accumulating evidence suggests that GABAergic neurons are present in physiological density, while a subset of them may be dysfunctional in SCH – but not uniformly in every patient. Several studies have suggested the possibility of SCH "subtypes" defined by certain cellular or molecular traits. Scarr and colleagues documented markedly lower M1 muscarinic receptor levels in the DLPFC present in 25% of the donors, establishing the "muscarinic receptor deficit form of schizophrenia" subtype [212, 213]. Dienel and colleagues reported that only a subset of cases demonstrated lower PV/SST mRNA levels [201]. Notably, Ruzicka and colleagues identified two subgroups of SCH-associated gene expression profiles when investigating almost 500,000 nuclei from control and SCH cases – one similar to the control group, and one very different from it. In addition, they also identified SCH-like patterns in some control cases, highlighting the spectrum–like nature of SCH [161].

SCH seems to be characterized by network-level functional disturbance across brain regions, affecting many, if not all, cell types. Traditional histo-pathological methods, however, only allow for the investigation of a handful of cell types at the same time on a rather limited scale. The fact that more than 30 years of extensive histological research did not establish clear cellular–molecular markers of SCH suggests that these methods may not be sufficient and/or adequate for doing so. Machine learning based object-detection algorithms and automatized multiplexed histological workstations are expected to upscale and expand the field of neurohistology [214], however, integrating multi-omic approaches in the workflow seems inevitable to understand the full picture.

1.5. Molecular psychiatry in the era of hight-throughput methods

High-throughput (HT) or new-generation sequencing technologies (NGS) opened new horizons in life sciences and allow scientists to address fundamental biological questions with unprecedented resolution. NGS enables the parallel sequencing of a vast number of DNA or RNA molecules simultaneously. Molecular psychiatry greatly benefits from NGS technologies. While gene expression was initially measured via hypothesis-driven

methods such as qPCR or in situ RNA hybridization methods for a few chosen transcripts, today, it is possible to assess the whole transcriptome with HT microarray or RNA sequencing technologies [215, 216]. NGS also upscaled genetic studies: genome-wide association studies (GWAS) conducted on large cohorts (>1000 cases) not only identified hundreds of genes potentially relevant to SCH [217–219], but also revealed previously unrecognized systems involved in SCH, such as the complement cascade [220] and drew attention to non-coding regions [221]. Today, some of the most promising causal genes include contactin-4 (*CNTN4*; neuronal adhesion molecule [222]), glycoprotein M6A (*GPM6A*; critically involved in neurodevelopment [223]), transcription factor 4 (*TCF4;* involved in synaptic plasticity, memory, and regulation of columnar distribution of layer 2–3 prefrontal pyramidal neurons [224]), and matrix mentalloproteinase-16 (*MMP16;* involved in breaking down the extracellular matrix, [225]), as reported in [226]. GWAS alone, however, did not tackle the SCH enigma [222]. Bulk RNA sequencing offers further valuable insight into major gene expression patterns in SCH (e.g., [227]), however, fails to capture subtle, cell-type specific changes. This challenge has been addressed by the development of single cell/nucleus RNA sequencing (scRNAseq or snRNAseq, respectively; [228]). Lake and colleagues were among the first to apply HT snRNAseq on post-mortem human brain tissue in 2016; a milestone in human neuroscience [229]. The possibility of quantifying the expression of all captured genes in thousands of individual cells/nuclei across many samples simultaneously opened exciting new perspectives. It was instantly clear that describing the transcriptomic landscape of the "healthy" human brain is equally important as exploring disease profiles. Such studies have been offering great insight (autism spectrum disorder [230], Alzheimer's disease [231], major depressive disorder [232], schizophrenia [160, 161]), but studies aiming to describe the integrative atlas of the human brain and establish a consensus cell-type taxonomy are of pivotal importance [142, 143]. Without understanding cell types of the healthy brain, we cannot truly comprehend the cell type-specific changes observed in disease. Recently, exploring individual heterogeneity on the transcriptomic level also became a hot topic, especially in connection with personalized medicine and pharmacogenomics [233, 160]. The single cell field is rapidly moving towards efficient integration of multi-scale data, including genetic, epigenetic, transcriptomic, proteomic,

and morpho-electro-physiological information, with the aim of at some point, finally, seeing the whole elephant (Figure 3).

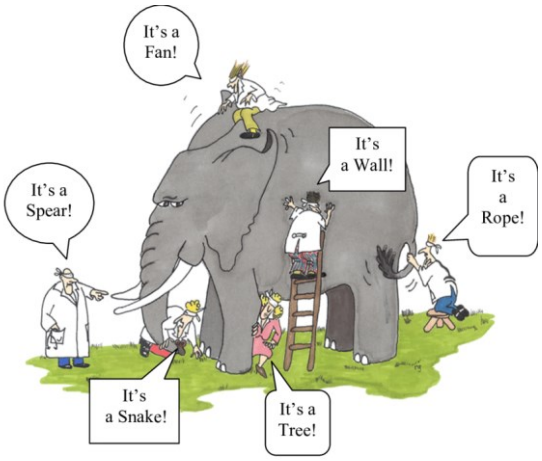

Figure 3. The inevitable struggle of science. *"The parable of the blind men and the elephant suggests that disputes among scholars arise … from differences of perspective – incomplete perceptions, each from a different angle of view, of a more complex reality." [234]*

Epigenetics, encompassing heritable alterations in chromatin structure and function [235], is extremely important in neuropsychiatric illness, as it mediates the effects of environmental factors on gene expression during neurodevelopment and throughout adult life [236]. Elusive non-coding elements, such an enhancer or promoter regions, can now be directly assessed by NGS technologies such as ChIP-Seq ("chromatin immunoprecipitation followed by sequencing"; [237]) or single cell ATAC-seq [238]. Regarding SCH, among many genes involved in dopaminergic (DRDs), serotonergic (*SLC6A4*), GABAergic (*GABRB2*) and glutamatergic (glutamate metabotropic receptors) systems, the most consistent findings in this line of studies was the hypomethylation of membrane-bound catechol-O-methyltransferase (*MB-COMT*), essentially involved in catabolizing catecholamine neurotransmitters such as dopamine, epinephrine, and norepinephrine in the brain (for an excellent review, see [239]). Notably, many studies reported methylation and histone-modification alterations associated with antipsychotics [240]: for example, haloperidol appeared to promote global hypermethylation [241].

Overall, the above-listed technologies are becoming indispensable tools for gaining insight into the mechanisms underlying healthy and pathological processes in biological systems.

2. Objectives

The aim of this work was to reveal SCH–associated cellular and molecular patterns in the DLPFC and the CN.

The main objectives were the following:

A) Perform quantitative histological assessment of **CR interneurons** in the human **CN** in SCH.

B) Perform quantitative histological assessment of **excitatory neurons, CR, and PV interneurons** in the human **DLPFC** in SCH.

C) Identify cell type–specific **gene expression** differences between **control and SCH** samples with **single nucleus RNA sequencing in the DLPFC**.

3. Methods

3.1. Materials

Formalin-fixed, paraffin embedded (FFPE) tissue blocks or sections containing Brodmann area 9 (Ba9) and the precommissural striatum containing the head of the CN were obtained from the following brain banks: Netherlands Brain Bank (NBB; Netherlands Institute for Neuroscience, The Netherlands); Oxford Brain Bank (OBB, Oxford University, United Kingdom); Newcastle Brain Tissue Resource, (NBTR, Newcastle University, United Kingdom); King's College London Neurodegenerative Diseases Brain Bank (KCL, King's College London, United Kingdom). From NBB, OBB, NBTR and furthermore the Human Brain Tissue Bank (HBTB, Semmelweis University, Budapest, Hungary), fresh frozen (FF) tissue samples were also requested from as many cases as possible and used for single nucleus RNA sequencing. Material was collected from donors from whom (or from their next of kin) written informed consent had been obtained. The experiments were approved by the Research Ethics Committee of the Hungarian Medical Research Council (reference number 38711-1/2019/EKU). Individuals in the control (CTR) group had no known history of psychiatric disorders. Demographics are described in Table 1, which also specifies which case was involved in which experiment. To minimalize biological variance between groups, we matched cases as closely as possible for PMI, age, and sex. Further details of NC samples can be viewed in the Supplementary Figure 1 and Supplementary Table 1 in [112], and of DLPFC samples in Supplementary Tables 1, 2, and 6 in [160].

Table 1. Demographic data of included cases and information regarding which case was included in certain experiments. "MB" *identifies cases which were included in the single nucleus RNA sequencing experiment. Cases* ***T1–T10*** *represent cases on which only IHC was performed in [160]. For cases* ***E1–10****, only CN data (not DLPFC data) has been published.* ***Abbreviations****: ID – identifier; Diag – diagnostic group; PMI – post-mortem interval (hours); SCH – schizophrenia; CTR – control; M – male; F – female; IHC – immunohistochemistry; CN – caudate nucleus; PFC – (dorsolateral) prefrontal cortex; SEQ – single nucleus RNA sequencing; Scope – RNAscope.* ***Colour code represents source****:* ***yellow*** *– Netherlands Brain Bank (Amsterdam, The Netherlands);* ***blue*** *– Oxford Brain Bank (Oxford University, Oxford, United Kingdom);* ***green*** *– Neurodegenerative Diseases Brain Bank (King's College London, United Kingdom);* ***pink*** *– Newcastle Brain Tissue Resource (Newcastle University, Newcastle upon Tyne, United Kingdom);* ***white*** *– Human Brain Tissue Bank (Semmelweis University, Budapest, Hungary).*

ID in [112]	ID [160]	Diag	Age	Sex	PMI (h)	Cause of death	IHC CN	IHC PFC	SEQ	Scope
-	MB6	SCH	71	M	13	Pulmonary failure			X	
#9	MB10	SCH	79	F	4.75	Cardiac failure	X	X	X	X
#10	MB12	SCH	55	F	9.83	Euthanasia	X	X	X	X
#7	MB14	SCH	66	F	11	Cancer	X	X	X	X
#11	MB22	SCH	63	F	5	Cancer			X	
-	MB8-2	SCH	59	M	12.5	Cardiac failure	X		X	X
#8	MB23	SCH	64	M	19	Pulmonary embolism	X		X	X
-	MB54	SCH	77	F	23	Pulmonary/ cardiac failure			X	
-	MB56	SCH	79	M	6	Stroke			X	
-	TT6	SCH	92	F	8	Pneumonia		X		
-	TT7	SCH	71	M	13	n/a		X		
-	TT8	SCH	60	M	41	n/a		X		
-	TT9	SCH	65	F	24	n/a		X		
-	TT10	SCH	55	M	50	n/a		X		
-	E1	SCH	67	M	5.75	Euthanasia		X		
-	E2	SCH	50	F	24	n/a	X	X		
-	E3	SCH	62	M	36	Pulmonary tuberculosis		X		
-	E4	SCH	32	F	46	Pulmonary embolism		X		
-	E5	SCH	75	F	50	Cerebro-vascular accident		X		
#1	MB7	CTR	57	F	7.66	Cancer, euthanasia	X	X	X	X
#3	MB9	CTR	78	F	4.58	Pulmonary failure, cancer	X	X	X	X
-	MB11	CTR	55	M	18.5	Cardiac failure			X	
-	MB13	CTR	61	M	5	Cardiac failure			X	
#4	MB15	CTR	70	F	6.25	Pulmonary failure, cancer	X	X	X	X

ID in [112]	ID [160]	Diag	Age	Sex	PMI (h)	Cause of death	IHC CN	IHC PFC	SEQ	Scope
#6	MB16	CTR	55	M	7.25	Intestinal ischemia	X	X	X	X
-	MB17	CTR	53	M	2	Cardiac failure			X	
-	MB19	CTR	64	M	4	Pulmonary failure			X	
-	MB21	CTR	54	F	19	Cancer			X	
#5	MB18 -2	CTR	55	M	7.5	Cancer; euthanasia	X	X	X	X
-	MB51	CTR	73	M	6	Cardiac failure			X	
-	MB53	CTR	88	F	2.5	Pulmonary/ cardiac failure			X	
-	MB55	CTR	51	M	10	Cardiac failure			X	
-	MB57	CTR	68	F	18	Pulmonary failure, cancer			X	
#2	TT1	CTR	60	F	8	Septicemia	X	X		
-	TT2	CTR	59	M	78	n/a		X		
-	TT3	CTR	65	M	55	n/a		X		
-	TT4	CTR	78	M	64	n/a		X		
-	TT5	CTR	69	F	63	n/a		X		
-	E6	CTR	92	M	8.45	Heart failure		X		
-	E7	CTR	102	M	5	Ileus		X		
-	E8	CTR	60	F	8.1	Cancer		X		
-	E9	CTR	67	M	25	Prostate cancer, metastasis		X		
-	E10	CTR	63	M	23	Colon cancer		X		
#14	-	SCH	50	M	34	Bleeding from esoph. varix	X			

We produced 6 µm thick serial coronal sections and air-dried them on SuperFrost Plus slides at room temperature (RT) for immunohistochemistry and RNAscope. For snRNAseq, approximately 100 mg grey matter was micro-dissected per case, containing

all cortical layers, from fresh frozen tissue stored at -80 °C. This was carried out by I. A. with scalpel under a stereotactic microscope while the stage was cooled with dry ice. Dissected tissue was immediately put into tubes and stored at -80 °C until processing.
Not all DLPFC samples could be used for both snRNAseq and IHC due to limitations such as limited tissue availability and PMI. For snRNAseq, we only included cases with a PMI under 24 hours to ensure sufficient RNA integrity.

3.2. Immunohistochemistry

Adjacent CN sections were stained for CR, Iba1, and TMEM119 [112]. Iba1 and TMEM119 markers were used to visualize microglia and reveal potential patterns of neuroinflammation. Adjacent DLPFC sections were stained for CR, PV, SMI-31.1, and cresyl violet (Nissl) [160]. SMI-31.1 is a neuronal filament marker which labels the neurofilament medium and heavy chains (NEFM, NEFH, respectively) and preferentially labels pyramidal neurons, making it useful for estimating the total density of cortical pyramidal cells [242]. Cresyl violet staining was used to estimate total neuronal density and to identify cortical layers.

Tissue sections were first deparaffinized using xylene and subsequently rehydrated through a graded ethanol series (absolute ethanol, 96%, 90%, and 70%), followed by rinsing in tap water. To block endogenous peroxidase activity, sections were incubated in 3% hydrogen peroxide (H_2O_2) prepared in phosphate-buffered saline (pH 7.4) for 20'. Antigen retrieval was performed by heat-induced epitope retrieval in citrate buffer (0.01 M, pH 6.0) at 121 °C for 10'. Slides were then mounted into the Sequenza System cover plates and racks, which generate a capillary gap between the glass slide and the cover plate, thereby minimizing reagent consumption (Thermo Scientific, 72110017, 73310017). Primary antibodies (listed in Table 2) were applied in Tris-buffered saline containing Triton X-100 (TBST, pH 7.6) and incubated for 1 hour at RT.

Table 2. List of antibodies used in immunohistochemical experiments.

Antibody	Species	Manufacturer	Catalogue number	Dilution
anti-calretinin	rabbit	Chemicon	AB5054	1:300
anti-parvalbumin	rabbit	Abcam	ab11427	1:500
anti-SMI-311	mouse	BioLegend	837801	1:500
anti-Iba1	rabbit	Wako	01919741	1:500
anti-TMEM119	rabbit	Abcam	ab185333	1:200

Sections were then incubated with horseradish peroxidase (HRP)-linked secondary antibody (Envision Kit, Dako, K-5007) for 1 hour at RT. Staining was visualized by 3-3'-diaminobenzidine (with the proportion of chromogen and substrate being 1:50) applied for 90''. Between steps, TBST wash was applied (3x1'). Finally, haematoxylin nuclear counterstain was applied for 20'' (in case of CN) or 90'' (in case of DLPFC) and sections were left in tap water for 5'. After dehydration in a graded alcohol series and xylene, sections were coverslipped with DePeX mounting medium. Negative control slides (where primary antibodies were omitted from protocol) demonstrated no specific staining.

3.3. Single nucleus mRNA sequencing

Fresh-frozen DLPFC tissue samples (~ 100 micrograms) from 9 SCH and 14 CTR samples were processed at the University of Copenhagen, Biotech Research and Innovation Centre by Mykhailo Y. Batiuk in the laboratory of Prof. Konstantin Khodosevich. SCH and CTR samples were coded and processed together. First, tissue was homogenized with a 1-ml Dounce homogenizer in homogenization buffer [250 mM sucrose, 25 mM KCl, 5 mM MgCl2, 10 mM TRIS with pH 8.0, 1 mM dithiothreitol, 1× protease inhibitor (Roche, #11873580001), ribonuclease inhibitor (0.4 U/µl; Takara, #2313B), SUPERase·In (0.2 U/µl; Invitrogen, #AM2696), and 0.1% Triton X-100] on ice. To isolate nuclei, the homogenate was first filtered through a 40-µm cell strainer and spun down at 1000g for 8' at 4 °C. After resuspending the pellet in 250 µl homogenization buffer, it was mixed with 250 µl of 50% iodixanol solution overlaid on top of a 29% iodixanol solution (for details see the Supplementary Methods in [160]), and spun down in an ultracentrifuge (Beckman Coulter, MAX-XP) using a swing bucket rotor (Beckman Coulter, TLS 55) at 14,000g_{max} for 22' at 4°C, with slow acceleration and deceleration. Once done, the supernatant was carefully removed, and pellets were resuspended in cold bovine serum albumin (BSA) solution and incubated for 15' on ice for blocking. After this, the suspension was split into '*target'* and control samples (e.g., NeuN-control, isotype control) for extensive quality control. To stain neuronal nuclei, NeuN antibody was used (Merck Millipore, MAB3777x, dilution: 1:1890) for 10' at 4 °C. Isotype control was stained using a control antibody (STEMCELL Technologies, 60070AD.1, 1:378) for 10' at 4 °C. Then, samples were mixed with 1 ml of BSA and centrifuged for 10' at 1000g

at 4°C using a swing bucket rotor. Pellets were resuspended, and filtered through a 35-µm strainer. Fluorescence-activated nucleus sorting (FANS) was carried out with a BD FACSAria III sorter using a 75-µm nozzle, using the 'BD FACSDiva' 8.0.1 software (for further details see Methods section of [160]). FANS was carried out on the NeuN-stained *'target'* sample to extract neuronal nuclei for sequencing. We chose to only include neurons due to financial reasons and based on evidence suggesting neuronal elements being more burdened in SCH than non-neuronal elements (further substantiated by [157], where the majority of transcriptomic burden accumulated in the neuronal compartment).
Library preparation was done according to standard 10X Genomics protocols with the Chromium Single Cell 3′ Reagent Kits v3 (10x Genomics, PN-1000075). Nuclei were quantified under a microscope, mixed with reverse transcription mix, and loaded onto Chromium (B) Chips (10x Genomics, PN-1000073) with partitioning oil and v3 Gel Beads. The Chromium Controller microfluidic equipment (10x Genomics, PN-120223) captured individual nuclei, reagents, and Gel Beads in single oil droplets, producing "Gel Beads-in-emulsion" or "GEMs". Gel Beads have short oligonucleotide sequences on their surface, which contain unique 10X barcodes ("cell barcodes"), unique molecular identifiers ("UMI"s, which serve as "mRNA molecule barcodes"), and polyDT sequences for capturing mature mRNA molecules by hybridizing to their poly–A tails. Then, reverse transcription of captured mRNA took place. Samples were stored at –20 °C and processed for cDNA cleanup and pre-amplification (12 polymerase chain reaction cycles) within a week. After cleanup using "SPRI–select" magnetic beads, cDNA was quantified and stored at −20 °C.
After these steps, fragments were cleaned up using the magnetic beads and processed through adapter ligation and sample index PCR with several steps of cleanups. Libraries were then cleaned up with magnetic beads and quantified with the Qubit HS dsDNA Assay Kit (Thermo Fisher Scientific, Q32854), Qubit Fluorometer, and the High Sensitivity DNA Kit (Agilent, 5067-4626) with the Agilent 2100 Bioanalyzer. Libraries were pooled based to the expected amounts of nuclei per sample. Pools were quantified and sequenced using either 100 or 200 cycles of NovaSeq 6000 S2 (Illumina, 20012861 and 20012862) runs on Illumina NovaSeq 6000 System (Illumina 20012850) controlled by the NovaSeq Control Software. Libraries were sequenced with 28 cycles for read 1, 8

cycles for i7 index, and 94 cycles for read 2. On average, sequencing yielded 54,230 reads and 4413 genes per nucleus.

3.4. RNAscope combined with immunohistochemistry

Combined in situ mRNA hybridization–immunohistochemistry experiments (RNAscope immune co-detection) for validating snRNAseq results were carried out on FFPE tissue containing DLPFC by Dora Sedmak and colleagues in the Zagreb Brain Research Centre in case of [160]. *CALB2*–CR RNAscope co-detection was carried out by T.T. at the Department of Pharmacology and Pharmacotherapy (Semmelweis University), in collaboration with Dr. Zoltan V. Varga. In all cases, experiments were carried out according to the manufacturer's guides (RNAscope Multiplex Fluorescent V2 Assay) [243]. Sections were pretreated at 60 °C on a heater for 1 hour, and deparaffinized (2x5' xylene, 2x2' absolute alcohol), after which excess alcohol was dried off at 30 °C and H_2O_2 solution was applied for 10' at RT (from the RNAscope™ Multiplex Fluorescent Detection Kit v2; #323110). To enhance antigen retrieval, slides were heat-treated in a rice cooker in Co-Detection Target Retrieval solution (ACDBio; RNA-Protein Co-Detection Ancillary Kit; #323180) for 12' at 100 °C. After 2x1' wash with distilled water (DW) and 1' in absolute alcohol, excess alcohol was dried off at 30 °C, and a hydrophobic barrier was drawn around tissue sections with an ImmEdge Hydrophobic Barrier PAP Pen (H-4000). Once the barrier was completely dry, sections were incubated with the Protease Plus solution (from the RNAscope™ Multiplex Fluorescent Detection Kit v2; #323110) for 30' in the RNAscope Hybez® oven at 40 °C. After 2x1' DW wash, sections were incubated with the probe solution (ACDBio, Hs-*CALB2* probe for channel C1, #422171; Hs-*CHRFAM7A* for channel 1, #833991; Negative Control Probe, #EF191515, 3-plex Positive Control Probe – *POLR2A* (channel C1), *PPIB* (channel C2), *UBC* (channel C3), #320881) for 2 hours in the RNAscope Hybez® oven at 40 °C. As this is an official breakpoint in the protocol, slides were removed from the RNAscope rack after 2 hours, washed 2x2' in wash buffer (WB), and stored in 5X saline-sodium citrate buffer overnight. The next day, slides were washed 2x2' in WB, then incubated with AMP1 reagent in the oven for 30'. After 2x2' in WB, slides were incubated with AMP2 reagents for 30'. During this incubation time, the fluorescent dyes were prepared (TSA Plus FITC/Cyanine 3/Cyanine 5, AKOYA Biosciences, #NEL741001KT, #NEL744001KT,

#NEL705A001KT, respectively; 180 µl/section; 1:1000 in TSA buffer #322810). After 2x2' in WB, slides were incubated with AMP3 reagents for 15'. After 2x2' in WB, the WB was discarded and replaced with new WB. Slides were incubated with HRP-C1 for 15'. After 2x2' in WB, fluorescent dye (dedicated to channel 1) was applied for 30'. After 2x2' in WB, slides were incubated with HRP blocker for 15'. After 2x2' WB, HRP-C2, fluorescent dye for channel 2, HRP-blocker, and HRP-C3, fluorescent dye for channel 3, and HRP blocker were also sequentially applied in the case of positive control probes. In the case of the target probe experiment, only the relevant channel was developed (channel 1), coupled with Cy3 fluorescent dye. In the case of immune co-detection, TBST wash was applied after the last HRP-blocker step, and slides were incubated with rabbit anti-calretinin antibody (Merck Millipore, ABN2191, 1:300 in TBST) at RT for one hour. After 3x5' TBST wash, donkey anti-rabbit secondary antibody (Alexa Fluor™ 488, Invitrogen, #A-11008, 1:500 in TBST) was applied for 45' and washed away with 3x5' in TBST.

Finally, 4′,6-diamidino-2-phenylindole (DAPI) was applied for 2' to label nuclei, and slides were coverslipped with Fluoromount-G mounting medium (Thermo Fisher Scientific; #00-4958-02). Slides were stored away from light, left to dry at RT overnight, and were finally transferred to 4 °C for long-term storage.

In the case of the CR–*CALB2* experiment, the finishing steps included incubation with TrueBlack Plus solution (Biotium #23014; 1:40 in 70% ethanol, for 40'') to quench autofluorescence.

3.5. Image analysis

Sections stained by immunohistochemistry were digitalized with whole-slide scanners (Aperio ScanScope AT Turbo, Leica Biosystems; Pannoramic Flash Desk DX, 3DHistech) at 20× and 40× magnification, respectively. Image analysis was carried out in digital pathology softwares (Aperio ImageScope v12.4.3.5008; Leica Biosystems; and SlideViewer v2.7.0.191696, 3DHistech).

Regarding striatal sections, the total CN was outlined and every immunoreactive neuron was annotated within the outlined region. One slide contained one section due to the large size of human tissue blocks. The annotation included measuring the longest diameter of neurons. Neurons were classified based on this measurement following the criteria

described by Petryszyn and colleagues with slight modifications [111]: small neurons (6 – 15 μm), medium-sized neurons (15 – 25 μm), large neurons (25 – 60 μm). Density values were calculated based on neuron number and measured area.

In the DLPFC, regions of interests (ROIs) were outlined (1 mm wide columns containing all cortical layers from the pial surface to the white matter where pial surface was perpendicular to the white matter; on average 5 ROIs/slide). Within each ROI, every cortical layer was separately outlined as well to measure their individual areas and neuron densities. Cortical layers were identified based on cytoarchitecture and adjacent sections which were stained with cresyl violet (which especially helped identifying L4). Immunoreactive cell bodies were annotated and density values were calculated from cell number and area. While this 2D method is not adequate for measuring absolute cell density, it is sufficient for measuring and comparing relative densities between groups [244]. Four investigators contributed to the quantification (*CN*: V.F, I.A, T.T; *DLPFC*: V.F, I.A, T.T, E.S), all blinded to the diagnoses of the subjects. Annotation was supervised by I.A. The annotation also included measuring the longest visible diameter of each immunoreactive neurons. Consistent with our earlier studies, only cell bodies with a diameter >6 μm were included [112, 245]. In the case of Iba1 and TMEM119 staining, the total immunoreactive area fraction was measured by the Aperio Positive Pixel Count Algorithm, as previously [245].

Fluorescently stained sections (RNAscope experiments) were digitized by an LSM780 confocal laser scanning microscope and a fluorescent whole-slide scanner (3DHistech Pannoramic MIDI II). The 20× and 63× objectives were used in the confocal microscope to produce tile scans containing all layers of the cortex within a 1 mm-wide column. RNAscope sections for [160] were evaluated by T.T. in the Aperio ImageScope program, similarly to IHC slides (cortical layers were outlined on tile scans and positive neurons were annotated). In case of the CR–*CALB2* experiment, the fluorescent scanner was used at 20× to produce whole-slide scans. At least two ROIs per section were outlined, in which neurons were annotated in the SlideViewer software by Örvényesi-Petik Sára undergraduate research student with the supervision of T.T. Because our previous results suggested that CR interneuron density was only significantly lower in L2, we focused on supragranular layers (L1–L3). We established 5 qualitative categories based on the expression level of both the CR protein and mRNA: 1) high protein – high mRNA; 2)

low protein – high mRNA; 3) no protein, high mRNA; 4) low protein – low mRNA; 5) high protein – low/no mRNA. The threshold between low and high mRNA content was set to 10 mRNA spots based on visual evaluation of all slides. *CALB2* mRNA positivity threshold was set at 3 spot/cell. We only considered cells in which the nucleus was visible. We acknowledge that this is approach could be further refined and we aim to increase the number of samples, the number of annotated ROIs, and establish a more objective semi-automated quantification protocol. After annotation, the percentage and number of each category in each ROI was extracted, and density was calculated based on neuron number and area.

3.6. Density heatmaps

For the visualization of CR neuron distribution and density as heatmaps, intact cortical areas (0.25 cm^2 – 1 cm^2) were delineated on the scanned sections, in which all immunoreactive cell bodies were annotated in the Aperio ImageScope software. Some sections had rips or insufficiently stained areas due to technical issues, therefore the available area of intact cortical areas varied across sections. Cases MB18-2, MB23, and TT5 were excluded due to having too many rips and bubbles present. From the remaining sections, over 45,000 CR-immunoreactive cells were annotated in over 18 cm^2 of cortical grey matter. Coordinates of annotated cells were loaded into a spatial informatics software (Quantum Geographic Information System "QGIS" v2.18.3, [246]). The metric projection EOV23700 was used. Maps were generated from the coordinates with the 'heatmap' module. We used a standard sampling radius of 565 μm, with a threshold of 30, meaning that on the red area of a computed heatmap in a [(0,565 mm^2) x π] area circle (~ 1 mm^2), at least 30 cells could be expected. Heatmaps were exported and merged with the respective tissue images to put the maps in spatial context using Gimp v2.10.22.

3.7. Bioinformatics analysis

The raw snRNAseq data provided by Illumina NovaSeq6000 platforms was processed by CellRanger, a free 10X Genomics tool, to produce FASTQ files by the *mkfastq* function, and raw/filtered count matrices by the *count* function, carried out by our collaborators at the University of Copenhagen. Raw data produced in the study can be accessed at https://zenodo.org/records/6921620. These matrices contain genes in the rows, individual

nuclei barcodes in the columns, and respective gene expression values in the cells. Code produced by our collaborators for the downstream analysis using "pagoda2" (https://github. com/kharchenkolab/pagoda2), "Conos" (https://github.com/ kharchenkolab/conos), and other packages to produce the results and plots presented in [160] can be found at https://github.com/khodosevichlab/Schizophrenia20, with extensive description in the Methods section of [160].

To briefly introduce the analyses applied by our research partners to produce the results and figures presented in [160]: datasets were normalized using "pagoda2", samples were aligned using "Conos", and the UMAP (Uniform Manifold Approximation and Projection) embedding was carried out with default parameters. Layer-specific locations of the identified cell types were estimated based on the Allen Brain Institute human motor cortex, temporal cortex, and anterior cingulate cortex datasets [140, 247]; for details, see [160]. Cell type-specific differentially expressed genes (DEGs) between groups were explored with a pseudo-bulk approach with the Wald test in DESeq2 [248] via the *estimatePerCellTypeDE*() function [249]: gene counts per cell type were pooled (per sample) to create pseudo-bulk gene counts. The p-values of DEGs were corrected for multiple comparison with the Benjamini-Hochberg method. To gain functional insight about the top DEGs, Gene Ontology analysis was carried out with the "clusterProfiler" package [250] for every cell type, focusing on Biological Pathway (BP) terms. Resulting BP terms were filtered by corrected p-values and clustered into 20 clusters based on the similarity of the genes involved in the categories. Additional analyses were also done, however, as I did not contribute to those in any way, I do not report them here.

For the unpublished figures presented here for the sake of better understanding cell types and marker gene expression (Figure 10 and 11), I used the raw count matrices (https://zenodo.org/records/6921620: snRNA-seq_raw_countmatrices.RDS) and carried out analyses in R (version 4.3.1.) with the "Seurat", "harmony", "tidyverse", and "patchwork" packages. Quality control was applied on each sample separately. Nuclei were filtered based on the number of unique genes detected ('*nFeature_RNA*') and the number of UMIs detected ('*nCount_RNA*') and mitochondrial gene expression level, to exclude low-quality nuclei and potential doublets (where two or more nuclei stick together and are registered as one). Filtered datasets were merged and "SCTransform" normalization was applied [251]. Despite the controlled experimental setup, the data

manifested some level of batch effect (when nuclei from certain batches, such as sample ID, tend to cluster together regardless of gene expression profiles), so I applied Harmony integration [252], which resulted in sufficient batch correction. The necessary steps of dimension reduction (Principal Component Analysis – PCA, Uniform Manifold Approximation and Projection – UMAP [253]) were followed by k-nearest-neighbours (KNN) clustering with *FindNeighbours*() and *FindClusters*(). Resolution is an important parameter of clustering, which directly impacts the number of clusters identified by the algorithm. Lower resolution highlights fewer, main cell types, while higher resolution allows for identification a higher number of smaller cellular subtypes. Achieving optimal high resolution can be challenging, as many cellular subtypes are not yet known and/or validated, one cannot be always sure if a small subcluster represents a biologically meaningful subtype or a technical artifact. Therefore, in my analysis, I chose a medium resolution which revealed the main cell types in the DLPFC which could be annotated based on known marker genes (in line with [160], Supplementary Table 3). As reported in the manuscript, despite FANS, there were some non-neuronal nuclei present in the dataset, originating from a few samples. I excluded such nuclei (mainly identified as astroglia and oligodendroglia based on aquaporin 4 and myelin basic protein expression) along with small, non-informative clusters, to achieve a clear, interpretable map of the investigated cell types.

3.8. Statistical analysis

Results are presented as mean ± sd. Alpha was set to 5%. In the case of [112], density values were statistically evaluated in the SPSS software (version 22.0) by I.A and T.T. Unpaired, two-tailed Student's t-tests were used to test whether the mean of age, PMI, and cross-sectional areas of the caudate nucleus were different between groups. Fisher's exact test was used to compare the distribution of sex between the groups. Finally, general linear models (GLM) were fitted on the data, which included cell density as dependent variable, diagnosis and cell type and explanatory variables, and PMI, age, and sex as potential confounders.

In the case of IHC and RNAscope results from the DLPFC in [160], density values of annotated neurons were analysed by T.T. in R environment (version 4.3.1.) by applying linear mixed models (LMM) using the "*lme*" function of "nlme" package [254] and post-

hoc comparison tests (via "*lsmeans*" from the "emmeans" package) with Bonferroni correction. This approach was chosen because several measurements were taken from the same sample (namely, 6 layer-specific density measurements), producing non-independent data. Each cell type was investigated in separate models. Cell density was set as the dependent variable, while sample ID was included as random effect. Layer (referring to respective cortical layer) was set as within-subject factor (6 levels), while diagnosis was set as a between-subject factor (2 levels). PMI, age, and sex were included as confounder variables. First, "full" models were constructed including diagnosis, PMI, age, sex, and their interactions with the Layer factor. This revealed which variables may affect the dependent variable significantly. Then, non-significant interactions and variables were dropped to achieve "final" models (see Supplementary Table 5 in [160]). To directly compare layers with each other across groups, post hoc multiple comparison tests were applied to these models using the "*lsmeans*" function. Reported p-values were corrected for multiple testing with the Bonferroni method. Because the *lsmeans* approach results in numerous comparison pairs, we only reported the p-values of comparisons relevant to our study (namely, CTR–SCH comparisons in layers 1–6). To compare average cortical width between groups, unpaired, two-tailed Student's t test was used.
The CR-*CALB2* RNAscope experiment was analysed similarly, however, instead of the "*lsmeans"* multiple comparison approach (producing numerous irrelevant, unnecessary comparison pairs), contrast matrices were constructed to directly test the biologically relevant questions (e.g., whether the ratio of a certain cell category differs between groups).

Regarding [112], my own work included whole-slide scanning, manual cell counting, carrying out descriptive statistics and correlation analyses, and participation in writing the manuscript. Regarding [160], my own work included sectioning paraffin-embedded tissue, immunohistochemical staining, whole-slide scanning and confocal microscopy, manual cell counting, statistical analyses, and participation in writing the manuscript. Unpublished, extra snRNAseq figures presented here are my own work based on the original, published dataset (https://zenodo.org/records/6921620). The CR-*CALB2* RNAscope experiment was carried out by me at the Department of Pharmacology and Pharmacotherapy (Semmelweis University), in collaboration with Dr. Zoltan V. Varga.

4. Results

4.1. Quantitative histological assessment of neuron density in SCH

4.1.1. Calretinin interneurons in the caudate nucleus

Analysing striatal sections from 6 SCH and 6 CTR cases confirmed the presence of small, medium, and large subtypes of CR neurons (Figure 4/A–R), and revealed significantly lower density of CR neurons in the CN (Figure 4/right panel) based on altogether 21,443 annotated neurons ($p = 0.018$; n = 6/group; GLM on total CR density). The densities of small, medium, and large CR interneurons were all relatively lower in SCH, however, statistical testing only revealed the density of small CR interneurons as significantly different ($p = 0.013$; n = 6/group; GLM). This was not confounded by PMI, age, or sex ($p > 0.05$, n = 6/group; GLM; see Supplementary Table 6 in [112]).

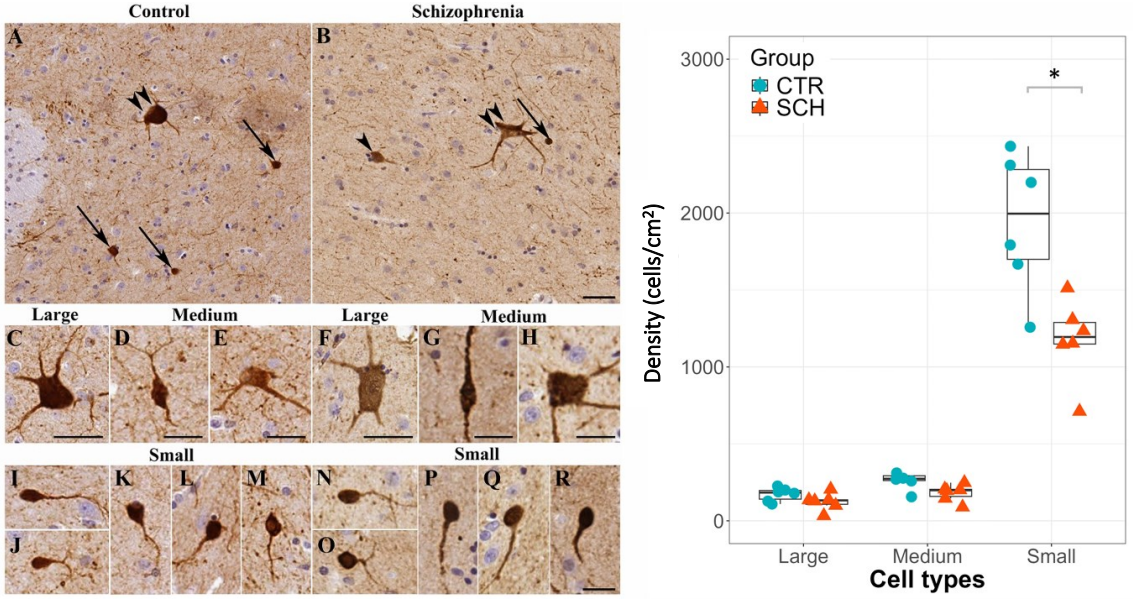

Figure 4. Morphology and density of calretinin subtypes in the caudate nucleus in control (CTR; blue) and schizophrenia (SCH; red) cases*. Large (C, F), medium (D, E, G, H), and small (I–R) cell types showed no gross morphological differences between groups. The density of large and medium subtypes did not differ significantly, while the density of small calretinin neurons was significantly lower in the SCH group (p = 0.013; n = 6/group; general linear model). Scale bars: (A, B, C, F): 40 µm; (D, E, G, H): 20 µm; (I–R): 15 µm. Images reused and modified from [112].*

Furthermore, there were no significant differences between the average longest diameter of annotated neurons between groups (**small**: $p = 0.803$; **medium**: $p = 0.975$; **large**: $p = 0.962$; n = 6/group; t-tests for SCH vs CTR).

To gain insight into whether potential volumetric changes of the CN may influence the measured neuronal density, we compared the cross-sectional caudate nucleus areas measured during annotation and found no significant difference between groups (**CTR**: 0.99 ± 0.09 cm^2, **SCH**: 0.90 ± 0.08 cm^2, p = 0.477, n = 6/group, t-test). Age and cross-sectional area were not significantly correlated in either group, although interestingly, SCH cases showed slight positive, while CTR cases showed slight negative correlation (**SCH**: r = 0.32, p = 0.59, n = 6, Pearson's correlation; **CTR**: r = -0.37, p = 0.46, n = 6, Pearson's correlation).

4.1.2. Striatal microglial activity in SCH

To determine whether the observed lower CR neuron density may be associated with increased neuroinflammation, we immunohistochemically visualized Iba1- and TMEM119-containing microglia in adjacent sections from the same cases. Qualitative evaluation conducted by three independent observers revealed no inflammatory patterns. In both groups, the large majority of microglia showed resting morphology (small cell bodies and fine ramified processes; see Figure 5).

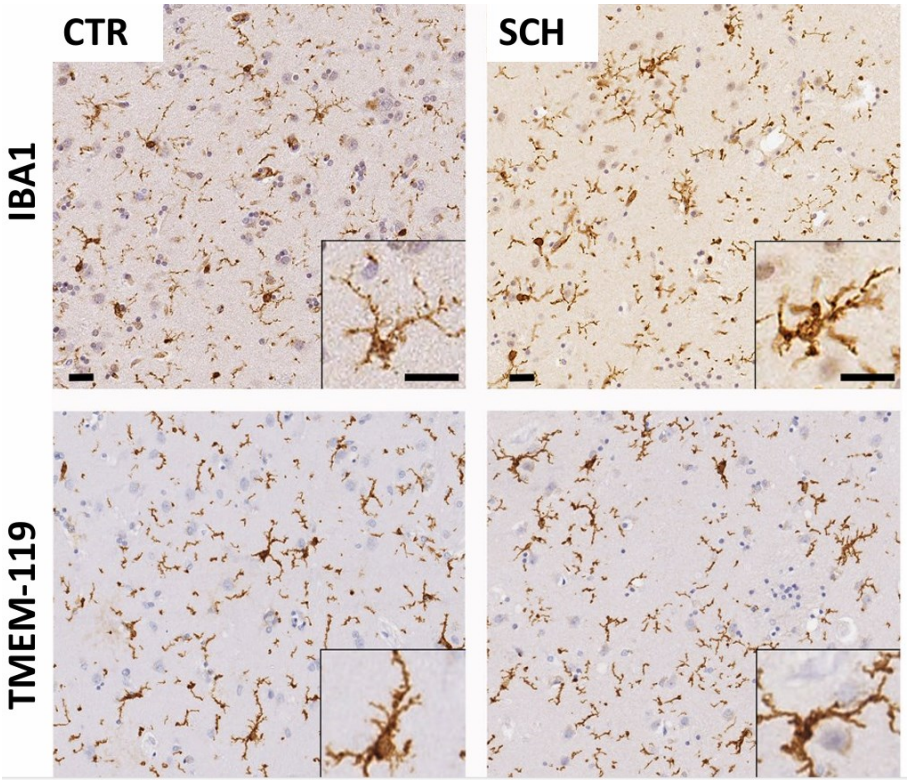

Figure 5. Qualitative assessment of general striatal microglial activity in control (CTR) and schizophrenia (SCH) cases. *The distribution and morphology of both Iba1 (top row) and*

TMEM119-expressing microglia (bottom row) showed no prominent differences visible upon qualitative evaluation. Most microglia cells demonstrated typical resting morphology with small cell bodies and fine, ramified processes in both groups (control: left; schizophrenia: right). Scale bars represent 20 µm. Images taken from [112].

Comparing the total immunoreactive area fractions revealed no significant differences between groups (**CTR/Iba1:** 5.04% ± 0.42%, **SCH/Iba1**: 3.66% ± 0.87%, p = 0.164; n = 6/group, t-test; **CTR/TMEM119:** 3.32% ± 0.46%, **SCH/TMEM119:** 2.96% ± 0.72%, p = 0.659; n = 6/group, t-test).

4.1.3. Calretinin and parvalbumin interneurons in the DLPFC

Analysing DLPFC sections from 10 SCH and 10 CTR samples revealed significantly lower density of CR neurons, specifically in cortical layer 2 (based on altogether 5254 neurons; p = 0.0028; n = 10/group; LMM followed by post-hoc multiple comparison; Figure 6/A–B). Notably, only a subset of SCH cases demonstrated strikingly lower density, which was not associated with PMI or other known confounding factors (Figure 6/B, cases highlighted with red circle). Unpublished data from an expanded dataset (n = 15/group) further substantiates the same result (p = 0.000165, LMM followed by post-hoc multiple comparison). PV neuron density was also markedly lower in cortical layer 2 (based on altogether 6507 annotated neurons) in the SCH group, however, this result was strongly confounded by PMI ($p = 8.3 \times 10^{-7}$; n = 10/group; LMM followed by post-hoc multiple comparison; Figure 6/C–D). Therefore, we excluded PV interneurons from further analyses.

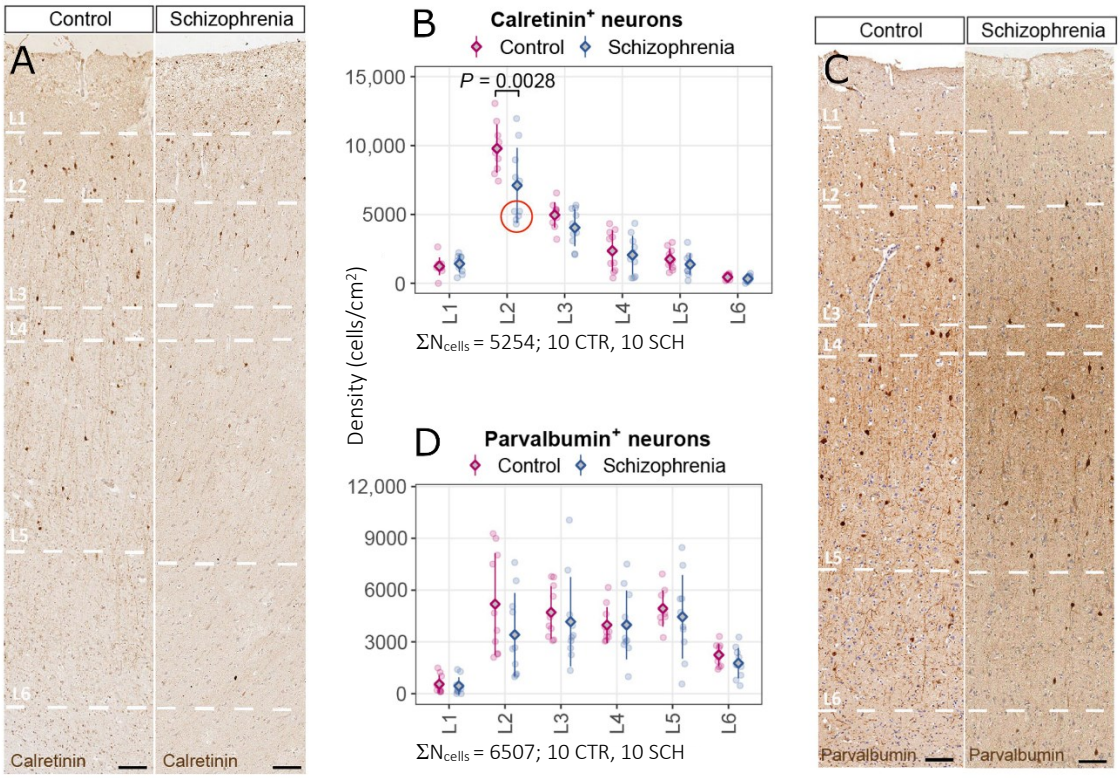

Figure 6. Density of cortical calretinin and parvalbumin interneurons in samples from the dorsolateral prefrontal cortex of neurotypical controls (CTR) and patients with schizophrenia (SCH). ***A)*** *Representative image of a cortical column stained against calretinin (CR) in both CTR (left) and SCH (right) cases.* ***B)*** *Scatterplot showing layer-specific CR interneuron density in CTR (red) and SCH (blue) cases. Red circle indicates the subset of SCH samples with markedly lower CR interneuron density (n = 10 cases/group, altogether 5254 neurons).* ***C)*** *Representative image of a cortical column stained against parvalbumin (PV) in both CTR (left) and SCH (right) cases.* ***D)*** *Scatterplot showing layer-specific PV interneuron density in CTR (red) and SCH (blue) cases (n = 10/group, altogether 6507 neurons). Diamonds represent group averages on the plots. Scale bars = 100 μm. Image taken and slightly modified from [160].*

During manual cell counting, we noticed high spatial heterogeneity in the density and distribution of CR neurons and we were curious whether this may be associated with any group-specific patterns. Mapping CR neuron distribution on a larger scale confirmed inhomogeneous CR cell body distribution (Figure 7/A–F), suggesting a "patchy" distribution pattern in SCH with visually striking low-density patches (Figure 7/A–C). Similar patterns were also visible in some CTR cases, although generally to a lower extent (e.g. Figure 7/F).

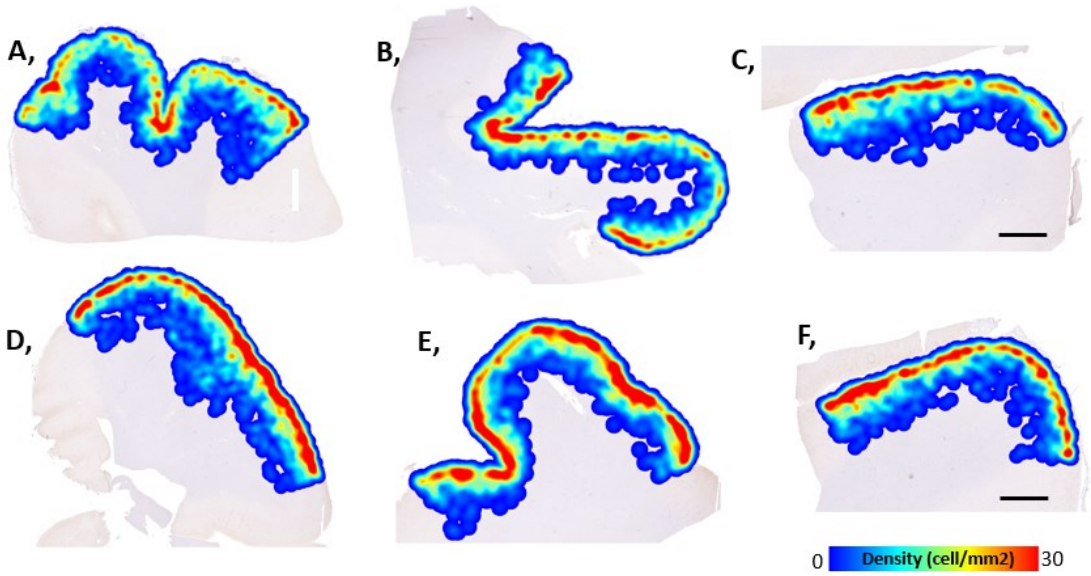

Figure 7. Representative heatmaps revealing the density and distribution of cortical calretinin interneurons. *Samples from patients with schizophrenia (**A**, **B**, **C**) generally demonstrated more "low-density patches" and more disrupted distribution compared to neurotypical controls (**D**, **E**, **F**). Scale bars represent 2 mm. Colour scale indicates neuronal density (0 – blue; 30 – red). Interpretation: in any point of a red area, at least 30 immunoreactive neurons are present in a 1 mm^2 circular area. Unpublished results.*

Diagnostic groups were not visually distinguishable during annotation. However, visual evaluation of the heatmaps (when knowing which group they belonged to) revealed that many SCH cases demonstrated higher level of spatial heterogeneity, with more low-density patches (Figure 7/A–C) compared to controls (Figure 7/D–F) – potentially suggesting disrupted upper layer structure of CR interneurons, which could be the result of developmental disturbances. At this stage, this is a qualitative assessment with no statistical corroboration.

4.1.4. Total neuron and excitatory neuron density in the DLPFC

Annotating all neuronal elements in a subset of cases stained with cresyl violet (Nissl) revealed no overall difference in total neuron density between the groups (based on altogether 45,446 neurons, $p = 0.875$; n = 6/group; LMM; Figure 8/A–B). Measuring the overall density of excitatory neurons stained by SMI-31.1 in the whole cohort, we found no significant difference between the two groups (based on altogether 58,964 neurons, $p = 0.721$; n = 10/group; LMM; Figure 8/C–D).

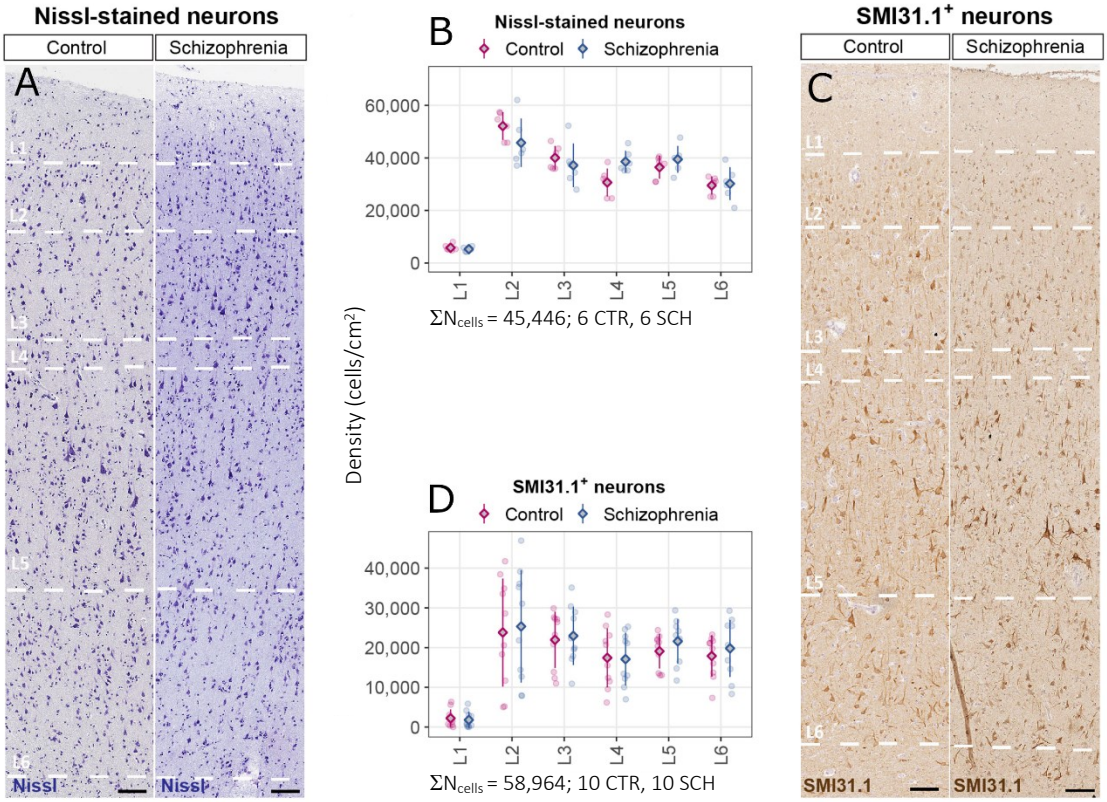

Figure 8. Total neuron density and total excitatory neuron density in the dorsolateral prefrontal cortex of patients with schizophrenia (SCH) and neurotypical controls (CTR)*. **A)** Representative image of a cortical column stained with cresyl violet in both CTR and SCH cases. **B)** Scatterplot showing layer-specific total neuron density in CTR (red) and SCH (blue) cases; no significant difference was found. **C)** Representative image of a cortical column stained against SMI31.1 in both CTR and SCH cases. **D)** Scatterplot showing layer-specific SMI31.1-immunoreactive excitatory neuron density in CTR and SCH cases. Diamonds represent group averages on the plots. Scale bars = 100 μm. Images taken and slightly modified from [160].*

4.2. Gene expression differences between CTR and SCH DLPFC

Raw data and results of bioinformatical analyses presented in Batiuk et al., 2022 [160] were produced by mainly by Mykhailo Y. Batiuk, Peter V. Kharchenko, Katerina Dragicevic, Rasmus Rydbirk, Viktor Petukhov, Shenglin Mei, Quiven Hu, and Ruslan Deviatiiarov. I participated in planning and conducting IHC and RNAscope experiments, slide scanning and confocal microscopy, image analysis, statistical analysis, and biological interpretation. For the sake of this dissertation, I re-analysed the raw sequencing data for visual purposes (Figures 10, 11).

4.2.1. Cortical interneuron diversity

To gain cell type-specific insight about gene expression differences in SCH, our research partners processed 9 SCH and 14 CTR DLPFC samples at the University of Copenhagen for snRNAseq. The process captured 225,012 nuclei, of which 209,053 passed quality control. High-resolution clustering produced 15 excitatory (EX) and 20 inhibitory (IN) neuronal subclusters (Figure 9/A), identified by canonical marker gene expression (Figure 9/B). Age, PMI, sex, disease condition, and other characteristics were also generally evenly distributed across the UMAP plots, suggesting that confounding effects did not influence clustering (Supplementary Figure 5 in [160]). IN and EX nuclei could be clearly distinguished based on the presence or absence of glutamic acid decarboxylase (*GAD1;* Figure 9/B). Main cell types were further annotated by cluster-specific marker genes (full list can be accessed in Supplementary Table 3 in [160]). Despite FANS, glial nuclei were also present in the dataset originating from a few cases [revealed by the expression of markers such as solute carrier family 1 member 3 (*SLC1A3;* astroglia), myelin basic protein (*MBP;* oligodendroglia), and protein tyrosine phosphatase receptor type C **(***PTPRC*; microglia)]**,** but these nuclei were excluded from further analyses.

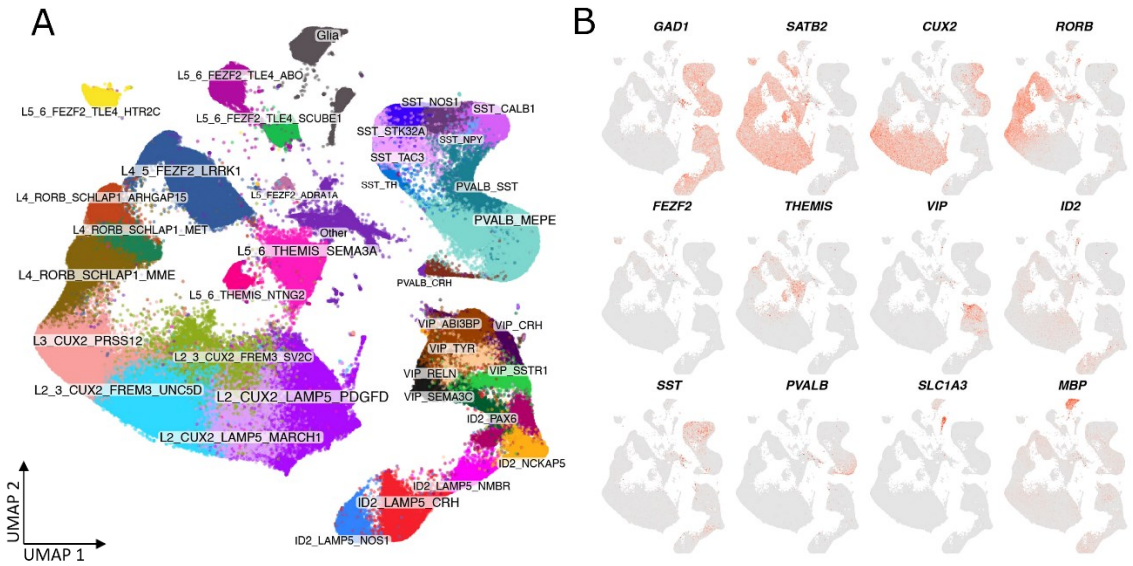

Figure 9. Single nucleus RNA sequencing analysis of the dorsolateral prefrontal cortex samples from patients with schizophrenia and matched neurotypical controls visualized in the same space. A) *Uniform manifold approximation and projection (UMAP) graph showing high-resolution cellular subtype clusters in the DLPFC including both groups. One point here represents one nucleus. Non-neuronal clusters are also show; however, these were excluded from further analyses. 15 excitatory clusters and 20 GABAergic inhibitory clusters were identified.* ***B)*** *Gene expression plots of selected marker genes. From left to write, top to down order: glutamic acid decarboxylase (**GAD1**) indicates GABAergic inhibitory interneurons. SATB homeobox 2 (**SATB2**) expression indicates principal excitatory neurons. Cut-like homeobox 2 (**CUX2**) identifies upper-layer excitatory cell types. RAR-related orphan receptor B (**RORB**) identifies layer 4-5 principal cell types. FEZ family zinc finger 2 (**FEZF2**) and thymocyte selection associated protein (**THEMIS**) identify subtypes of layer 5-6 principal cell types. Main GABAergic interneuron cell types can be identified by vasoactive intestinal peptide (**VIP**), inhibitor of DNA binding 2 (**ID2**), somatostatin (**SST**), and parvalbumin (**PVALB**) expression. Solute carrier family 1 member 3 (**SLC1A3**) and myelin basic protein (**MBP**) expression reveal astroglia and oligodendroglia contamination, respectively. Images taken from [160].*

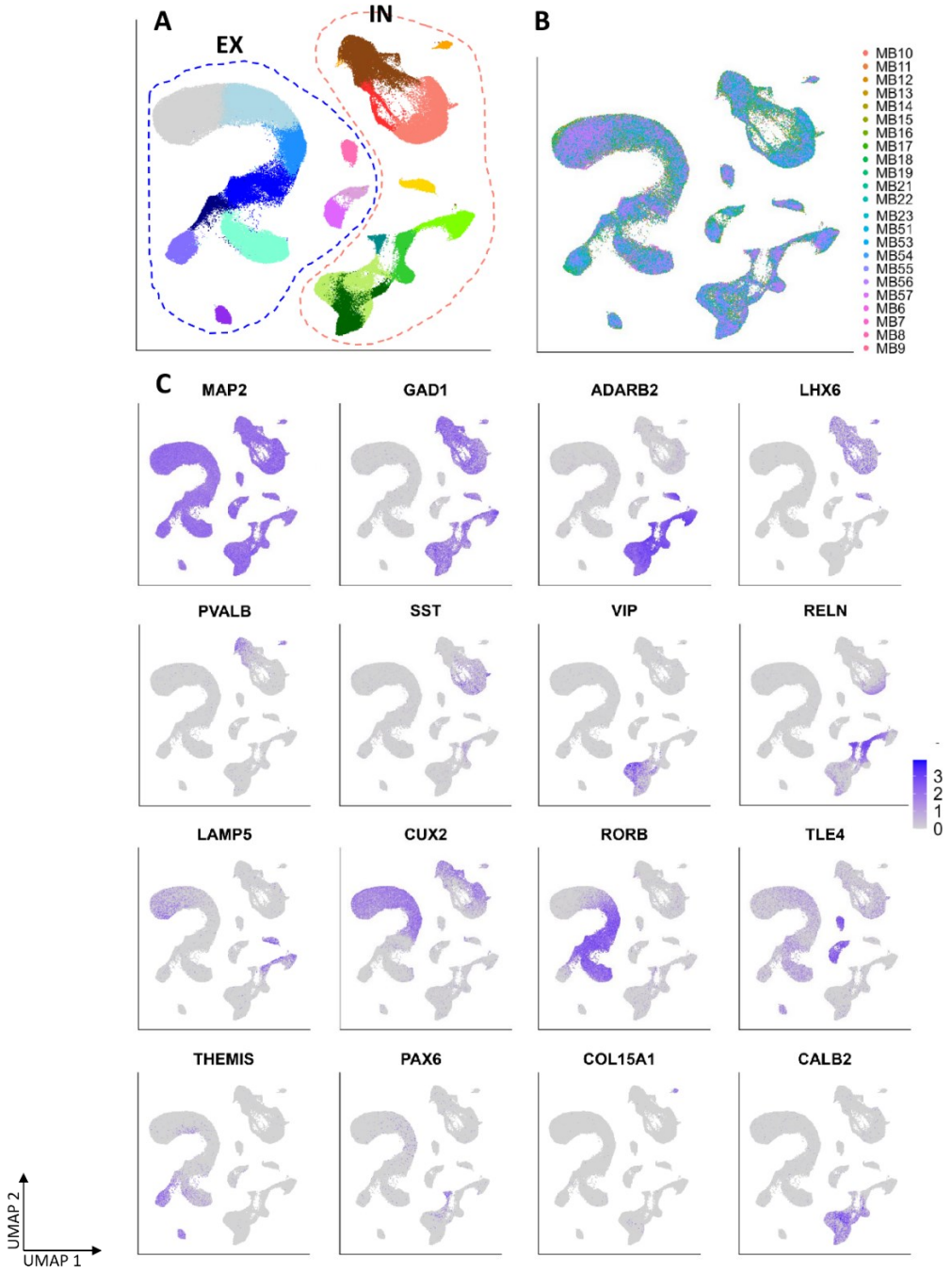

Figure 10. Expanded figure for demonstrating main cell types and selected marker genes. Nuclei from both diagnostic groups are presented together, in the same space. A) *Lower-resolution clustering highlighted main cell types in the uniform manifold approximation and projection (UMAP) graph including all samples from both groups. One point represents one nucleus.* ***B)*** *No batch effect visible (nuclei from every sample are represented in every cluster), confirming that after integration, nuclei formed clusters based on gene expression profiles, not based on technical or biological confounder variables.* ***C)*** *Gene expression plots of selected markers identify main cell types. From left to write, top-down order:* ***MAP2*** *– neuronal cells;* ***GAD1*** *– GABAergic interneurons (INs);* ***ADARB*** *– INs of caudal ganglionic eminence-origin;* ***LHX6*** *– INs of medial ganglionic eminence-origin;* ***PVALB*** *– parvalbumin INs;* ***SST*** *–*

somatostatin INs; ***VIP*** *– vasoactive intestinal peptide/calretinin INs;* ***RELN*** *– reelin-expressing neurogliaform INs;* ***LAMP5*** *– upper-layer pyramidal neurons (PNs) and neurogliaform/rosehip INs;* ***CUX2*** *– upper-layer PNs and PVALB, SST INs;* ***RORB*** *– layer 4-5 PNs;* ***TLE4*** *– layer 5-6 PN subtypes;* ***THEMIS*** *– layer 5-6 PN subtypes;* ***PAX6*** *– putative cholecystokinin INs;* ***COL15A1*** *– chandelier PV INs;* ***CALB2*** *– calretinin gene expression. Gene names are resolved in the List of Abbreviations. Unpublished supplementary figure based on original, openly available data published in [160].*

Main cortical EX and IN cell types were identified (Figure 10/A), and each cluster contained nuclei from all subjects, indicating that potential technical differences between subjects ("batch effects") were successfully corrected during data processing (Figure 10/B). EX cell types were identified based on the expression of known marker genes such as *CUX2* (supragranular cell types); *RORB* (layer 4 cell types); *FEZF2*, *TLE4*, and *THEMIS* (infragranular cell types), as shown in Figure 10/C. Cell types were assigned to the layers they primarily reside in based on Allen Brain Institute resources (for details, see [160]). Main IN cell types were identified based on the expression of known marker genes including *LHX6*, *ADARB2, PVALB, SST, VIP, RELN, PAX6, COL15A1,* and *CALB2* (Figure 10/C).

Cell types identified here aligned well with Allen Brain Institute reference databases (Supplementary Figure 4 in [160]). Main EX and GABAergic IN cell types were further clustered based on secondary and tertiary markers achieving 15 EX and 20 IN clusters (Figure 9/A; full marker gene list in Supplementary Table 3 in [160]).

For example, the heterogenous ***VIP*** cluster could be subdivided into further putative subclusters based on corticotropin-releasing hormone (*CRH*), ABI family member 3 binding protein (*ABI3BP*), semaphorin 3 (*SEMA3C*), NCK associated protein 5 (*NCKAP5*), inhibitor of DNA binding 2 (*ID2*), reelin (*RELN*), tyrosinase (*TYR*), and somatostatin receptor 1 (*SSTR1*) expression (Figure 11 panels, respectively). Notably, *CALB2* expression was not confined to ***VIP*** clusters – *CALB2, ID2* and *NCKAP5* expression overlapped in a substantial proportion of nuclei, which suggests that a subset of putative neurogliaform neurons may also express *CALB2* (Figure 11).

It must be noted that high-resolution, small transcriptomic subtypes are in many cases not yet validated and their biological relevance as a "cell type" is not always clear [255]; future studies are necessary to confirm such cellular subtypes with in situ RNA hybridization and immunohistochemistry.

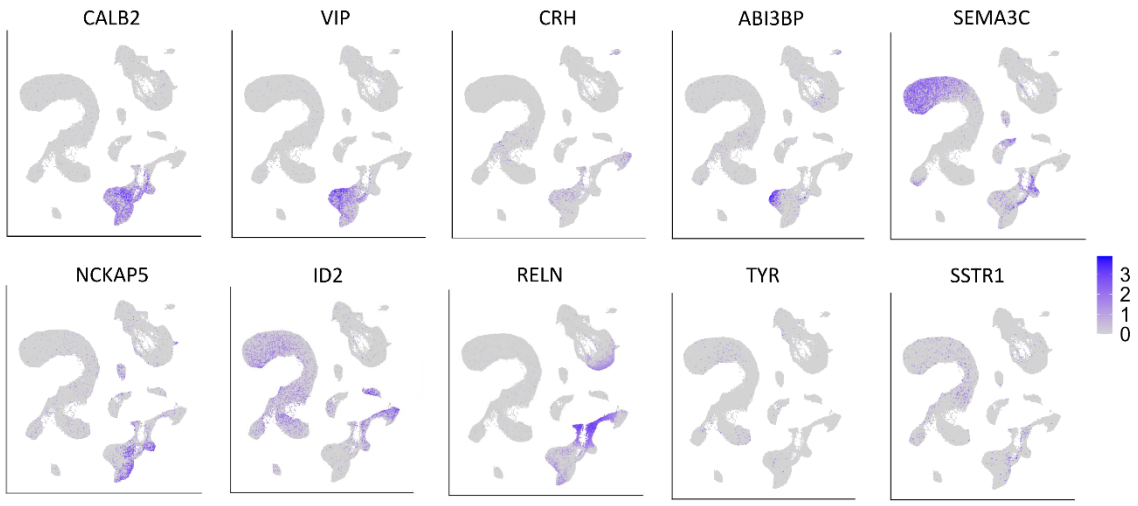

Figure 11. Gene expression plots depicting expression of markers for putative cortical VIP interneuron subtypes presented in [160]. *Full names of included marker genes can be found in the List of Abbreviations. Although these putative subclusters are intriguing, further in situ validation is necessary to confirm their existence as discrete cell types. Scale bar represents normalized gene expression. Unpublished supplementary figure derived from published, openly available data [160].*

Chandelier and basket ***PVALB*** cell types could be clearly identified based on additional *CRH/COL15A1* and *MEPE* expression, respectively (in line [161]). Within the ***SST*** cluster, upper-layer- and lower-layer-residing neurons could be identified based on *CALB1* and *NPY* expression, respectively, along with other potential subtypes. ***RELN*** cell types formed a bridge between ***VIP*** and ***ID2/rosehip*** clusters. *CCK* and *PAX6* expression identified putative CCK basket cells, some of which also expressed *CALB2* at low levels. Rosehip neurons could be identified based on *ID2*, *LAMP5*, *TRPC3* and *CHST9* expression [178, 161].

To explore the extent of within- and between-group heterogeneity, expression distance values were calculated via Pearson's linear correlation (for details, see [160]). Inter-sample expression distances were significantly higher in the SCH group compared to the CTR group ($p < 0.0001$), and when projecting expression distances into 2D space for visualization, CTR samples clustered together, while SCH appeared more scattered (see Figure 2/E–F in [160]) – as expected, based on the heterogenous manifestation characteristic of SCH. Some SCH samples aligned closer with CTR cases, while others were located farther, which is a pattern that has been also noted by others [161, 227].

4.2.2. Differentially expressed genes

Cell-type specific differentially expressed genes (DEGs) in SCH compared to CTR are listed in Supplementary Dataset Table 1 in [160] (available to download at https://zenodo.org/records/6921620). Nearly all cell types presented with a high number of DEGs however, only a fraction of them remained strongly significant after statistically correcting p-values for multiple testing ("*p.adj*" column). ***PVALB_CRH*** neurons (corresponding to PV chandelier cells), and certain ***SST*** subtypes presented with the highest proportion of highly expressed, significant DEGs. It should be noted that a number of significant DEGs were shared among both IN and EX cell types, for example *FP236383.1*, *C5orf17*, and *HES4* (known to be involved in early developmental processes based on the Gene Ontology database). *C5orf63*, *CRYAB* (which codes an anti-apoptotic, protective small heat shock protein B5; [256]) and *H1FX* (H1 histone family member X; involved in early developmental processes in mice [257]) were reported in several EX subtypes. In contrast, INs presented with more subtype-specific DEGs. For example, *ADARB2* was upregulated in several ***SST*** clusters, which is interesting, since those neurons are known to derive from the MGE and do not typically express *ADARB2* (see Figure 10). Ionotropic kainite glutamate receptors 3 and 4 (*GRIK3; GRIK4*), which play key roles in mediating excitatory neurotransmission crucial for both development and cognitive functioning, were upregulated in the chandelier ***PVALB*** cluster. Thrombospondin type 1 domain containing 7A (*THS7DA;* involved in endothelial cell migration and angiogenesis, [258]), EYA transcriptional coactivator and phosphatase 4 (*EYA4;* involved in cell proliferation and migration, reported to be upregulated in breast cancer [259]) and cadherin 9 (*CDH9;* involved in synaptogenesis and neurotransmission by mediating calcium-dependent cell-cell adhesion [260], also associated with autism spectrum disorder [261]) was downregulated, while heat shock protein family A member 1 (*HSP1A;* involved in proteostasis and protection under stress, previously associated with paranoid SCH [262, 263]) was upregulated in the ***SST_NPY*** cluster. Furthermore, semaphorin 3C (*SEMA3C;* crucial for the development of cortical interneurons [264]) and tubulin alpha 4a (*TUBA4A;* involved in cytoskeleton formation) were downregulated, while heat shock protein family B (small) member 1 (*HSPB1*) was upregulated in ***VIP*** clusters.

In addition to extracting DEGs in a data-driven approach, we also applied a more hypothesis-driven approach, directly testing a few clinically relevant, "interesting" transcripts (involved in GABAergic, glutamatergic, monoaminergic, or for example, oxytocinergic signalling; see Supplementary Figure 12/G in [160]). Intriguingly, oxytocin receptor mRNA (*OXTR*) was downregulated in SCH (p = 0.0168; n = 9 SCH/14 CTR; Wald test) in the ***SST_NPY*** subtype. The ***PVALB*** chandelier cluster showed significantly downregulated gamma-aminobutyric acid type A receptor subunit alpha1 (*GABRA1*) and glutamate ionotropic receptor NMDA type subunit 2A (*GRIN2A*) expression (p = 0.00573, p = 0.0446, respectively; n = 9 SCH/14 CTR; Wald test). Similarly, several ***SST*** subtypes also demonstrated lower levels of *GABRA1* mRNA, and a cholinergic neurotransmission-related gene, *CHRFAM7A* was markedly lower in SCH in both ***ID2*** and ***VIP*** subtypes, suggesting that its expression largely coincides with calretinin expression (Figure 12/A). This gene encodes the human-specific fusion protein CHRNA7–FAM7A [265], which has been previously associated with several psychiatric disorders [266].

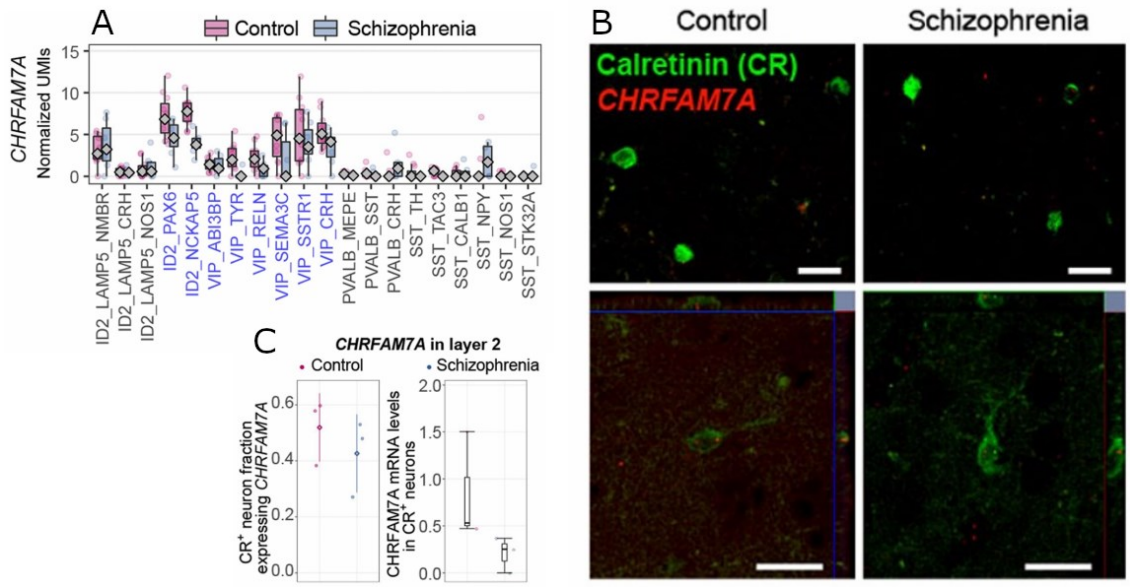

Figure 12. Validation of expression differences of CHRFAM7A between control (CTR) and schizophrenia (SCH) groups. A) *Normalized expression level of CHRFAM7A based on single nucleus RNA sequencing data (only main interneuron groups shown; UMI stands for unique molecular identifier). CHRFAM7A was mainly expressed by VIP/ID2 cell types, highlighted in blue.* ***B)*** *In situ validation of CHRFAM7A (red) being expressed in calretinin protein-expressing neurons (green), although at very low levels, which could be expected based on the low normalized expression levels, shown in panel A. Scale bars represent 20 µm.* ***C) Left:*** *Plot showing no prominent difference in the proportion of layer 2 calretinin neurons co-expressing*

CHRFAM7A mRNA in CTR and SCH DLPFC sections (n = 3/group). ***Right****: Plot showing markedly lower level of CHRFAM7A in layer 2 calretinin neurons of SCH cases (n = 3/group).*

We confirmed with RNAscope that *CHRFAM7A* is largely expressed by CR protein-expressing interneurons (Figure 12/B), and that the average expression level of *CHRFAM7A* in L2 CR neurons was lower in the SCH group by 77% (Figure 12/C), although *CHRFAM7A* signal was very low, making evaluation and statistical testing somewhat challenging.

4.2.3. Gene Ontology pathway analysis

To gain insight into the functional relevance of the significant DEGs, we performed pathway analyses utilizing the Gene Ontology Database. The complete list of cell type-specific GO terms can be found in Supplementary Dataset Table 2 and Supplementary Figures 10–11 in [160]. The most significantly **downregulated** pathways were associated to mitochondrial function (oxidative phosphorylation, mitochondrial ATP synthesis, and other processes linked to cellular respiration), translation, protein localization, and transmembrane transport (Figure 13/top panel). The cell types most strongly affected by such alterations belonged to ***VIP***, ***PVALB***, ***ID2***, and certain EX (***L4-5_FEZF2_LRRK1; L4_RORB_SCHLAP1_MET***) clusters (Figure 13/top panel). Notably, translation-associated pathways were downregulated in the ***VIP_SEMA3C*** and ***VIP_ABI3BP*** subclusters, belonging to traditional "CR interneurons" based on their *CALB2* expression. Furthermore, genes associated with synapse organization were specifically downregulated in SCH in the ***SST_NPY*** cell cluster. In contrast, the most significantly **upregulated** pathways were associated with neuronal transmission (regulating membrane potential and ion transport, synaptic signalling) and developmental processes, most prominently affecting EX ***L5-6_FEZF2_TLE4, L2_CUX2-LAMP5_PDGFD*** cell types, and the IN ***ID2_LAMP5_NOS1, PVALB_SST,*** and ***ID2_NCKAP5*** cell types (Figure 13/bottom panel).

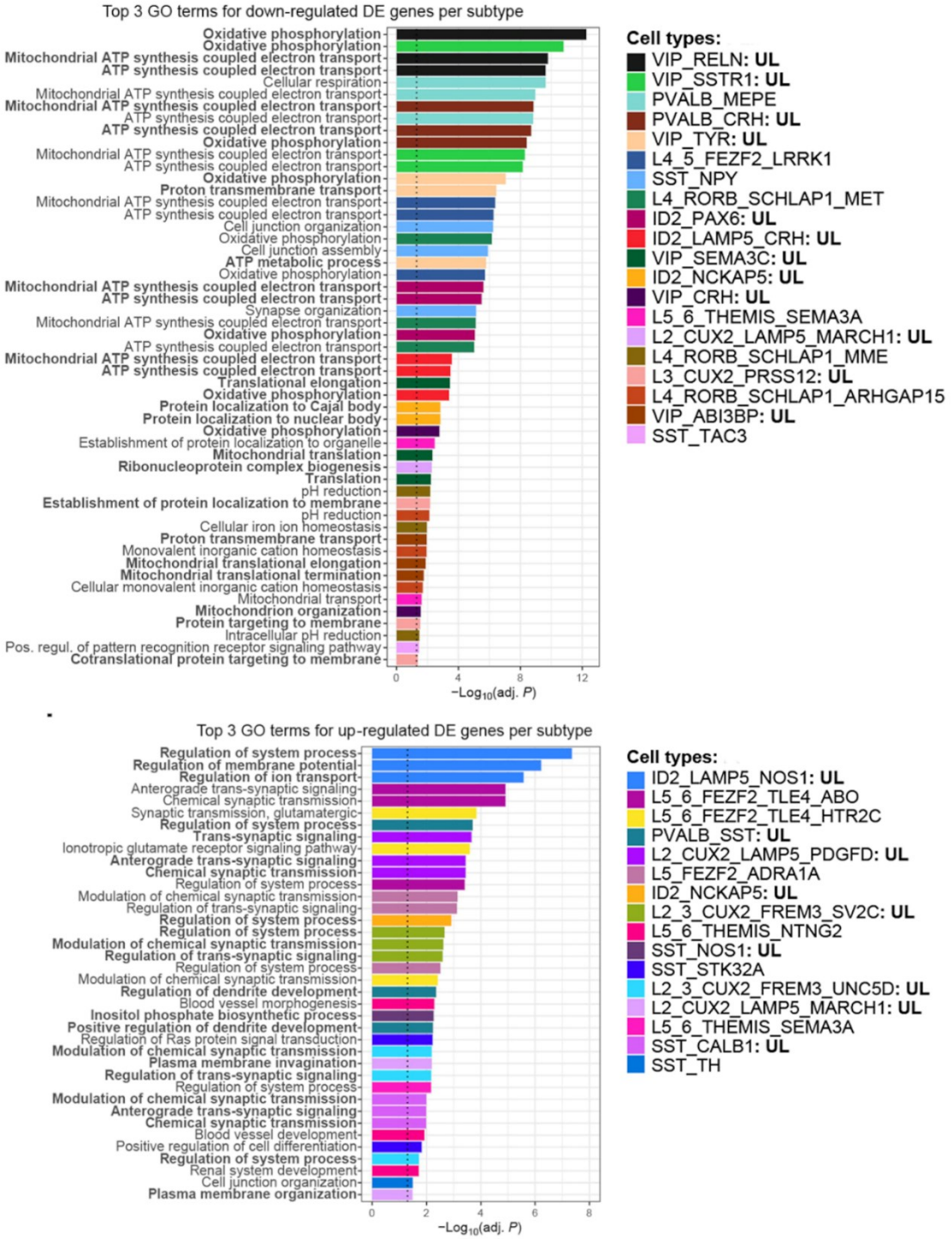

Figure 13. Functional interpretation of cell type-specific differentially expressed genes in SCH. *The x axis shows significancy (log-transformed for visual purposes); dotted line represents the significancy cutoff (p = 0.05 or lower after Bonferroni correction). Cell types are colour coded and listed on legends. Gene names can be found in the List of abbreviations. "UL" indicates upper-layer localization of given cell types based on Allen Brain Institute reference materials. Images from [160].*

These results suggest that many cell types, presumably organized in both local upper-layer and wider neuronal networks are affected transcriptionally in SCH, which is most probably central to the mechanisms and symptoms of the condition, although such results must be interpreted considering potential confounding and limiting factors. Although many cell types are widely affected, systematic, biologically meaningful patterns seem to emerge, which can aid our understanding of the dysfunction present in SCH and guide future pharmaceutical research.

4.2.4. Calretinin mRNA and protein expression in the DLFPC

While we observed significantly lower L2 CR interneuron density in our histological analysis, the average *CALB2* expression was not significantly different between groups according to snRNAseq data. Although we cannot directly compare IHC (visualizing cellular protein) and snRNAseq (capturing mRNA in the nucleus) results, this raised the possibility that CR neurons may be present in physiological density in SCH with a subset of them failing to produce detectable amounts of CR protein. To directly address this question, we simultaneously labelled CR protein and *CALB2* mRNA on a subset of cases (n = 5/group) from which we had both IHC and snRNAseq results (Figure 14/A). We categorized neurons based on expression pattern (high, low, or no protein expression together with high, low or no mRNA expression), demonstrated in Figure 14/1–5. Based on our hypothesis, we expected more neurons in the SCH cases that only express *CALB2* mRNA, but not (or only very low levels of) CR protein.

Further substantiating previous results, we observed lower proportion of "high protein, high mRNA" expressing neurons in SCH (Figure 14/right–1; $p < 0.0001$; n = 5/group; LMM with post hoc multiple comparison). In support of our hypothesis, we also revealed higher proportion of "low protein, high mRNA" expressing neurons (Figure 14/right–2; $p < 0.05$; n = 5/group; LMM with post hoc multiple comparison) and higher proportion of "no protein, only mRNA" expressing neurons in SCH (Figure 14/right–3; $p < 0.001$; n = 5/group; LMM with post hoc multiple comparison). These preliminary results support the notion that a subset of cortical CR interneurons may fail to express detectable levels of CR protein in SCH. We aim to expand the sample number up to n = 10/group and carry out layer-specific annotation to gain more robust statistical results.

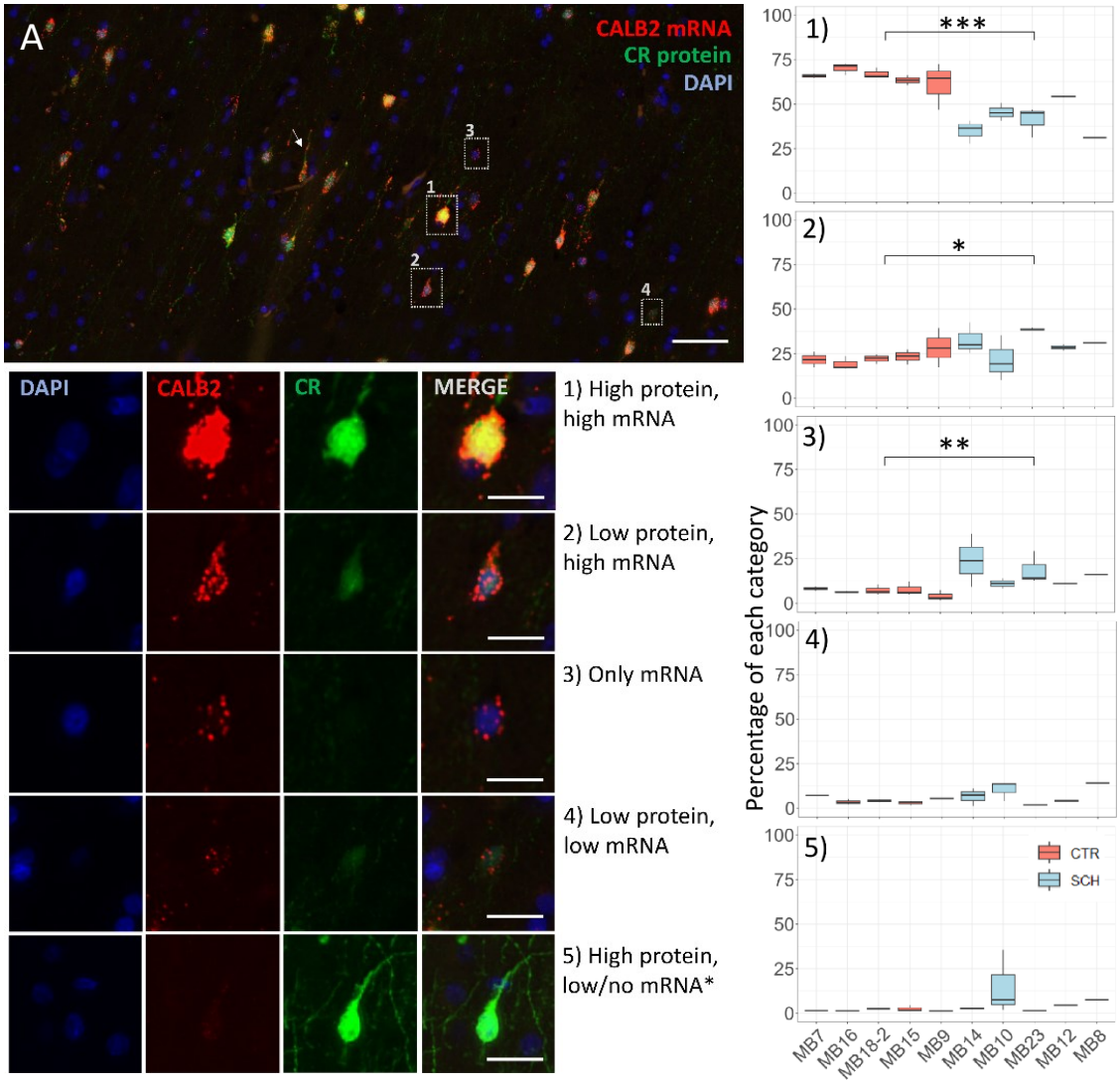

Figure 14. Patterns of calretinin mRNA and protein expression in the dorsolateral prefrontal cortex in control and schizophrenia cases. Left: *A) Representative images of CR protein (green) and CALB2 mRNA (red) co-detection from a control case (scale bar represents 100 μm) and annotation categories based on expression patterns (1–5; scale bars represent 20 μm). On panel A, note that calretinin mRNA is widely present in neuronal processes too (white arrow). The 5. category "High protein–low/no mRNA" was very rare, only present in relevant numbers in case MB10.* ***Right:*** *Boxplots showing statistical evaluation of the percentage of respective categories (1–5; * represents adjusted $p < 0.05$; ** represents adjusted $p < 0.001$; *** represents adjusted $p < 0.0001$).*

5. Discussion

During my doctoral research we revealed lower calretinin neuron density in the caudate nucleus and the second layer of the dorsolateral prefrontal cortex. Furthermore, we identified cell type-specific differentially expressed genes with single nucleus RNA sequencing, suggesting network-wide functional disturbances. Although CR interneurons have not been in the focus of SCH research, the gene encoding CR (*CALB2*) has been identified as a candidate locus by a meta-analysis of genome-wide association studies [267]. Moreover, interneurons, including CR interneurons, have been implicated in SCH-related neurodevelopmental disruption in organoid models derived from SCH patient-specific induced pluripotent stem cells (iPSCs) [268, 60], underscoring the need for further investigating this neuron population.

We detected lower density of CR interneurons in the caudate nucleus in SCH. The only previous histological assessments of striatal interneurons in SCH revealed lower density of large cholinergic neurons [113, 119] in the ventral striatum. A substantial proportion of striatal large cholinergic neurons co-express CR (109, 113, 269). However, in our dataset, the observed difference was driven by the significantly lower density of small CR interneurons, while medium and large subtype densities did not differ significantly between groups. The difference was not influenced by known confounding factors such as age, sex, or post-mortem interval. The total analysed area was substantially larger in our study (~10 cm^2) than in the case of Holt and colleagues (~2 cm^2; [113]), perhaps making it more representative. Since CR neurons are among the most abundant interneuron types in the human striatum, they are important modulators of striatal activity and output. Therefore, the lower density of functional CR neurons could directly impact fronto-striatal function in SCH [112]. Measuring the density of CR interneurons in the putamen of the same cases as presented here, Kelmer and colleagues revealed similar patterns of significantly lower density of small CR interneurons [270], while medium spiny neuron density was found unaltered. These results may suggest that small striatal CR interneurons are generally affected in SCH. The consequently impaired local inhibition and calcium buffering could even be directly associated with the overactivated state of the striatum, a well-established feature of SCH.

We also detected lower CR interneuron density in the DLPFC (*published*: n = 10 SCH/ 10 CTR [160]; *unpublished*: n = 15 SCH/15 CTR). This difference was driven by markedly lower density in a subset of cases (~ 50%). To minimize the confounding effect of biological and technical variables, we matched SCH and CTR cases as closely as possible for PMI, age, and gender, in this order of importance, because in our experience, PMI has the strongest confounding effect on neuronal density [160]. Lower cortical CR neuron density was not significantly affected by PMI, age or gender based on visual and statistical evaluation. Furthermore, every brain bank was represented in the lower–CR group. The involvement of CR neurons in SCH is intriguing because according to Hladnik and colleagues, this neuron class became the dominant GABAergic population in the PFC during primate evolution: in rodents, CR neurons represent 2-3% of all neurons, while in the monkey and human prefrontal cortex their proportion can extend to 15% of all neurons [271]. Our preliminary results of simultaneous staining of CR mRNA and protein support the hypothesis that cortical CR neurons are not lost in SCH, but the expression of CR protein is lower or lacking in a subset of neurons. This could be more reliably assessed by using SCH-independent markers of CR neurons; however, as the transcriptomic studies revealed, "CR interneurons" represent a heterogenous neuronal population, with no obvious, selective marker described yet. Using developmental markers can be applied in the case of SST/PV neurons, as they selectively express SOX6 for example [201]; however, CR neurons share most of their known developmental markers with other CGE-derived populations such as neurogliaform neurons and rosehip neurons – furthermore, it is unclear whether the expression of *LHX6* or other such markers is unchanged in SCH.

Why haven't previous studies detected lower CR density in the DLPFC? To my knowledge, 18 post-mortem human studies employed immunohistochemistry or in situ mRNA hybridization to assess dorsolateral prefrontal cortical interneuron density in SCH, of which only 9 included CR neurons [202–211] and none of them revealed well-supported significant differences. **Daviss and Lewis** [202] analysed 5 SCH and 5 matched CTR case pairs, and measured neuronal density in the DLPFC using 40 μm thick free-floating sections. Although the overall result did not reveal significant differences in CR neuron density, the case-wise density plots generously included by the authors show that 2 cases out of 5 demonstrated markedly lower density, and 3 had density values similar to their control pairs. This notion is extremely important, as it highlights the need

for individual evaluation, and corroborates our observation that only a subset of cases may demonstrate lower CR neuron density. Low sample number greatly limits this study. **Reynolds and Beasley** [203] measured CR and PV neuron density in 18 SCH and 22 CTR cases focusing on the Ba10. The authors report significantly decreased PV neuron density in cortical layers III and IV along with unaltered CR neuron density. However, the study did not include individual results, only group averages. When within-group heterogeneity is so high (as stated in the article), presenting only group averages is insufficient: even if 30-50% cases present with low neuron density, that can be easily masked in the group average by the other cases with CTR-like density values. Furthermore, information regarding PMI was missing in 11 cases, hindering the evaluation of confounding effects. In our analysis, we found that PMI strongly affects cortical PV neuron density (or more likely, protein detectability; [173, 201]). **Beasley and Reynolds** [204] measured the density of PV, CB, and CR interneurons in the Ba9 of 15 SCH and 15 CTR cases. The authors reported significantly lower density of PV neurons in layer III with a p-value of 0.049, and of CB neurons in layers II, III, and IV ($p = 0.004$, 0.026, 0.031, respectively). However, both PMI and time spent in fixative was markedly higher in the SCH group. Interestingly, when checking correlations between neuronal density and PMI, the authors applied an alpha of 10% in contrast with the usually applied 5% (which they did apply when evaluating neuronal densities). **Reynolds and Beasley** [205] investigated the Ba46 of the same cases, and detected lower PV neuron density with a similar approach. Here, the authors found both CR and CB neuron density as unaltered. **Tooney and Cahl** [207] measured PV, CR, and CB neuronal density in 6 SCH and 6 CTR cases within the Ba9 and found no significant differences. Although presenting group averages on barplots for 6 cases is not very informative, their results suggest non-significantly higher PV neuron density in SCH. Investigating 7 SCH and 5 CTR cases, **Sakai and colleagues** [208] found no significant overall difference in the density of PV, CB, or CR interneurons. However, they showed significant secondary results, such as lower layer 2 CB and layer 6 PV neuron density ($p = 0.0007$; $p = 0.031$, respectively) through somewhat complicated, estimation-based techniques. This is the only study where the authors classified cortical PV, CR, and CB neurons into “medium” and “large” morphological subtypes, which has no clear neuroanatomical basis to our knowledge, but it did complicate statistical evaluation, which furthermore did not account for multiple

comparison. Demographic data were presented only as group averages and notably, information regarding PMI was missing. **Chung and colleagues** [211] applied multiplex fluorescent in situ hybridization and immune co-detection to quantify excitatory synapses (identified by VGLUT-1 and PSD95-positivity) on the surface areas of CR and PV interneurons in the Ba9 of 20 SCH and 20 matched CTR cases. The authors reported 18% lower mean density of VGLUT1+/PSD95+ spots on PV-expressing neurons in SCH. This was not influenced by confounding factors, and the same patterns was not present in monkeys chronically exposed to haloperidol. Similar pattern was not present in CR-immunoreactive neurons, suggesting that CR interneurons receive physiological amounts of excitatory synapses in SCH. Thus, the authors provided evidence for selectively deficient excitatory drive on PV neurons in the Ba9. **Fung and colleagues** [210] applied multiplex fluorescent in situ hybridization and western blot analyses on a large cohort (37 SCH, 37 CTR) to assess the levels of several interneuron markers in the DLPFC during development and in SCH. The authors found it challenging to decide whether to exclude outliers, therefore presented results both with and without outliers. *CALB2* mRNA was lower in the SCH group when the authors excluded outlier cases, but significancy was lost when outliers were included. Western blot analysis showed no significant difference in CR protein content between groups (importantly, this method may not be able to detect subtle layer-specific differences). Still, the authors report an intriguing pattern possibly contradicting our results. **Hashimoto and colleagues** reported that *PVALB*, but not *CALB2* mRNA levels were lower in SCH compared to the CTR group [206, 209]. Strictly speaking, the last 4 studies may not be directly relevant since they did not assess neuronal density. However, the last two studies [206, 209] support our observation of no significant difference in *CALB2* gene expression levels between CTR and SCH group in snRNAseq data.

In conclusion, although several post-mortem studies quantified CR neuron density in the human DLPFC, most of them dismissed possible within-group patterns, and presented results as group averages. This may be a possible explanation of why none of the previous studies detected lower CR neuron density. Another interesting reason which could contribute to this may be the inhomogeneous distribution of CR interneurons even in samples from neurotypical control donors. The fewer and narrower the ROIs are, the less representative the measured densities will be. The range of applied cortical traverses in

the aforementioned studies varied from 250 to 1000 μm. The number of ROIs per slide varied from to 2 to 10. Although this may seem like nit-picking, results would be better comparable if the ROI sampling method would be more standardized. Interestingly, building on early observations noting abnormal cytoarchitectural patterns in the entorhinal cortex in SCH [272], Arnold and colleagues spatially analysed Nissl-stained sections (via "point-pattern analysis") from the same region in SCH [273, 274], and found increased disorganization and "dead space" around layer 2 neurons, suggesting abnormal distribution of neurons. In our analyses, mapping the density and distribution of CR neurons as heatmaps also indicated potential disruption in the distribution of this neuron type in SCH. This notion could be further tested with cluster analysis approaches, which we aim to carry out in the future. Machine learning-based object detection algorithms can be expected to upscale and reshape the field of histology. With the aid of trained, standard algorithms, scientists are already able to process sections at a much larger scale with measurable error rates [214]. With this, it becomes possible to think and reveal patterns at a much larger scale, and, so to say, think outside the ROIs.

In both brain regions, the observed lower density of CR neurons could have several explanations. It could result from the lower levels of CR protein without the loss of neurons, suggesting potential disruption of transcription and/or translation. Supporting this hypothesis, microRNA – crucial regulators of transcription and translation [275] – have been implicated in SCH [276]. However, the observed pattern could also be associated with lower density of CR neurons present in the tissue. For example, developmental disturbances may lead to fewer CR neurons maturing and integrating successfully into the circuitry. In support of this hypothesis, patient-derived cerebral organoid models showed altered CR neuron morphology, connectivity, and density in the SCH group [268], while patient-derived ventral forebrain organoids revealed pathologically accelerated maturation of inhibitory neurons in the SCH group [60]. In addition, even if physiological numbers of CR neurons integrate into the circuitry during development, the lower level of CR protein could disrupt intracellular calcium-buffering, which may eventually lead to neuronal degeneration on the long term [277]. Decreased CR protein expression could also be, hypothetically, an active neuronal response to certain stimuli; an adaptation to pathological conditions present in the schizophrenic brain [168]. A handful of interesting studies showed that the expression of SST and CR is

directly linked to neuronal activity in the maturing hippocampus (in rat slices; [278, 279]). This could also be a highly relevant factor in the case of SCH, especially during the development and maturation of cortical circuits.

Applying single nucleus RNA sequencing on CTR and SCH DLPFC samples pinpointed a hub of network-level dysfunction in the upper cortical layers involving both inhibitory and excitatory subtypes [160]. Both populations demonstrated substantial transcriptomic burden. Interestingly, such patterns were not confirmed by Ruzicka and colleagues on a larger cohort of samples, where the majority of DEGs were associated with excitatory neurons (many previously identified as candidate genes in genetic studies, such as *SHANK2* and *NRXN3*). In contrast with our results, interneuron subtypes demonstrated low levels of disturbance compared to excitatory cell types [161]. At this point it is difficult to interpret these differences. Importantly, both studies highlighted that SCH DEGs are targets of transcription factors already identified as SCH risk genes, and pinpointed cell-type specific differential expression of high-confidence SCH risk genes [280]. It would be interesting to integrate the data from both studies and focus on individual heterogeneity and potential cellular–molecular phenotypes present in SCH.

In our study, the top upregulated biological pathways involved neurotransmission and neurodevelopmental processes primarily in excitatory cell types, while downregulated biological pathways included energy metabolism in ***PVALB*** and ***VIP*** cell types, translation within the ***VIP*** group (which could potentially be associated with cellular metabolic disturbance), and synapse organization in the ***SST-NPY*** subtype. Although this is usually not in the spotlight of attention, a series of studies have suggested abnormal energy metabolism and oxidative stress as central features of SCH [281]. For example, the levels of glutathione, an important intracellular antioxidant have been reported significantly lower in both in vivo and post-mortem experiments [282, 283]. Knockout mice with impaired glutathione synthesis demonstrate high oxidative stress and interestingly, reduced PV immunoreactivity and reductions in PV-dependent neuronal oscillations [284]. Accordingly, some studies reported that additional antioxidant treatments have been successful in improving negative and cognitive symptoms SCH patients [285], although other studies have not been able to confirm this [281]. It may be the case that antioxidant treatment is most effective before disease onset, during critical neurodevelopmental periods [281]. However, brain energy metabolism is also impacted

by antipsychotic medications; an effect often challenging to separate from the effect of SCH itself.

Post-mortem human SCH research faces several important limitations. One of the most important general limitations is the effect of post-mortem interval; the biochemical changes that occur in the brain tissue after death and before fixation – along with pH changes, gene expression changes, protein and RNA degradation, etc. The method of fixation has also been shown to impact neuronal density (in the case of hippocampal CR neurons [286]). Interestingly, we did not reveal clear correlation between post mortem interval and striatal or cortical CR neuron density, even though the PMI ranged from 4.75 to over 50 hours. This may suggest that certain CR interneuron populations are differently vulnerable to PMI. It may also be the case that CR protein degrades very fast in a subset of CR neurons and/or a subset of CR neurons degenerate very early after death, in the first 2-4 hours. Such vulnerability of CR neurons has been shown in the rat hippocampus following ischemia [287]). If this were the case, the samples included in our project may all be impacted by this early degeneration. Further experiments are necessary to clarify this question regarding the striatum and the DLPFC, involving control cases with very low (2-4 hours) and higher (over 8 hours) PMI; as demonstrated exemplarily on human hippocampus samples by Tóth and colleagues [288]). Most importantly, one must closely match control and diagnostic cases regarding fixation type, PMI, age, and sex to mitigate the potential confounding effects of these variables [201]. Another challenging limitation is the complex local and global effect of long-term antipsychotic medication on brain structure and chemistry [289]. For example, basal ganglia volume has been proposed to be positively correlated with antipsychotic medication [290, 123], and some studies reported that medication-naïve patients had lower-than-average caudate nucleus volume, which was normalized by antipsychotic treatment [122]. Our analysis of CN cross-sectional areas (including 1 medication-naïve case) did not reveal differences between SCH and CTR cases. Antipsychotics are also known to impact fundamental cellular–molecular functions in the brain, such as glucose metabolism [291], neurotransmission, and many other aspects [292]. Reliably separating the effects of antipsychotics from those of SCH itself remains challenging due to the scarcity of samples from medication-naïve SCH patients and the complex mechanisms involved [289]. In our snRNAseq study [160], our collaborating partners compared our data to human bulk RNA-seq data [293] and

clozapine/haloperidol-treated rhesus macaque [294] bulk DLPFC data to assess the potential effects of antipsychotics. Comparing the human antipsychotic–associated DEGs and macaque drug treatment–associated DEGs with the DEGs identified in our study resulted in only a small overlap. This indicated that the majority of DEGs found were likely not associated with antipsychotic treatment. Ruzicka and colleagues reported similar observations [161].

Another frequent and significant limitation is the inconsistent availability of autopsy reports and medical history from brain banks. This can complicate the reliable assessment of potential confounding factors (e.g., cerebrospinal fluid pH, substance use, duration and nature of antipsychotic treatment), and restrict the investigation of potential correlations (e.g., age of onset, SCH "subtype", symptomatology, and social environment). In the current state of our project with 15 SCH cases involved, we have some level of detail regarding the SCH diagnosis in 12 cases. Of these, paranoid SCH was noted in 7 cases, uncategorized chronic defect state was noted in 2 cases, while no such detail was noted in the other 3 cases, however, those were additionally diagnosed with various disorders including schizoaffective syndrome, bipolar disorder, obsessive-compulsive disorder, and depression. No pattern could be seen regarding CR neuron density and paranoid SCH diagnosis. The one completely medication-naïve case included in our study also demonstrated markedly lower CN and layer 2 DLPFC CR neuron density, suggesting that the phenomenon cannot be solely attributable to antipsychotic treatment. Cerebrospinal fluid pH values are known in 6 cases, from which no pattern could be seen regarding CR neuron density. A critical documentation gap is the frequently missing data regarding the hemisphere from which tissue blocks were taken, introducing an unknown confounding factor, particularly in light of the known functional lateralization of the DLPFC [295, 296]. This is a rarely discussed, potentially significant factor in post-mortem SCH research, as in vivo studies indicate abnormal, or lack of such lateralization in SCH patients [297–299]. Additionally, interhemispheric differences on the cellular level have been shown, such as lower Betz cell density in the right primary motor cortices of patients with SCH [300]. The scarcity and heterogeneity of documentation is unfortunate but not unique to our study, and represents a major limitation and challenge in post-mortem brain research.

In conclusion, our findings indicate the involvement of CR-expressing neurons – or more precisely, the expression of CR protein – in SCH, and reinforce the importance of considering both individual and within-group heterogeneity in SCH research. CR interneurons represent a particularly intriguing target due to their unique evolutionary trajectory and functional role in cortical and striatal circuits. By combining insights from multi-omics, advanced histology, and patient-derived organoid models, future research focusing on interneurons may uncover new biomarkers and specific therapeutic targets, ultimately improving outcomes for patients with SCH and better understanding the mechanisms causing SCH.

6. Conclusions

The presented results suggest that both cortical and striatal calretinin interneurons may be functionally disturbed in schizophrenia.

A) In the caudate nucleus, the lower density of small, calretinin-expressing neurons presumably affects local calcium homeostasis, synaptic signalling, and local inhibition. Altogether these are expected to impact striatal activity and output, and may directly contribute to the disrupted fronto-striatal function in SCH.

B) In the dorsolateral prefrontal cortex, calretinin neurons showed significantly lower density in layer 2 in SCH. However, this was only present in 50% of SCH cases. This, in line with other studies, highlights the importance of within-group heterogeneity in SCH. Since calretinin neurons have been shown to demonstrate disturbed maturation and integration into the circuitry in patient-derived cerebral organoids, it is imperative to further study their potential developmental disturbance in SCH. Our preliminary results suggest that these neurons are present in SCH, but a subset of them fail to express detectable levels of calretinin protein.

C) Single nucleus RNA sequencing confirmed that many, primarily upper-layer residing neuron subtypes are disturbed in the DLPFC in SCH, with energy metabolism-related pathways primarily downregulated in GABAergic interneurons and neurotransmission-related pathways primarily upregulated in excitatory cell types.

Together, our results suggest that calretinin protein expression is affected in SCH, which could contribute to disrupted neurotransmission. Today, the integration of multi-omic approaches and advanced histological techniques allows for a more comprehensive analyses of cellular subtypes both in neurotypical control tissue and in complex conditions such as SCH. Revealing and targeting disturbed molecular pathways may help restore cellular homeostasis in vulnerable neuron populations. However, it must be noted that discovering and validating the cellular and molecular composition of neurotypical control tissue is of equal importance, as without understanding the healthy brain, we cannot comprehend the disturbances detected in disease.

7. Summary

Schizophrenia (SCH) is a devastating neuropsychiatric disorder with poorly understood etiology. Despite extensive research, literature regarding underlying cell-type-specific alterations in SCH remains controversial. Here, we applied quantitative immunohistochemistry to measure the relative density of certain cell types in the dorsolateral prefrontal cortex (DLPFC) and the caudate nucleus (CN); single nucleus RNA sequencing to measure cell type specific gene expression in the DLPFC; and in situ mRNA hybridization to validate differentially expressed genes and further examine protein- and mRNA expression patterns in the DLPFC.

The density of calretinin-expressing interneurons was lower in the caudate nucleus and in cortical layer 2 of the DLPFC, which was not influenced by known confounder factors. Single nucleus RNA sequencing conducted on a sample cohort overlapping with the cohort used for histology revealed network-level dysfunction in various excitatory and inhibitory cell types mostly localized to upper cortical layers. Cell types demonstrating the most profound disturbance involved transcriptomic subtypes of somatostatin, parvalbumin, and calretinin inhibitory neurons, and various excitatory neuron types. Pathway analyses of differentially expressed genes suggested disturbance in energy metabolism, protein biogenesis and localization primarily in inhibitory interneurons, while genes disturbed in excitatory neurons types were rather associated with neurotransmission- and development-related pathways.

Because the sequencing did not reveal significantly lower calretinin mRNA levels in SCH, we applied in situ mRNA hybridization with immune co-detection to simoultaneously assess CR protein and mRNA levels (n = 5 CTR/5 SCH). The results indicated disrupted calretinin protein translation in SCH, with a higher proportion of neurons expressing calretinin mRNA without the protein.

Together, our results suggest that calretinin protein expression is affected in SCH, which, seeing its important role in calcium buffering and calcium signalling, could contribute to disrupted neurotransmission. The presented evidence is intriguing, albeit modest: it underlines the need for better understanding of the neurochemical and functional properties of human cortical and striatal calretinin interneurons in both healthy and pathological conditions.

8. References

1. Bromet EJ, Fennig S. Epidemiology and natural history of schizophrenia. *Biol Psychiatry* 1999;46:871–81.
2. GBD 2017 Disease and Injury Incidence and Prevalence Collaborators, Global, regional, and national incidence, prevalence, and years lived with disability for 354 Diseases and Injuries for 195 countries and territories, 1990–2017: A systematic analysis for the Global Burden of Disease Study 2017. *Lancet* 2018; 392, 1789–1858.
3. Sullivan PF, Kendler KS, Neale MC. Schizophrenia as a complex trait: evidence from a meta-analysis of twin studies. *Arch Gen Psychiatry*. 2003;60:1187–92.
4. Owen MJ, Legge SE, Rees E, Walters JTR, O'Donovan MC. Genomic findings in schizophrenia and their implications. *Mol Psychiatry* 2023;28:3638–47.
5. Tao Y, Zhao R, Yang B, Han J, Li Y. Dissecting the shared genetic landscape of anxiety, depression, and schizophrenia. *J Transl Med* 2024;22:373.
6. McCutcheon RA, Marques RT, Howes OD. Schizophrenia—An Overview. *JAMA Psychiatry* 2020;77:201.
7. Green MF, Nuechterlein KH, Gold JM, Barch DM, Cohen J, Essock S, Fenton FS, Frese F, Goldberg TE, Heaton RK, Keefe RSE, Kern RS, Kraemer H, Stover E, Weinberger DR, Zalcman S, Marder SR. Approaching a consensus cognitive battery for clinical trials in schizophrenia: The NIMH-MATRICS conference to select cognitive domains and test criteria. *Biol Psychiatry* 2004;56:301–7.
8. Lesh TA, Niendam TA, Minzenberg MJ, Carter CS. Cognitive Control Deficits in Schizophrenia: Mechanisms and Meaning. *Neuropsychopharmacology* 2011;36:316–38.
9. Heinrichs RW. The Primacy of Cognition in Schizophrenia. *Am Psychol* 2005;60:229–42.
10. Kahn RS, Keefe RSE. Schizophrenia Is a Cognitive Illness: Time for a Change in Focus. *JAMA Psychiatry* 2013;70:1107.
11. Bosia M, Bechi M, Bosinelli F, Politi E, Buonocore M, Spangaro M, Bianchi L, Cocchi F, Guglielmino C, Cavallaro R. From cognitive and clinical substrates to functional profiles: Disentangling heterogeneity in schizophrenia. *Psychiatry Research* 2019;271:446–53.

12. Schmitt A, Falkai P, Papiol S. Neurodevelopmental disturbances in schizophrenia: evidence from genetic and environmental factors. *J Neural Transm* 2023;130:195–205.
13. Lieberman JA. Neurobiology and the Natural History of Schizophrenia. *J Clin Psychiatry* 2006;67:e11.
14. Spear LP. The adolescent brain and age-related behavioral manifestations. *Neurosci Biobehav Rev* 2000;24:417–63.
15. Andersen SL. Trajectories of brain development: point of vulnerability or window of opportunity? *Neurosci & Biobehav Rev* 2003;27:3–18.
16. Lipska B. To model a psychiatric disorder in animals: schizophrenia as a reality test. *Neuropsychopharmacology* 2000;23:223–39.
17. Nakamura T, Takata A. The molecular pathology of schizophrenia: an overview of existing knowledge and new directions for future research. *Mol Psychiatry* 2023;28:1868–89.
18. Tandon R, Nasrallah H, Akbarian S, Carpenter WT, DeLisi LE, Gaebel W, Green MF, Gur RE, Heckers S, Kane JM, Malaspina D, Meyer-Lindenberg A, Murray R, Owen M, Smoller JW, Yassin W, Keshavan M. The schizophrenia syndrome, circa 2024: What we know and how that informs its nature. *Schizophrenia Research* 2024;264:1–28.
19. Jablensky A. The diagnostic concept of schizophrenia: its history, evolution, and future prospects. *Dialogues Clin Neurosci* 2010;12:271–87.
20. Fujihara K. Beyond the γ-aminobutyric acid hypothesis of schizophrenia. *Front Cell Neurosci* 2023;17:1161608.
21. Kraepelin E. Dementia Praecox and Paraphrenia. Edinburgh: Livingstone; 1919.
22. Abi-Dargham A. Recent evidence for dopamine abnormalities in schizophrenia. *Eur Psychiatr* 2002;17:341s–7s.
23. Abi-Dargham A, Rodenhiser J, Printz D, Zea-Ponce Y, Gil R, Kegeles LS, Weiss R, Cooper TB, Mann JJ, Van Heertum RL, Gorman JM, Laruelle M. Increased baseline occupancy of D_2 receptors by dopamine in schizophrenia. *Proc Natl Acad Sci USA* 2000;97:8104–9.
24. Lewis DA. Cortical circuit dysfunction and cognitive deficits in schizophrenia – implications for preemptive interventions. *Eur J of Neuroscience* 2012;35:1871–8.

25. Gao R, Penzes P. Common mechanisms of excitatory and inhibitory imbalance in schizophrenia and autism spectrum disorders. *Curr Mol Med.* 2015;15(2):146-67.
26. Laborit H, Huguenard P, Alluaume R. Un nouveau stabilisateur végétatif; le 4560 RP [A new vegetative stabilizer; 4560 R.P.]. *Presse Med* 1952;13;60(10):206-8.
27. Carlsson A, Lindqvist M. Effect of Chlorpromazine or Haloperidol on Formation of 3-Methoxytyramine and Normetanephrine in Mouse Brain. *Acta Pharmacol et Toxicol* 1963;20:140–4.
28. Creese I, Burt DR, Snyder SH. Dopamine Receptor Binding Predicts Clinical and Pharmacological Potencies of Antischizophrenic Drugs. *Science* 1976;192:481–3.
29. Johnstone EC, Frith CD, Crow TJ, Carney MWP, Price JS. Mechanism of the antipsychotic effect in the treatment of acute schizophrenia. *Lancet* 1978;311:848–51.
30. Snyder SH. The dopamine hypothesis of schizophrenia: focus on the dopamine receptor. *Am J Psychiatry.* 1976;133(2):197-202.
31. Davis KL, Kahn RS, Ko G, Davidson M. Dopamine in schizophrenia: a review and reconceptualization. *Am J Psychiatry.* 1991 Nov;148(11):1474-86.
32. Knable MB, Weinberger DR. Dopamine, the prefrontal cortex and schizophrenia. *J Psychopharmacol* 1997;11:123–31.
33. Goldman-Rakic PS, Muly EC 3rd, Williams GV. D(1) receptors in prefrontal cells and circuits. *Brain Res Brain Res Rev.* 2000 Mar;31(2-3):295-301.
34. Pycock CJ, Kerwin RW, Carter CJ. Effect of lesion of cortical dopamine terminals on subcortical dopamine receptors in rats. *Nature* 1980;286:74–7.
35. Jaskiw GE, Karoum FK, Weinberger DR. Persistent elevations in dopamine and its metabolites in the nucleus accumbens after mild subchronic stress in rats with ibotenic acid lesions of the medial prefrontal cortex. *Brain Research* 1990;534:321–3.
36. Weinberger DR. Implications of Normal Brain Development for the Pathogenesis of Schizophrenia. *Arch Gen Psychiatry* 1987;44:660.
37. Weinberger DR. Physiological Dysfunction of Dorsolateral Prefrontal Cortex in Schizophrenia: III. A New Cohort and Evidence for a Monoaminergic Mechanism. *Arch Gen Psychiatry* 1988;45:609.

38. Deutch AY. The regulation of subcortical dopamine systems by the prefrontal cortex: interactions of central dopamine systems and the pathogenesis of schizophrenia. In: Tuma AH, Stricker EM, Gershon S, editors. Advances in Neuroscience and Schizophrenia, Vienna: Springer Vienna; 1992, p. 61–89.
39. Grace AA. Cortical regulation of subcortical dopamine systems and its possible relevance to schizophrenia. *J Neural Transmission* 1993;91:111–34.
40. Meyer-Lindenberg A, Straub RE, Lipska BK, Verchinski BA, Goldberg T, Callicott JH, Egan MF, Huffaker SS, Mattay VS, Kolachana B, Kleinman JE, Weinberger DR. Genetic evidence implicating DARPP-32 in human frontostriatal structure, function, and cognition. *J Clin Invest* 2007;117:672–82.
41. Weinberger DR. Physiologic Dysfunction of Dorsolateral Prefrontal Cortex in Schizophrenia: I. Regional Cerebral Blood Flow Evidence. *Arch Gen Psychiatry* 1986;43:114.
42. Howes OD, Kapur S. The dopamine hypothesis of schizophrenia: version iii--the final common pathway. *Schizophr Bull* 2009;35:549–62.
43. Laruelle M. Dopamine Transmission in the Schizophrenic Brain. In: Hirsch SR, Weinberger DR, editors. Schizophrenia. 1st ed., Wiley; 2003, p. 365–87.
44. Sohal VS, Rubenstein JLR. Excitation-inhibition balance as a framework for investigating mechanisms in neuropsychiatric disorders. *Mol Psychiatry* 2019;24:1248–57.
45. Clark SD. The Role of Dynorphin and the Kappa Opioid Receptor in Schizophrenia and Major Depressive Disorder: A Translational Approach. In: Liu-Chen L-Y, Inan S, editors. The Kappa Opioid Receptor, vol. 271, Cham: Springer International Publishing; 2020, p. 525–46.
46. Buck SA, Quincy Erickson-Oberg M, Logan RW, Freyberg Z. Relevance of interactions between dopamine and glutamate neurotransmission in schizophrenia. *Mol Psychiatry* 2022;27:3583–91.
47. Dean B, Bakker G, Ueda HR, Tobin AB, Brown A, Kanaan RAA. A growing understanding of the role of muscarinic receptors in the molecular pathology and treatment of schizophrenia. *Front Cell Neurosci* 2023;17:1124333.

48. Trépanier MO, Hopperton KE, Mizrahi R, Mechawar N, Bazinet RP. Postmortem evidence of cerebral inflammation in schizophrenia: a systematic review. *Mol Psychiatry* 2016;21:1009–26.
49. Zhuo C, Tian H, Song X, Jiang D, Chen G, Cai Z, Ping J, Cheng L, Zhou C, Chen C. Microglia and cognitive impairment in schizophrenia: translating scientific progress into novel therapeutic interventions. *Schizophrenia* 2023;9:42.
50. Sellgren CM, Gracias J, Watmuff B, Biag JD, Thanos JM, Whittredge PB, Fu T, Worringer K, Brown HE, Wang J, Kaykas A, Karmacharya R, Goold CP, Sheridan SD, Perlis RH. Increased synapse elimination by microglia in schizophrenia patient-derived models of synaptic pruning. *Nat Neurosci* 2019;22:374–85.
51. Ormel PR, Böttcher C, Gigase FAJ, Missall RD, Van Zuiden W, Fernández Zapata MC, Ilhan D, De Goeij M, Udine E, Sommer IEC, Priller J, Raj T, Kahn RS, Hol EM, De Witte LD. A characterization of the molecular phenotype and inflammatory response of schizophrenia patient-derived microglia-like cells. *Brain Behav Immun* 2020;90:196–207.
52. Howes OD, Onwordi EC. The synaptic hypothesis of schizophrenia version III: a master mechanism. *Mol Psychiatry* 2023;28:1843–56.
53. De Jonge JC, Vinkers CH, Hulshoff Pol HE, Marsman A. GABAergic Mechanisms in Schizophrenia: Linking Postmortem and In Vivo Studies. *Front Psychiatry* 2017;8:118.
54. Akbarian S, Kim JJ, Potkin SG, Hagman JO, Tafazzoli A, Bunney WE Jr, Jones EG. Gene expression for glutamic acid decarboxylase is reduced without loss of neurons in prefrontal cortex of schizophrenics. *Arch Gen Psychiatry* 1995;52(4):258–66.
55. Volk DW, Austin MC, Pierri JN, Sampson AR, Lewis DA. Decreased glutamic acid decarboxylase67 messenger RNA expression in a subset of prefrontal cortical gamma-aminobutyric acid neurons in subjects with schizophrenia. *Arch Gen Psychiatry* 2000; 57(3):237–45.
56. Thompson M, Weickert CS, Wyatt E, Webster MJ. Decreased glutamic acid decarboxylase(67) mRNA expression in multiple brain areas of patients with schizophrenia and mood disorders. *J Psychiatr Res* 2009;43(11):970–7.

57. Lewis DA, Hashimoto T, Volk DW. Cortical inhibitory neurons and schizophrenia. *Nat Rev Neurosci* 2005;6:312–24.
58. Olney JW. Glutamate Receptor Dysfunction and Schizophrenia. *Arch Gen Psychiatry* 1995;52:998.
59. Volk DW, Lewis DA. Early Developmental Disturbances of Cortical Inhibitory Neurons: Contribution to Cognitive Deficits in Schizophrenia. *Schizophr Bull* 2014;40:952–7.
60. Sawada T, Barbosa AR, Araujo B, McCord AE, D'Ignazio L, Benjamin KJM, Sheehan B, Zabolocki M, Feltrin A, Arora R, Brandtjen AC, Kleinman JE, Hyde TM, Bardy C, Weinberger DR, Paquola ACM, Erwin JA. Recapitulation of Perturbed Striatal Gene Expression Dynamics of Donors' Brains With Ventral Forebrain Organoids Derived From the Same Individuals With Schizophrenia. *Am J Psychiatry* 2024;181:493–511.
61. Lieberman JA, Small SA, Girgis RR. Early Detection and Preventive Intervention in Schizophrenia: From Fantasy to Reality. *Am J Psychiatry* 2019;176:794–810.
62. Morris LS, Kundu P, Dowell N, Mechelmans DJ, Favre P, Irvine MA, Robbins TW, Daw N, Bullmore ET, Harrison NA, Voon V. Fronto-striatal organization: Defining functional and microstructural substrates of behavioural flexibility. *Cortex* 2016;74:118–33.
63. Alexander GE, DeLong MR. Microstimulation of the primate neostriatum. I. Physiological properties of striatal microexcitable zones. *J Neurophysiol* 1985;53:1401–16.
64. Alexander GE, DeLong MR, Strick PL. Parallel Organization of Functionally Segregated Circuits Linking Basal Ganglia and Cortex. *Annu Rev Neurosci* 1986;9:357–81.
65. Alexander GE, Crutcher MD. Functional architecture of basal ganglia circuits: neural substrates of parallel processing. *Trends Neurosci* 1990;13:266–71.
66. Haber SN. Corticostriatal circuitry. *Dialogues Clinical Neurosci* 2016;18:7–21.
67. Jarbo K, Verstynen TD. Converging Structural and Functional Connectivity of Orbitofrontal, Dorsolateral Prefrontal, and Posterior Parietal Cortex in the Human Striatum. *J Neurosci* 2015;35:3865–78.

68. Saga Y, Hoshi E, Tremblay L. Roles of Multiple Globus Pallidus Territories of Monkeys and Humans in Motivation, Cognition and Action: An Anatomical, Physiological and Pathophysiological Review. *Front Neuroanat* 2017;11.
69. Zikereya T, Shi K, Chen W. Goal-directed and habitual control: from circuits and functions to exercise-induced neuroplasticity targets for the treatment of Parkinson's disease. *Front Neurol* 2023;14:1254447.
70. Märtin A, Calvigioni D, Tzortzi O, Fuzik J, Wärnberg E, Meletis K. A Spatiomolecular Map of the Striatum. *Cell Reports* 2019;29:4320-4333.e5.
71. Garma LD, Harder L, Barba-Reyes JM, Marco Salas S, Díez-Salguero M, Nilsson M, Serrano-Pozo A, Hyman BT, Muñoz-Manchado AB. Interneuron diversity in the human dorsal striatum. *Nat Commun* 2024;15:6164.
72. Graybiel AM, Aosaki T, Flaherty AW, Kimura M. The Basal Ganglia and Adaptive Motor Control. *Science* 1994;265:1826–31.
73. Bogacz R, Gurney K. The Basal Ganglia and Cortex Implement Optimal Decision Making Between Alternative Actions. *Neural Comput* 2007;19:442–77.
74. Tecuapetla F, Jin X, Lima SQ, Costa RM. Complementary Contributions of Striatal Projection Pathways to Action Initiation and Execution. *Cell* 2016;166:703–15.
75. Yartsev MM, Hanks TD, Yoon AM, Brody CD. Causal contribution and dynamical encoding in the striatum during evidence accumulation. *eLife* 2018;7:e34929.
76. Stephenson-Jones M, Samuelsson E, Ericsson J, Robertson B, Grillner S. Evolutionary Conservation of the Basal Ganglia as a Common Vertebrate Mechanism for Action Selection. *Current Biology 2*011;21:1081–91.
77. Krienen FM, Goldman M, Zhang Q, C. H. Del Rosario R, Florio M, Machold R, Saunders A, Levandowski K, Zaniewski H, Schuman B, Wu C, Lutservitz A, Mullally CD, Reed N, Bien E, Bortolin L, Fernandez-Otero M, Lin JD, Wysoker A, Nemesh J, Kulp D, Burns M, Tkachev V, Smith R, Walsh CA, Dimidschstein J, Rudy B, S. Kean L, Berretta S, Fishell G, Feng G, McCarroll SA. Innovations present in the primate interneuron repertoire. *Nature* 2020;586:262–9.
78. Gerfen CR, Engber TM, Mahan LC, Susel Z, Chase TN, Monsma FJ, Sibley DR. D_1 and D_2 dopamine receptor-regulated gene expression of striatonigral and striatopallidal neurons. *Science* 1990;250:1429–32.

79. Rocha GS, Freire MAM, Britto AM, Paiva KM, Oliveira RF, Fonseca IAT, Araújo DP, Oliveira LC, Guzen FP, Morais PLAG, Cavalcanti JRLP. Basal ganglia for beginners: the basic concepts you need to know and their role in movement control. *Front Syst Neurosci* 2023;17:1242929.
80. Moustafa AA, Chakravarthy S, Phillips JR, Gupta A, Keri S, Polner B, Frank MJ, Jahanshahi M. Motor symptoms in Parkinson's disease: A unified framework. *Neurosci Biobehav Rev* 2016;68:727–40.
81. Howes OD, Kambeitz J, Kim E, Stahl D, Slifstein M, Abi-Dargham A, Kapur S. The Nature of Dopamine Dysfunction in Schizophrenia and What This Means for Treatment: Meta-analysis of Imaging Studies. *Arch Gen Psychiatry* 2012;69.
82. Ernst M, Zametkin A, Matochik J, Pascualvaca D, Cohen R. Low medial prefrontal dopaminergic activity in autistic children. *Lancet* 1997;350:638.
83. Abbott AE, Linke AC, Nair A, Jahedi A, Alba LA, Keown CL, Fishman I, Müller RA. Repetitive behaviors in autism are linked to imbalance of corticostriatal connectivity: a functional connectivity MRI study. *Soc Cogn and Affect Neurosci* 2018;13:32–42.
84. DiMaio S, Grizenko N, Joober R. Dopamine genes and attention-deficit hyperactivity disorder: a review. *J Psychiatry Neurosci.* 2003 Jan;28(1):27-38.
85. Diana M. The Dopamine Hypothesis of Drug Addiction and Its Potential Therapeutic Value. *Front Psychiatry* 2011;2.
86. Floresco SB, Magyar O. Mesocortical dopamine modulation of executive functions: beyond working memory. *Psychopharmacology* 2006;188:567–85.
87. Haber SN, Knutson B. The Reward Circuit: Linking Primate Anatomy and Human Imaging. *Neuropsychopharmacology* 2010;35:4–26.
88. Mink JW. The basal ganglia: focused selection and inhibition of competing motor programs. *Prog Neurobiol* 1996;50:381–425.
89. Kosillo P, Zhang Y-F, Threlfell S, Cragg SJ. Cortical Control of Striatal Dopamine Transmission via Striatal Cholinergic Interneurons. *Cereb Cortex* 2016;26:4160–9.
90. Nelson BG, Bassett DS, Camchong J, Bullmore ET, Lim KO. Comparison of large-scale human brain functional and anatomical networks in schizophrenia. *NeuroImage: Clinical* 2017;15:439–48.

91. Kristensen TD, Ambrosen KS, Raghava JM, Syeda WT, Dhollander T, Lemvigh CK, Bojesen KB, Barber AD, Nielsen MØ, Rostrup E, Pantelis C, Fagerlund B, Glenthøj BY, Ebdrup BH. Structural and functional connectivity in relation to executive functions in antipsychotic-naïve patients with first episode schizophrenia. *Schizophrenia* 2024;10:77.
92. Kottaram A, Johnston LA, Tian Y, Ganella EP, Laskaris L, Cocchi L, McGorry P, Pantelis C, Kotagiri R, Cropley V, Zalesky A. Predicting individual improvement in schizophrenia symptom severity at 1-year follow-up: Comparison of connectomic, structural, and clinical predictors. *Human Brain Mapping* 2020;41:3342–57.
93. Zhang Z, Zhuo K, Xiang Q, Sun Y, Suckling J, Wang J, Liu D, Sun Y. Dynamic functional connectivity and its anatomical substrate reveal treatment outcome in first-episode drug-naïve schizophrenia. *Transl Psychiatry* 2021;11:282.
94. Yoon JH, Westphal AJ, Minzenberg MJ, Niendam T, Ragland JD, Lesh T, Solomon M, Carter CS. Task-evoked substantia nigra hyperactivity associated with prefrontal hypofunction, prefrontonigral disconnectivity and nigrostriatal connectivity predicting psychosis severity in medication naïve first episode schizophrenia. *Schizophr Res* 2014;159:521–6.
95. Graveland GA, Difiglia M. The frequency and distribution of medium-sized neurons with indented nuclei in the primate and rodent neostriatum. *Brain Research* 1985;327:307–11.
96. Graveland GA, Williams RS, Difiglia M. A Golgi study of the human neostriatum: Neurons and afferent fibers. *J of Comp Neurology* 1985;234:317–33.
97. Gerfen CR, Bolam JP. The Neuroanatomical Organization of the Basal Ganglia. Handbook of Behavioral Neuroscience, vol. 20, Elsevier; 2010, p. 3–28.
98. Aubert I, Ghorayeb I, Normand E, Bloch B. Phenotypical characterization of the neurons expressing the D1 and D2 dopamine receptors in the monkey striatum. *J Comp Neurol* 2000;418:22–32.
99. Stanley G, Gokce O, Malenka RC, Südhof TC, Quake SR. Continuous and Discrete Neuron Types of the Adult Murine Striatum. *Neuron* 2020;105:688-699.e8.

100. He J, Kleyman M, Chen J, Alikaya A, Rothenhoefer KM, Ozturk BE, Wirthlin M, Fish K, Byrne LC, Pfenning AR, Stauffer WR. Transcriptional and Anatomical Diversity of Medium Spiny Neurons in the Primate Striatum. *SSRN Journal* 2021.
101. Bernácer J, Prensa L, Giménez-Amaya JM. Distribution of GABAergic interneurons and dopaminergic cells in the functional territories of the human striatum. *PLoS ONE* 2012;7:e30504.
102. Lecumberri A, Lopez-Janeiro A, Corral-Domenge C, Bernacer J. Neuronal density and proportion of interneurons in the associative, sensorimotor and limbic human striatum. *Brain Struct Funct* 2017.
103. Garas FN, Kormann E, Shah RS, Vinciati F, Smith Y, Magill PJ, Sharott A. Structural and molecular heterogeneity of calretinin-expressing interneurons in the rodent and primate striatum. *J of Comparative Neurology* 2018;526:877–98
104. Del Rey NL, Trigo-Damas I, Obeso JA, Cavada C, Blesa J. Neuron types in the primate striatum: Stereological analysis of projection neurons and interneurons in control and parkinsonian monkeys. *Neuropathology Appl Neurobio* 2022;48:e12812.
105. Muñoz-Manchado AB, Bengtsson Gonzales C, Zeisel A, Munguba H, Bekkouche B, Skene NG, Lönnerberg P, Ryge J, Harris KD, Linnarsson S, Hjerling-Leffler J. Diversity of Interneurons in the Dorsal Striatum Revealed by Single-Cell RNA Sequencing and PatchSeq. *Cell Reports* 2018;24:2179-2190.e7.
106. Tepper JM, Koós T, Ibanez-Sandoval O, Tecuapetla F, Faust TW, Assous M. Heterogeneity and Diversity of Striatal GABAergic Interneurons: Update 2018. *Front Neuroanat* 2018;12:91.
107. Corrigan EK, DeBerardine M, Poddar A, Turrero Garcia M, Schmitz MT, Harwell C, Paredes M, Krienen FM, Pollen AA. Conservation, alteration, and redistribution of mammalian striatal interneurons. 2024 [*preprint*]
108. Kawaguchi Y. Physiological, morphological, and histochemical characterization of three classes of interneurons in rat neostriatum. *J Neurosci* 1993;13:4908–23.
109. Cicchetti F, Beach TG, Parent A. Chemical phenotype of calretinin interneurons in the human striatum. *Synapse* 1998;30:284–97.

110. Wu Y, Parent A. Striatal interneurons expressing calretinin, parvalbumin or NADPH-diaphorase: a comparative study in the rat, monkey and human. *Brain Research* 2000;863:182–91.
111. Petryszyn S, Beaulieu J-M, Parent A, Parent M. Distribution and morphological characteristics of striatal interneurons expressing calretinin in mice: A comparison with human and nonhuman primates. *J Chem Neuroanat* 2014;59–60:51–61.
112. Adorjan I, Sun B, Feher V, Tyler T, Veres D, Chance SA, Szele FG. Evidence for decreased density of calretinin-immunopositive neurons in the caudate nucleus in patients with schizophrenia. *Front Neuroanat* 2020;14:581685.
113. Holt DJ, Herman MM, Hyde TM, Kleinman JE, Sinton CM, German DC, Hersh LB, Graybiel AM, Saper CB. Evidence for a deficit in cholinergic interneurons in the striatum in schizophrenia. *Neuroscience* 1999;94:21–31.
114. Marín O, Anderson SA, Rubenstein JLR. Origin and Molecular Specification of Striatal Interneurons. *J Neurosci* 2000;20:6063–76.
115. Tasic B, Yao Z, Graybuck LT, Smith KA, Nguyen TN, Bertagnolli D, Goldy J, Garren E, Economo MN, Viswanathan S, Penn O, Bakken T, Menon V, Miller J, Fong O, Hirokawa KE, Lathia K, Rimorin C, Tieu M, Larsen R, Casper T, Barkan E, Kroll M, Parry S, Shapovalova NV, Hirschstein D, Pendergraft J, Sullivan HA, Kim TK, Szafer A, Dee N, Groblewski P, Wickersham I, Cetin A, Harris JA, Levi BP, Sunkin SM, Madisen L, Daigle TL, Looger L, Bernard A, Phillips J, Lein E, Hawrylycz M, Svoboda K, Jones AR, Koch C, Zeng H. Shared and distinct transcriptomic cell types across neocortical areas. *Nature* 2018;563:72–8.
116. Knowles R, Dehorter N, Ellender T. From Progenitors to Progeny: Shaping Striatal Circuit Development and Function. *J Neurosci* 2021;41:9483–502.
117. Kegeles LS, Abi-Dargham A, Frankle WG, Gil R, Cooper TB, Slifstein M, Hwang DR, Huang Y, Haber SN, Laruelle M. Increased synaptic dopamine function in associative regions of the striatum in schizophrenia. *Arch Gen Psychiatry* 2010;67:231.
118. McCutcheon RA, Abi-Dargham A, Howes OD. Schizophrenia, dopamine and the striatum: from biology to symptoms. *Trends Neurosci* 2019;42:205–20.

119. Holt DJ, Bachus SE, Hyde TM, Wittie M, Herman MM, Vangel M, Saper CB, Kleinman JE. Reduced Density of Cholinergic Interneurons in the Ventral Striatum in Schizophrenia: An In Situ Hybridization Study. *Biol Psych* 2005;58:408–16.
120. Brandt GN, Bonelli RM. Structural neuroimaging of the basal ganglia in schizophrenic patients: a review. *Wien Med Wochenschr* 2008;158:84–90.
121. ENIGMA Schizophrenia Working Group, van Erp TG, Hibar DP, Rasmussen JM, Glahn DC, Pearlson GD, Andreassen OA, Agartz I, Westlye LT, Haukvik UK, Dale AM, Melle I, Hartberg CB, Gruber O, Kraemer B, Zilles D, Donohoe G, Kelly S, McDonald C, Morris DW, Cannon DM, Corvin A, Machielsen MW, Koenders L, de Haan L, Veltman DJ, Satterthwaite TD, Wolf DH, Gur RC, Gur RE, Potkin SG, Mathalon DH, Mueller BA, Preda A, Macciardi F, Ehrlich S, Walton E, Hass J, Calhoun VD, Bockholt HJ, Sponheim SR, Shoemaker JM, van Haren NE, Hulshoff Pol HE, Ophoff RA, Kahn RS, Roiz-Santiañez R, Crespo-Facorro B, Wang L, Alpert KI, Jönsson EG, Dimitrova R, Bois C, Whalley HC, McIntosh AM, Lawrie SM, Hashimoto R, Thompson PM, Turner JA. Subcortical brain volume abnormalities in 2028 individuals with schizophrenia and 2540 healthy controls via the ENIGMA consortium. *Mol Psychiatry* 2016;21:547–53.
122. Haijma SV, Van Haren N, Cahn W, Koolschijn PCMP, Hulshoff Pol HE, Kahn RS. Brain Volumes in Schizophrenia: A Meta-Analysis in Over 18 000 Subjects. *Schizophr Bull* 2013;39:1129–38.
123. Andersen HG, Raghava JM, Svarer C, Wulff S, Johansen LB, Antonsen PK, Nielsen MØ, Rostrup E, Vernon AC, Jensen LT, Pinborg LH, Glenthøj BY, Ebdrup BH. Striatal Volume Increase After Six Weeks of Selective Dopamine D2/3 Receptor Blockade in First-Episode, Antipsychotic-Naïve Schizophrenia Patients. *Front Neurosci* 2020;14:484.
124. Benjamin KJM, Chen Q, Jaffe AE, Stolz JM, Collado-Torres L, Huuki-Myers LA, Burke EE, Arora R, Feltrin AS, Barbosa AR, Radulescu E, Pergola G, Shin JH, Ulrich WS, Deep-Soboslay A, Tao R; BrainSeq Consortium; Hyde TM, Kleinman JE, Erwin JA, Weinberger DR, Paquola ACM. Analysis of the caudate nucleus transcriptome in individuals with schizophrenia highlights effects of antipsychotics and new risk genes. *Nat Neurosci* 2022;25:1559–68.

125. Friedman NP, Robbins TW. The role of prefrontal cortex in cognitive control and executive function. *Neuropsychopharmacology* 2022;47:72–89.
126. Hoshi E. Functional specialization within the dorsolateral prefrontal cortex: A review of anatomical and physiological studies of non-human primates. *Neurosci Res* 2006;54:73–84.
127. Mylius V, Ayache SS, Ahdab R, Farhat WH, Zouari HG, Belke M, Brugières P, Wehrmann E, Krakow K, Timmesfeld N, Schmidt S, Oertel WH, Knake S, Lefaucheur JP. Definition of DLPFC and M1 according to anatomical landmarks for navigated brain stimulation: Inter-rater reliability, accuracy, and influence of gender and age. *NeuroImage* 2013;78:224–32.
128. Szczepanski SM, Knight RT. Insights into Human Behavior from Lesions to the Prefrontal Cortex. *Neuron* 2014;83:1002–18.
129. Panikratova YR, Vlasova RM, Akhutina TV, Korneev AA, Sinitsyn VE, Pechenkova EV. Functional connectivity of the dorsolateral prefrontal cortex contributes to different components of executive functions. *Int J Psychophysiol.* 2020;151:70–79.
130. Semendeferi K, Lu A, Schenker N, Damasio H. Humans and great apes share a large frontal cortex. *Nat Neurosci* 2002;5:272–6.
131. Rakic P. Specification of Cerebral Cortical Areas. *Science* 1988;241:170–6.
132. Buxhoeveden DP, Casanova MF. The minicolumn hypothesis in neuroscience. *Brain* 2002;125:935–51.
133. Leyva-Díaz E, López-Bendito G. In and out from the cortex: Development of major forebrain connections. *Neuroscience* 2013;254:26–44.
134. Markram H, Toledo-Rodriguez M, Wang Y, Gupta A, Silberberg G, Wu C. Interneurons of the neocortical inhibitory system. *Nat Rev Neurosci* 2004;5:793–807.
135. Tomioka R, Okamoto K, Furuta T, Fujiyama F, Iwasato T, Yanagawa Y, Obata K, Kaneko T, Tamamaki N. Demonstration of long-range GABAergic connections distributed throughout the mouse neocortex. *Eur J of Neuroscience* 2005;21:1587–600.
136. Rowitch DH, Kriegstein AR. Developmental genetics of vertebrate glial–cell specification. *Nature* 2010;468:214–22.

137. Cornell J, Salinas S, Huang H-Y, Zhou M. Microglia regulation of synaptic plasticity and learning and memory. *Neural Regen Res* 2022;17:705.
138. Mariani MM, Kielian T. Microglia in Infectious Diseases of the Central Nervous System. *J Neuroimmune Pharmacol* 2009;4:448–61.
139. Abbott NJ, Patabendige AAK, Dolman DEM, Yusof SR, Begley DJ. Structure and function of the blood–brain barrier. *Neurobiol Dis* 2010;37:13–25.
140. Schuman B, Dellal S, Prönneke A, Machold R, Rudy B. Neocortical Layer 1: An Elegant Solution to Top-Down and Bottom-Up Integration. *Annu Rev Neurosci* 2021;44:221–52.
141. Markram H, Muller E, Ramaswamy S, Reimann MW, Abdellah M, Sanchez CA, Ailamaki A, Alonso-Nanclares L, Antille N, Arsever S, Kahou GA, Berger TK, Bilgili A, Buncic N, Chalimourda A, Chindemi G, Courcol JD, Delalondre F, Delattre V, Druckmann S, Dumusc R, Dynes J, Eilemann S, Gal E, Gevaert ME, Ghobril JP, Gidon A, Graham JW, Gupta A, Haenel V, Hay E, Heinis T, Hernando JB, Hines M, Kanari L, Keller D, Kenyon J, Khazen G, Kim Y, King JG, Kisvarday Z, Kumbhar P, Lasserre S, Le Bé JV, Magalhães BR, Merchán-Pérez A, Meystre J, Morrice BR, Muller J, Muñoz-Céspedes A, Muralidhar S, Muthurasa K, Nachbaur D, Newton TH, Nolte M, Ovcharenko A, Palacios J, Pastor L, Perin R, Ranjan R, Riachi I, Rodríguez JR, Riquelme JL, Rössert C, Sfyrakis K, Shi Y, Shillcock JC, Silberberg G, Silva R, Tauheed F, Telefont M, Toledo-Rodriguez M, Tränkler T, Van Geit W, Díaz JV, Walker R, Wang Y, Zaninetta SM, DeFelipe J, Hill SL, Segev I, Schürmann F. Reconstruction and Simulation of Neocortical Microcircuitry. *Cell* 2015;163:456–92.
142. Kim B, Kim D, Schulmann A, Patel Y, Caban-Rivera C, Kim P, Jambhale A, Johnson KR, Feng N, Xu Q, Kang SJ, Mandal A, Kelly M, Akula N, McMahon FJ, Lipska B, Marenco S, Auluck PK. Cellular Diversity in Human Subgenual Anterior Cingulate and Dorsolateral Prefrontal Cortex by Single-Nucleus RNA-Sequencing. *J Neurosci* 2023;43:3582–97.
143. Hodge RD, Bakken TE, Miller JA, Smith KA, Barkan ER, Graybuck LT, Close JL, Long B, Johansen N, Penn O, Yao Z, Eggermont J, Höllt T, Levi BP, Shehata SI, Aevermann B, Beller A, Bertagnolli D, Brouner K, Casper T, Cobbs C, Dalley R, Dee N, Ding SL, Ellenbogen RG, Fong O, Garren E, Goldy J, Gwinn RP,

Hirschstein D, Keene CD, Keshk M, Ko AL, Lathia K, Mahfouz A, Maltzer Z, McGraw M, Nguyen TN, Nyhus J, Ojemann JG, Oldre A, Parry S, Reynolds S, Rimorin C, Shapovalova NV, Somasundaram S, Szafer A, Thomsen ER, Tieu M, Quon G, Scheuermann RH, Yuste R, Sunkin SM, Lelieveldt B, Feng D, Ng L, Bernard A, Hawrylycz M, Phillips JW, Tasic B, Zeng H, Jones AR, Koch C, Lein ES. Conserved cell types with divergent features in human versus mouse cortex. *Nature* 2019;573:61–8.

144. Condé F, Lund JS, Jacobowitz DM, Baimbridge KG, Lewis DA. Local circuit neurons immunoreactive for calretinin, calbindin D-28k or parvalbumin in monkey prefronatal cortex: Distribution and morphology. *J Comp Neurol* 1994;341:95–116.
145. Hornung J-P, Tribolet N. Distribution of GABA-containing neurons in human frontal cortex: a quantitative immunocytochemical study. *Anat Embryol* 1994;189.
146. Fishell G, Kepecs A. Interneuron Types as Attractors and Controllers. *Annu Rev Neurosci* 2020;43:1–30.
147. Gouwens NW, Sorensen SA, Baftizadeh F, Budzillo A, Lee BR, Jarsky T, Alfiler L, Baker K, Barkan E, Berry K, Bertagnolli D, Bickley K, Bomben J, Braun T, Brouner K, Casper T, Crichton K, Daigle TL, Dalley R, de Frates RA, Dee N, Desta T, Lee SD, Dotson N, Egdorf T, Ellingwood L, Enstrom R, Esposito L, Farrell C, Feng D, Fong O, Gala R, Gamlin C, Gary A, Glandon A, Goldy J, Gorham M, Graybuck L, Gu H, Hadley K, Hawrylycz MJ, Henry AM, Hill D, Hupp M, Kebede S, Kim TK, Kim L, Kroll M, Lee C, Link KE, Mallory M, Mann R, Maxwell M, McGraw M, McMillen D, Mukora A, Ng L, Ng L, Ngo K, Nicovich PR, Oldre A, Park D, Peng H, Penn O, Pham T, Pom A, Popović Z, Potekhina L, Rajanbabu R, Ransford S, Reid D, Rimorin C, Robertson M, Ronellenfitch K, Ruiz A, Sandman D, Smith K, Sulc J, Sunkin SM, Szafer A, Tieu M, Torkelson A, Trinh J, Tung H, Wakeman W, Ward K, Williams G, Zhou Z, Ting JT, Arkhipov A, Sümbül U, Lein ES, Koch C, Yao Z, Tasic B, Berg J, Murphy GJ, Zeng H. Integrated Morphoelectric and Transcriptomic Classification of Cortical GABAergic Cells. *Cell* 2020;183:935-953.e19.
148. Tremblay R, Lee S, Rudy B. GABAergic Interneurons in the Neocortex: From Cellular Properties to Circuits. *Neuron* 2016;91:260–92.

149. Machold R, Dellal S, Valero M, Zurita H, Kruglikov I, Meng JH, Hanson JL, Hashikawa Y, Schuman B, Buzsáki G, Rudy B. Id2 GABAergic interneurons comprise a neglected fourth major group of cortical inhibitory cells. *eLife* 2023;12:e85893.
150. González-Burgos G, Krimer LS, Povysheva NV, Barrionuevo G, Lewis DA. Functional Properties of Fast Spiking Interneurons and Their Synaptic Connections With Pyramidal Cells in Primate Dorsolateral Prefrontal Cortex. *J Neurophysiol* 2005;93:942–53.
151. Melchitzky DS. Pyramidal Neuron Local Axon Terminals in Monkey Prefrontal Cortex: Differential Targeting of Subclasses of GABA Neurons. *Cerebral Cortex* 2003;13:452–60.
152. DeFelipe J, Hendry SHC, Jones EG, Schmechel D. Variability in the terminations of GABAergic chandelier cell axons on initial segments of pyramidal cell axons in the monkey sensory-motor cortex. *J Comp Neurol* 1985;231:364–84.
153. Inan M, Anderson SA. The chandelier cell, form and function. *Curr Opin Neurobiol* 2014;26:142–8.
154. Szabadics J, Varga C, Molnár G, Oláh S, Barzó P, Tamás G. Excitatory Effect of GABAergic Axo-Axonic Cells in Cortical Microcircuits. *Science* 2006;311:233–5.
155. Woodruff AR, McGarry LM, Vogels TP, Inan M, Anderson SA, Yuste R. State-Dependent Function of Neocortical Chandelier Cells. *J Neurosci* 2011;31:17872–86.
156. Sohal VS, Zhang F, Yizhar O, Deisseroth K. Parvalbumin neurons and gamma rhythms enhance cortical circuit performance. *Nature* 2009;459:698–702.
157. Buzsáki G, Wang X-J. Mechanisms of Gamma Oscillations. *Annu Rev Neurosci* 2012;35:203–25.
158. Cardin JA, Carlén M, Meletis K, Knoblich U, Zhang F, Deisseroth K, Tsai LH, Moore CI. Driving fast-spiking cells induces gamma rhythm and controls sensory responses. *Nature* 2009;459:663–7.
159. Gonzalez-Burgos G, Cho RY, Lewis DA. Alterations in Cortical Network Oscillations and Parvalbumin Neurons in Schizophrenia. *Biol Psych* 2015;77:1031–40.

160. Batiuk MY, Tyler T, Dragicevic K, Mei S, Rydbirk R, Petukhov V, Deviatiiarov R, Sedmak D, Frank E, Feher V, Habek N, Hu Q, Igolkina A, Roszik L, Pfisterer U, Garcia-Gonzalez D, Petanjek Z, Adorjan I, Kharchenko PV, Khodosevich K. Upper cortical layer–driven network impairment in schizophrenia. *Sci Adv* 2022;8:eabn8367.
161. Ruzicka WB, Mohammadi S, Fullard JF, Davila-Velderrain J, Subburaju S, Tso DR, Hourihan M, Jiang S, Lee HC, Bendl J; Voloudakis G, Haroutunian V, Hoffman GE, Roussos P, Kellis M; PsychENCODE Consortium. Single-cell multi-cohort dissection of the schizophrenia transcriptome. *Science* 2024;384:eadg5136.
162. Gabbott PLA, Bacon SJ. Vasoactive intestinal polypeptide containing neurones in monkey medial prefrontal cortex (mPFC): colocalisation with calretinin. *Brain Research* 1997;744:179–84.
163. Kullander K, Topolnik L. Cortical disinhibitory circuits: cell types, connectivity and function. *Trends Neurosci* 2021;44:643–57.
164. Del Río MR, DeFelipe J. Synaptic Connections of Calretinin-Immunoreactive Neurons in the Human Neocortex. *J Neurosci* 1997;17:5143–54.
165. Pi H-J, Hangya B, Kvitsiani D, Sanders JI, Huang ZJ, Kepecs A. Cortical interneurons that specialize in disinhibitory control. *Nature* 2013;503:521–4.
166. Gabbott PLA, Bacon SJ. Local circuit neurons in the medial prefrontal cortex (areas 24a,b,c, 25 and 32) in the monkey: I. Cell morphology and morphometrics. *J Comp Neurol* 1996;364:567–608.
167. Baimbridge KG, Celio MR, Rogers JH. Calcium-binding proteins in the nervous system. *Trends Neurosci* 1992;15:303–8.
168. Fairless R, Williams SK, Diem R. Calcium-Binding Proteins as Determinants of Central Nervous System Neuronal Vulnerability to Disease. *IJMS* 2019;20:2146.
169. Schurmans S, Schiffmann SN, Gurden H, Lemaire M, Lipp H-P, Schwam V, Pochet R, Imperato A, Böhme GA, Parmentier M. Impaired long-term potentiation induction in dentate gyrus of calretinin-deficient mice. *Proc Natl Acad Sci USA* 1997;94:10415–20.
170. Melchitzky DS, Lewis DA. Dendritic-targeting GABA neurons in monkey prefrontal cortex: Comparison of somatostatin- and calretinin-immunoreactive axon terminals. *Synapse* 2008;62:456–65.

171. Martinotti, C.Contributo allo studio della corteccia cerebrale, ed all'origine centrale dei nervi. *Ann Freniatr Sci Affini* 1889; 14–381.
172. Kubota Y, Shigematsu N, Karube F, Sekigawa A, Kato S, Yamaguchi N, Hirai Y, Morishima M, Kawaguchi Y. Selective Coexpression of Multiple Chemical Markers Defines Discrete Populations of Neocortical GABAergic Neurons. *Cerebral Cortex* 2011;21:1803–17.
173. Banovac I, Sedmak D, Esclapez M, Petanjek Z. The Distinct Characteristics of Somatostatin Neurons in the Human Brain. *Mol Neurobiol* 2022;59:4953–65.
174. Xu H, Jeong H-Y, Tremblay R, Rudy B. Neocortical Somatostatin-Expressing GABAergic Interneurons Disinhibit the Thalamorecipient Layer 4. *Neuron* 2013;77:155–67.
175. Mengod G, Rigo M, Savasta M, Probst A, Palacios JM. Regional distribution of neuropeptide somatostatin gene expression in the human brain. *Synapse* 1992;12:62–74.
176. Gonzalez-Albo MC. The Human Temporal Cortex: Characterization of Neurons Expressing Nitric Oxide Synthase, Neuropeptides and Calcium-binding Proteins, and their Glutamate Receptor Subunit Profiles. *Cerebral Cortex* 2001;11:1170–81.
177. Machold R, Dellal S, Valero M, Zurita H, Kruglikov I, Meng JH, Hanson JL, Hashikawa Y, Schuman B, Buzsáki G, Rudy B. Id2 GABAergic interneurons comprise a neglected fourth major group of cortical inhibitory cells. *eLife* 2023;12:e85893.
178. Boldog E, Bakken TE, Hodge RD, Novotny M, Aevermann BD, Baka J, Bordé S, Close JL, Diez-Fuertes F, Ding SL, Faragó N, Kocsis ÁK, Kovács B, Maltzer Z, McCorrison JM, Miller JA, Molnár G, Oláh G, Ozsvár A, Rózsa M, Shehata SI, Smith KA, Sunkin SM, Tran DN, Venepally P, Wall A, Puskás LG, Barzó P, Steemers FJ, Schork NJ, Scheuermann RH, Lasken RS, Lein ES, Tamás G. Transcriptomic and morphophysiological evidence for a specialized human cortical GABAergic cell type. *Nat Neurosci* 2018;21:1185–95.
179. Kisvárday ZF, Gulyas A, Beroukas D, North JB, Chubb IW, Somogyi P. Synapses, axonal and dendritic patterns of GABA-immunoreactive neurons in human cerebral cortex. *Brain* 1990;113:793–812.

180. Kubota Y, Kawaguchi Y. Two distinct subgroups of cholecystokinin-immunoreactive cortical interneurons. *Brain Research* 1997;752:175–83.
181. Ibrahim LA, Huang S, Fernandez-Otero M, Sherer M, Qiu Y, Vemuri S, Xu Q, Machold R, Pouchelon G, Rudy B, Fishell G. Bottom-up inputs are required for establishment of top-down connectivity onto cortical layer 1 neurogliaform cells. *Neuron* 2021;109:3473-3485.e5.
182. Nguyen R, Venkatesan S, Binko M, Bang JY, Cajanding JD, Briggs C, Sargin D, Imayoshi I, Lambe EK, Kim JC. Cholecystokinin-Expressing Interneurons of the Medial Prefrontal Cortex Mediate Working Memory Retrieval. *J Neurosci* 2020;40:2314–31.
183. Rafelski SM, Theriot JA. Establishing a conceptual framework for holistic cell states and state transitions. *Cell* 2024;187:2633–51.
184. Dienel SJ, Lewis DA. Alterations in cortical interneurons and cognitive function in schizophrenia. *Neurobiol Dis* 2019;131:104208.
185. Shepherd AM, Laurens KR, Matheson SL, Carr VJ, Green MJ. Systematic meta-review and quality assessment of the structural brain alterations in schizophrenia. *Neurosci Biobehav Rev* 2012;36:1342–56.
186. Van Haren NEM. Changes in Cortical Thickness During the Course of Illness in Schizophrenia. *Arch Gen Psychiatry* 2011;68:871.
187. Lesh TA, Tanase C, Geib BR, Niendam TA, Yoon JH, Minzenberg MJ, Ragland JD, Solomon M, Carter CS. A Multimodal Analysis of Antipsychotic Effects on Brain Structure and Function in First-Episode Schizophrenia. *JAMA Psychiatry* 2015;72:226.
188. Ellison-Wright I, Bullmore E. Meta-analysis of diffusion tensor imaging studies in schizophrenia. *Schizophr Res* 2009;108:3–10.
189. Weinberger DR. Physiologic Dysfunction of Dorsolateral Prefrontal Cortex in Schizophrenia: I. Regional Cerebral Blood Flow Evidence. *Arch Gen Psychiatry* 1986;43:114.
190. Perlstein WM, Carter CS, Noll DC, Cohen JD. Relation of Prefrontal Cortex Dysfunction to Working Memory and Symptoms in Schizophrenia. *AJP* 2001;158:1105–13.

191. Yoon JH, Minzenberg MJ, Ursu S, Walters R, Wendelken C, Ragland JD, Carter CS. Association of Dorsolateral Prefrontal Cortex Dysfunction With Disrupted Coordinated Brain Activity in Schizophrenia: Relationship With Impaired Cognition, Behavioral Disorganization, and Global Function. *AJP* 2008;165:1006–14.
192. Smucny J, Lesh TA, Newton K, Niendam TA, Ragland JD, Carter CS. Levels of Cognitive Control: A Functional Magnetic Resonance Imaging-Based Test of an RDoC Domain Across Bipolar Disorder and Schizophrenia. *Neuropsychopharmacology* 2018;43:598–606.
193. Roux F, Uhlhaas PJ. Working memory and neural oscillations: alpha–gamma versus theta–gamma codes for distinct WM information? *Trends in Cognitive Sciences* 2014;18:16–25.
194. Bastos AM, Loonis R, Kornblith S, Lundqvist M, Miller EK. Laminar recordings in frontal cortex suggest distinct layers for maintenance and control of working memory. *Proc Natl Acad Sci USA* 2018;115:1117–22.
195. Buzsáki G, Wang X-J. Mechanisms of Gamma Oscillations. *Annu Rev Neurosci* 2012;35:203–25.
196. Lewis DA, Hashimoto T, Volk DW. Cortical inhibitory neurons and schizophrenia. *Nat Rev Neurosci* 2005;6:312–24.
197. Brisch R, Bielau H, Saniotis A, Wolf R, Bogerts B, Krell D, Steiner J, Braun K, Krzyżanowska M, Krzyżanowski M, Jankowski Z, Kaliszan M, Bernstein HG, Gos T. Calretinin and parvalbumin in schizophrenia and affective disorders: a mini-review, a perspective on the evolutionary role of calretinin in schizophrenia, and a preliminary post-mortem study of calretinin in the septal nuclei. *Front Cell Neurosci* 2015;9.
198. Prkačin MV, Banovac I, Petanjek Z, Hladnik A. Cortical interneurons in schizophrenia – cause or effect? *Croat Med J* 2023;64:110–22.
199. Kaar SJ, Angelescu I, Marques TR, Howes OD. Pre-frontal parvalbumin interneurons in schizophrenia: a meta-analysis of post-mortem studies. *J Neural Transm* 2019;126:1637–51.

200. Benes FM, McSparren J, Bird ED, SanGiovanni JP, Vincent SL. Deficits in small interneurons in prefrontal and cingulate cortices of schizophrenic and schizoaffective patients. *Arch Gen Psychiatry* 1991;48:996.
201. Dienel SJ, Fish KN, Lewis DA. The Nature of Prefrontal Cortical GABA Neuron Alterations in Schizophrenia: Markedly Lower Somatostatin and Parvalbumin Gene Expression Without Missing Neurons. *AJP* 2023;180:495–507.
202. Daviss SR, Lewis DA. Local circuit neurons of the prefrontal cortex in schizophrenia: selective increase in the density of calbindin-immunoreactive neurons. *Psychiatry Res* 1995;59:81–96.
203. Reynolds GP, Beasley CL. GABAergic neuronal subtypes in the human frontal cortex — development and deficits in schizophrenia. *J Chem Neuroanat* 2001;22:95–100.
204. Beasley CL, Zhang ZJ, Patten I, Reynolds GP. Selective deficits in prefrontal cortical GABAergic neurons in schizophrenia defined by the presence of calcium-binding proteins. *Biological Psychiatry* 2002;52:708–15.
205. Reynolds GP, Beasley CL, Zhang ZJ. Understanding the neurotransmitter pathology of schizophrenia: selective deficits of subtypes of cortical GABAergic neurons. *J Neural Transm* 2002;109:881–9.
206. Hashimoto T, Volk DW, Eggan SM, Mirnics K, Pierri JN, Sun Z, Sampson AR, Lewis DA. Gene Expression Deficits in a Subclass of GABA Neurons in the Prefrontal Cortex of Subjects with Schizophrenia. *J Neurosci* 2003;23:6315–26.
207. Tooney PA, Chahl LA. Neurons expressing calcium-binding proteins in the prefrontal cortex in schizophrenia. Progress in Neuro-Psychopharmacology and *Biol Psych* 2004;28:273–8.
208. Sakai T, Oshima A, Nozaki Y, Ida I, Haga C, Akiyama H, Nakazato Y, Mikuni M. Changes in density of calcium-binding-protein-immunoreactive GABAergic neurons in prefrontal cortex in schizophrenia and bipolar disorder. *Neuropathology* 2008;28:143–50.
209. Hashimoto T, Arion D, Unger T, Maldonado-Avilés JG, Morris HM, Volk DW Mirnics K, Lewis DA. Alterations in GABA-related transcriptome in the dorsolateral prefrontal cortex of subjects with schizophrenia. *Mol Psychiatry* 2008;13:147–61.

210. Fung SJ, Webster MJ, Sivagnanasundaram S, Duncan C, Elashoff M, Weickert CS. Expression of Interneuron Markers in the Dorsolateral Prefrontal Cortex of the Developing Human and in Schizophrenia. *AJP* 2010;167:1479–88.
211. Chung DW, Fish KN, Lewis DA. Pathological Basis for Deficient Excitatory Drive to Cortical Parvalbumin Interneurons in Schizophrenia. *AJP* 2016;173:1131–9.
212. Scarr E, Cowie TF, Kanellakis S, Sundram S, Pantelis C, Dean B. Decreased cortical muscarinic receptors define a subgroup of subjects with schizophrenia. *Mol Psychiatry* 2009;14:1017–23.
213. Scarr E, Hopper S, Vos V, Seo MS, Everall IP, Aumann TD, Chana G, Dean B. Low levels of muscarinic M1 receptor–positive neurons in cortical layers III and V in Brodmann areas 9 and 17 from individuals with schizophrenia. *J Psychiatry Neurosci.* 2018;43:338–46.
214. Olar A, Tyler T, Hoppa P, Frank E, Csabai I, Adorjan I, Pollner P. Annotated dataset for training deep learning models to detect astrocytes in human brain tissue. *Sci Data* 2024;11:96.
215. Jiang Z, Zhou X, Li R, Michal JJ, Zhang S, Dodson MV, Zhang Z, Harland RM. Whole transcriptome analysis with sequencing: methods, challenges and potential solutions. *Cell Mol Life Sci* 2015;72:3425–39.
216. Sforzini L, Marizzoni M, Bottanelli C, Kunšteková V, Zonca V, Saleri S, Kose M, Lombardo G, Mariani N, Nettis MA, Nikkheslat N, Worrell C, Zajkowska Z, Pointon L, Cowen PJ, Cavanagh J, Harrison NA, Riva MA, Mondelli V, Bullmore ET; Neuroimmunology of Mood Disorders and Alzheimer's Disease (NIMA) Consortium; Cattaneo A, Pariante CM. Transcriptomic profiles in major depressive disorder: the role of immunometabolic and cell-cycle-related pathways in depression with different levels of inflammation. *Mol Psychiatry*. 2025 Apr;30(4):1308-1318.
217. Schizophrenia Working Group of the Psychiatric Genomics Consortium. Biological insights from 108 schizophrenia-associated genetic loci. *Nature* 2014;511:421–7.
218. Fromer M, Pocklington AJ, Kavanagh DH, Williams HJ, Dwyer S, Gormley P, Georgieva L, Rees E, Palta P, Ruderfer DM, Carrera N, Humphreys I, Johnson JS, Roussos P, Barker DD, Banks E, Milanova V, Grant SG, Hannon E, Rose SA, Chambert K, Mahajan M, Scolnick EM, Moran JL, Kirov G, Palotie A, McCarroll

SA, Holmans P, Sklar P, Owen MJ, Purcell SM, O'Donovan MC. De novo mutations in schizophrenia implicate synaptic networks. *Nature* 2014;506:179–84.

219. Marshall CR, Howrigan DP, Merico D, Thiruvahindrapuram B, Wu W, Greer DS, Antaki D, Shetty A, Holmans PA, Pinto D, Gujral M, Brandler WM, Malhotra D, Wang Z, Fajarado KVF, Maile MS, Ripke S, Agartz I, Albus M, Alexander M, Amin F, Atkins J, Bacanu SA, Belliveau RA Jr, Bergen SE, Bertalan M, Bevilacqua E, Bigdeli TB, Black DW, Bruggeman R, Buccola NG, Buckner RL, Bulik-Sullivan B, Byerley W, Cahn W, Cai G, Cairns MJ, Campion D, Cantor RM, Carr VJ, Carrera N, Catts SV, Chambert KD, Cheng W, Cloninger CR, Cohen D, Cormican P, Craddock N, Crespo-Facorro B, Crowley JJ, Curtis D, Davidson M, Davis KL, Degenhardt F, Del Favero J, DeLisi LE, Dikeos D, Dinan T, Djurovic S, Donohoe G, Drapeau E, Duan J, Dudbridge F, Eichhammer P, Eriksson J, Escott-Price V, Essioux L, Fanous AH, Farh KH, Farrell MS, Frank J, Franke L, Freedman R, Freimer NB, Friedman JI, Forstner AJ, Fromer M, Genovese G, Georgieva L, Gershon ES, Giegling I, Giusti-Rodríguez P, Godard S, Goldstein JI, Gratten J, de Haan L, Hamshere ML, Hansen M, Hansen T, Haroutunian V, Hartmann AM, Henskens FA, Herms S, Hirschhorn JN, Hoffmann P, Hofman A, Huang H, Ikeda M, Joa I, Kähler AK, Kahn RS, Kalaydjieva L, Karjalainen J, Kavanagh D, Keller MC, Kelly BJ, Kennedy JL, Kim Y, Knowles JA, Konte B, Laurent C, Lee P, Lee SH, Legge SE, Lerer B, Levy DL, Liang KY, Lieberman J, Lönnqvist J, Loughland CM, Magnusson PKE, Maher BS, Maier W, Mallet J, Mattheisen M, Mattingsdal M, McCarley RW, McDonald C, McIntosh AM, Meier S, Meijer CJ, Melle I, Mesholam-Gately RI, Metspalu A, Michie PT, Milani L, Milanova V, Mokrab Y, Morris DW, Müller-Myhsok B, Murphy KC, Murray RM, Myin-Germeys I, Nenadic I, Nertney DA, Nestadt G, Nicodemus KK, Nisenbaum L, Nordin A, O'Callaghan E, O'Dushlaine C, Oh SY, Olincy A, Olsen L, O'Neill FA, Van Os J, Pantelis C, Papadimitriou GN, Parkhomenko E, Pato MT, Paunio T; Psychosis Endophenotypes International Consortium; Perkins DO, Pers TH, Pietiläinen O, Pimm J, Pocklington AJ, Powell J, Price A, Pulver AE, Purcell SM, Quested D, Rasmussen HB, Reichenberg A, Reimers MA, Richards AL, Roffman JL, Roussos P, Ruderfer DM, Salomaa V, Sanders AR, Savitz A, Schall U, Schulze TG, Schwab SG, Scolnick EM, Scott RJ, Seidman LJ, Shi J, Silverman JM, Smoller JW,

Söderman E, Spencer CCA, Stahl EA, Strengman E, Strohmaier J, Stroup TS, Suvisaari J, Svrakic DM, Szatkiewicz JP, Thirumalai S, Tooney PA, Veijola J, Visscher PM, Waddington J, Walsh D, Webb BT, Weiser M, Wildenauer DB, Williams NM, Williams S, Witt SH, Wolen AR, Wormley BK, Wray NR, Wu JQ, Zai CC, Adolfsson R, Andreassen OA, Blackwood DHR, Bramon E, Buxbaum JD, Cichon S, Collier DA, Corvin A, Daly MJ, Darvasi A, Domenici E, Esko T, Gejman PV, Gill M, Gurling H, Hultman CM, Iwata N, Jablensky AV, Jönsson EG, Kendler KS, Kirov G, Knight J, Levinson DF, Li QS, McCarroll SA, McQuillin A, Moran JL, Mowry BJ, Nöthen MM, Ophoff RA, Owen MJ, Palotie A, Pato CN, Petryshen TL, Posthuma D, Rietschel M, Riley BP, Rujescu D, Sklar P, St Clair D, Walters JTR, Werge T, Sullivan PF, O'Donovan MC, Scherer SW, Neale BM, Sebat J; CNV and Schizophrenia Working Groups of the Psychiatric Genomics Consortium. Contribution of copy number variants to schizophrenia from a genome-wide study of 41,321 subjects. *Nat Genet* 2017;49:27–35.

220. Sekar A, Bialas AR, De Rivera H, Davis A, Hammond TR, Kamitaki N, Tooley K, Presumey J, Baum M, Van Doren V, Genovese G, Rose SA, Handsaker RE; Schizophrenia Working Group of the Psychiatric Genomics Consortium; Daly MJ, Carroll MC, Stevens B, McCarroll SA. Schizophrenia risk from complex variation of complement component 4. *Nature* 2016;530:177–83.
221. Chen S, Sun X, Niu W, Kong L, He M, Li W, Zhong A, Lu J, Zhang L. Aberrant Expression of Long Non-Coding RNAs in Schizophrenia Patients. *Med Sci Monit* 2016;22:3340–51.
222. Oguro-Ando A, Bamford RA, Sital W, Sprengers JJ, Zuko A, Matser JM, Oppelaar H, Sarabdjitsingh A, Joëls M, Burbach JPH, Kas MJ. Cntn4, a risk gene for neuropsychiatric disorders, modulates hippocampal synaptic plasticity and behavior. *Transl Psychiatry* 2021;11:106.
223. León A, Aparicio GI, Scorticati C. Neuronal Glycoprotein M6a: An Emerging Molecule in Chemical Synapse Formation and Dysfunction. *Front Synaptic Neurosci* 2021;13:661681.
224. Page SC, Hamersky GR, Gallo RA, Rannals MD, Calcaterra NE, Campbell MN, Mayfield B, Briley A, Phan BN, Jaffe AE, Maher BJ. The schizophrenia- and autism-associated gene, transcription factor 4 regulates the columnar distribution of

layer 2/3 prefrontal pyramidal neurons in an activity-dependent manner. *Mol Psychiatry* 2018;23:304–15.

225. Laronha H, Caldeira J. Structure and Function of Human Matrix Metalloproteinases. *Cells* 2020;9:1076.
226. Ma C, Gu C, Huo Y, Li X, Luo X-J. The integrated landscape of causal genes and pathways in schizophrenia. *Transl Psychiatry* 2018;8:67.
227. Bowen EFW, Burgess JL, Granger R, Kleinman JE, Rhodes CH. DLPFC transcriptome defines two molecular subtypes of schizophrenia. *Transl Psychiatry* 2019;9:147.
228. Macosko EZ, Basu A, Satija R, Nemesh J, Shekhar K, Goldman M, Tirosh I, Bialas AR, Kamitaki N, Martersteck EM, Trombetta JJ, Weitz DA, Sanes JR, Shalek AK, Regev A, McCarroll SA. Highly Parallel Genome-wide Expression Profiling of Individual Cells Using Nanoliter Droplets. *Cell* 2015;161:1202–14.
229. Lake BB, Ai R, Kaeser GE, Salathia NS, Yung YC, Liu R, Wildberg A, Gao D, Fung HL, Chen S, Vijayaraghavan R, Wong J, Chen A, Sheng X, Kaper F, Shen R, Ronaghi M, Fan JB, Wang W, Chun J, Zhang K. Neuronal subtypes and diversity revealed by single-nucleus RNA sequencing of the human brain. *Science* 2016;352:1586–90.
230. Velmeshev D, Schirmer L, Jung D, Haeussler M, Perez Y, Mayer S, Bhaduri A, Goyal N, Rowitch DH, Kriegstein AR. Single-cell genomics identifies cell type–specific molecular changes in autism. *Science* 2019;364:685–9.
231. Mathys H, Davila-Velderrain J, Peng Z, Gao F, Mohammadi S, Young JZ, Menon M, He L, Abdurrob F, Jiang X, Martorell AJ, Ransohoff RM, Hafler BP, Bennett DA, Kellis M, Tsai LH. Single-cell transcriptomic analysis of Alzheimer's disease. *Nature* 2019;570:332–7.
232. Nagy C, Maitra M, Tanti A, Suderman M, Théroux JF, Davoli MA, Perlman K, Yerko V, Wang YC, Tripathy SJ, Pavlidis P, Mechawar N, Ragoussis J, Turecki G. Single-nucleus transcriptomics of the prefrontal cortex in major depressive disorder implicates oligodendrocyte precursor cells and excitatory neurons. *Nat Neurosci* 2020;23:771–81.
233. Zhu Q, Zhao X, Zhang Y, Li Y, Liu S, Han J, Sun Z, Wang C, Deng D, Wang S, Tang Y, Huang Y, Jiang S, Tian C, Chen X, Yuan Y, Li Z, Yang T, Lai T, Liu Y,

Yang W, Zou X, Zhang M, Cui H, Liu C, Jin X, Hu Y, Chen A, Xu X, Li G, Hou Y, Liu L, Liu S, Fang L, Chen W, Wu L. Single cell multi-omics reveal intra-cell-line heterogeneity across human cancer cell lines. *Nat Commun* 2023;14:8170.

234. Evans RG. The blind men, the elephant and the CT scanner. *Healthc Policy.* 2006 Mar;1(3):12-8.
235. Dupont C, Armant D, Brenner C. Epigenetics: Definition, Mechanisms and Clinical Perspective. *Semin Reprod Med* 2009;27:351–7.
236. Egervari G, Kozlenkov A, Dracheva S, Hurd YL. Molecular windows into the human brain for psychiatric disorders. *Mol Psychiatry* 2019;24:653–73.
237. Mikkelsen TS, Ku M, Jaffe DB, Issac B, Lieberman E, Giannoukos G, Alvarez P, Brockman W, Kim TK, Koche RP, Lee W, Mendenhall E, O'Donovan A, Presser A, Russ C, Xie X, Meissner A, Wernig M, Jaenisch R, Nusbaum C, Lander ES, Bernstein BE. Genome-wide maps of chromatin state in pluripotent and lineage-committed cells. *Nature* 2007;448:553–60.
238. Buenrostro JD, Wu B, Chang HY, Greenleaf WJ. ATAC-seq: A Method for Assaying Chromatin Accessibility Genome-Wide. *C P Mol Biology* 2015;109.
239. Smigielski L, Jagannath V, Rössler W, Walitza S, Grünblatt E. Epigenetic mechanisms in schizophrenia and other psychotic disorders: a systematic review of empirical human findings. *Mol Psychiatry* 2020;25:1718–48.
240. Marques D, Vaziri N, Greenway SC, Bousman C. DNA methylation and histone modifications associated with antipsychotic treatment: a systematic review. *Mol Psychiatry* 2024.
241. Swathy B, Banerjee M. Haloperidol induces pharmacoepigenetic response by modulating miRNA expression, global DNA methylation and expression profiles of methylation maintenance genes and genes involved in neurotransmission in neuronal cells. *PLoS ONE* 2017;12:e0184209.
242. Cipelletti B, Avanzini G, Vitellaro-Zuccarello L, Franceschetti S, Sancini G, Lavazza T, Acampora D, Simeone A, Spreafico R, Frassoni C. Morphological organization of somatosensory cortex in Otx1−/− mice. *Neuroscience* 2002;115:657–67.
243. Wang F, Flanagan J, Su N, Wang L-C, Bui S, Nielson A, Wu X, Vo HT, Ma XJ, Luo Y. RNAscope. *J Mol Diag* 2012;14:22–9.

244. Benes FM, Lange N. Two-dimensional versus three-dimensional cell counting: a practical perspective. *Trends Neurosci* 2001;24:11–7.
245. Adorjan I, Ahmed B, Feher V, Torso M, Krug K, Esiri M, Chance SA, Szele FG. Calretinin interneuron density in the caudate nucleus is lower in autism spectrum disorder. *Brain* 2017;140:2028–40.
246. QGIS.org (2024). QGIS Geographic Information System. Open Source Geospatial Foundation Project. http://qgis.org
247. Allen Institute Cell Types Database: RNA-Seq Data; Multiple Cortical Areas - SMART-SEQ Database (2019).
248. Love MI, Huber W, Anders S. Moderated estimation of fold change and dispersion for RNA-seq data with DESeq2. *Genome Biol* 2014;15:550.
249. Petukhov V, Igolkina A, Rydbirk R, Mei S, Christoffersen L, Khodosevich K, Kharchenko PV. Case-control analysis of single-cell RNA-seq studies 2022. [Preprint]
250. Yu G, Wang L-G, Han Y, He Q-Y. clusterProfiler: an R Package for Comparing Biological Themes Among Gene Clusters. *OMICS: A Journal of Integrative Biology* 2012;16:284–7.
251. Hafemeister C, Satija R. Normalization and variance stabilization of single-cell RNA-seq data using regularized negative binomial regression. *Genome Biol* 2019;20:296.
252. Korsunsky I, Millard N, Fan J, Slowikowski K, Zhang F, Wei K, Baglaenko Y, Brenner M, Loh PR, Raychaudhuri S. Fast, sensitive and accurate integration of single-cell data with Harmony. *Nat Methods* 2019;16:1289–96.
253. Becht E, McInnes L, Healy J, Dutertre C-A, Kwok IWH, Ng LG, Ginhoux F, Newell EW. Dimensionality reduction for visualizing single-cell data using UMAP. *Nat Biotechnol* 2019;37:38–44.
254. Pinheiro J, Bates D, DebRoy S, Sarkar D, Heisterkamp S, Willigen B. Linear and nonlinear mixed effects models contact: Package 'nlme' 2020; https://bugs.r-project.org.
255. Trapnell C. Defining cell types and states with single-cell genomics. *Genome Res* 2015;25:1491–8.

256. Zhang J, Liu J, Wu J, Li W, Chen Z, Yang L. Progression of the role of CRYAB in signaling pathways and cancers. *Onco Targets Ther* 2019;12:4129–39.
257. Ichihara-Tanaka K, Kadomatsu K, Kishida S. Temporally and Spatially Regulated Expression of the Linker Histone H1fx During Mouse Development. *J Histochem Cytochem* 2017;65:513–30.
258. Kuo M-W, Wang C-H, Wu H-C, Chang S-J, Chuang Y-J. Soluble THSD7A is an N-glycoprotein that promotes endothelial cell migration and tube formation in angiogenesis. *PLoS One* 2011;6:e29000.
259. De La Peña Avalos B, Tropée R, Duijf PHG, Dray E. EYA4 promotes breast cancer progression and metastasis through its role in replication stress avoidance. *Mol Cancer* 2023;22:158.
260. Takeichi M. The cadherin superfamily in neuronal connections and interactions. *Nat Rev Neurosci*. 2007;8(1):11–20.
261. Wang C, Pan Y-H, Wang Y, Blatt G, Yuan X-B. Segregated expressions of autism risk genes Cdh11 and Cdh9 in autism-relevant regions of developing cerebellum. *Mol Brain* 2019;12:40.
262. Murshid A, Prince TL, Lang B, Calderwood SK. Role of heat shock factors in stress-induced transcription. *Methods Mol Biol*. 2018;1709:23-34.
263. Kowalczyk M, Owczarek A, Suchanek R, Paul-Samojedny M, Fila-Danilow A, Borkowska P, Kucia K, Kowalski J. Heat shock protein 70 gene polymorphisms are associated with paranoid schizophrenia in the Polish population. *Cell Stress and Chaperones* 2014;19:205–15.
264. Andrews WD, Barber M, Nemitz M, Memi F, Parnavelas JG. Semaphorin3A–neuropilin1 signalling is involved in the generation of cortical interneurons. *Brain Struct Funct* 2017;222:2217–33.
265. Sinkus ML, Graw S, Freedman R, Ross RG, Lester HA, Leonard S. The human CHRNA7 and CHRFAM7A genes: A review of the genetics, regulation, and function. *Neuropharmacology* 2015;96:274–88.
266. Ihnatovych I, Saddler R-A, Sule N, Szigeti K. Translational implications of CHRFAM7A, an elusive human-restricted fusion gene. *Mol Psychiatry* 2024;29:1020–32.

267. Pardiñas AF, Holmans P, Pocklington AJ, Escott-Price V, Ripke S, Carrera N, Legge SE, Bishop S, Cameron D, Hamshere ML, Han J, Hubbard L, Lynham A, Mantripragada K, Rees E, MacCabe JH, McCarroll SA, Baune BT, Breen G, Byrne EM, Dannlowski U, Eley TC, Hayward C, Martin NG, McIntosh AM, Plomin R, Porteous DJ, Wray NR, Caballero A, Geschwind DH, Huckins LM, Ruderfer DM, Santiago E, Sklar P, Stahl EA, Won H, Agerbo E, Als TD, Andreassen OA, Bækvad-Hansen M, Mortensen PB, Pedersen CB, Børglum AD, Bybjerg-Grauholm J, Djurovic S, Durmishi N, Pedersen MG, Golimbet V, Grove J, Hougaard DM, Mattheisen M, Molden E, Mors O, Nordentoft M, Pejovic-Milovancevic M, Sigurdsson E, Silagadze T, Hansen CS, Stefansson K, Stefansson H, Steinberg S, Tosato S, Werge T; GERAD1 Consortium; CRESTAR Consortium; Collier DA, Rujescu D, Kirov G, Owen MJ, O'Donovan MC, Walters JTR. Common schizophrenia alleles are enriched in mutation-intolerant genes and in regions under strong background selection. *Nat Genet* 2018;50:381–9.

268. Stachowiak EK, Benson CA, Narla ST, Dimitri A, Chuye LEB, Dhiman S, Harikrishnan K, Elahi S, Freedman D, Brennand KJ, Sarder P, Stachowiak MK. Cerebral organoids reveal early cortical maldevelopment in schizophrenia—computational anatomy and genomics, role of FGFR1. *Transl Psychiatry* 2017;7:6.

269. Massouh M, Wallman M-J, Pourcher E, Parent A. The fate of the large striatal interneurons expressing calretinin in Huntington's disease. *Neuroscience Research* 2008;62:216–24.

270. Kelmer P, Hoppa P, Frank E, Tyler T, Adorjan I. Lower density of calretinin-immunopositive neurons in the putamen of subjects with schizophrenia. *J Anat* 2024:joa.14180.

271. Hladnik A, Dzaja D, Darmopil S, Jovanov-MiloÅ¡eviÄ‡ N, Petanjek Z. Spatio-temporal extension in site of origin for cortical calretinin neurons in primates. *Front Neuroanat* 2014;8.

272. Jakob H, Beckmann H. Circumscribed malformation and nerve cell alterations in the entorhinal cortex of schizophrenics: Pathogenetic and clinical aspects. *J Neural Transmission* 1994;98:83–106.

273. Arnold SE. Some Cytoarchitectural Abnormalities of the Entorhinal Cortex in Schizophrenia. *Arch Gen Psychiatry* 1991;48:625.

274. Arnold SE, Ruscheinsky DD, Han L-Y. Further Evidence of Abnormal Cytoarchitecture of the Entorhinal Cortex in Schizophrenia Using Spatial Point Pattern Analyses. *Biol Psychiatry* 1997;42:639–47.
275. Kiriakidou M, Tan GS, Lamprinaki S, De Planell-Saguer M, Nelson PT, Mourelatos Z. An mRNA m7G Cap Binding-like Motif within Human Ago2 Represses Translation. *Cell* 2007;129:1141–51.
276. Zhang H-C, Du Y, Chen L, Yuan Z-Q, Cheng Y. MicroRNA schizophrenia: Etiology, biomarkers and therapeutic targets. *Neurosci Biobehav Rev* 2023;146:105064.
277. Schiffmann SN, Cheron G, Lohof A, d'Alcantara P, Meyer M, Parmentier M, Schurmans S. Impaired motor coordination and Purkinje cell excitability in mice lacking calretinin. *Proc Natl Acad Sci USA* 1999;96:5257–62.
278. Marty S, Onténiente B. The expression pattern of somatostatin and calretinin by postnatal hippocampal interneurons is regulated by activity-dependent and -independent determinants. *Neuroscience* 1997;80:79–88.
279. Hou Z-H, Yu X. Activity-regulated Somatostatin Expression Reduces Dendritic Spine Density and Lowers Excitatory Synaptic Transmission via Postsynaptic Somatostatin Receptor 4. *J Biol Chem* 2013;288:2501–9.
280. Trubetskoy V, Pardiñas AF, Qi T, Panagiotaropoulou G, Awasthi S, Bigdeli TB, Bryois J, Chen CY, Dennison CA, Hall LS, Lam M, Watanabe K, Frei O, Ge T, Harwood JC, Koopmans F, Magnusson S, Richards AL, Sidorenko J, Wu Y, Zeng J, Grove J, Kim M, Li Z, Voloudakis G, Zhang W, Adams M, Agartz I, Atkinson EG, Agerbo E, Al Eissa M, Albus M, Alexander M, Alizadeh BZ, Alptekin K, Als TD, Amin F, Arolt V, Arrojo M, Athanasiu L, Azevedo MH, Bacanu SA, Bass NJ, Begemann M, Belliveau RA, Bene J, Benyamin B, Bergen SE, Blasi G, Bobes J, Bonassi S, Braun A, Bressan RA, Bromet EJ, Bruggeman R, Buckley PF, Buckner RL, Bybjerg-Grauholm J, Cahn W, Cairns MJ, Calkins ME, Carr VJ, Castle D, Catts SV, Chambert KD, Chan RCK, Chaumette B, Cheng W, Cheung EFC, Chong SA, Cohen D, Consoli A, Cordeiro Q, Costas J, Curtis C, Davidson M, Davis KL, de Haan L, Degenhardt F, DeLisi LE, Demontis D, Dickerson F, Dikeos D, Dinan T, Djurovic S, Duan J, Ducci G, Dudbridge F, Eriksson JG, Fañanás L, Faraone SV, Fiorentino A, Forstner A, Frank J, Freimer NB, Fromer M, Frustaci A, Gadelha

A, Genovese G, Gershon ES, Giannitelli M, Giegling I, Giusti-Rodríguez P, Godard S, Goldstein JI, González Peñas J, González-Pinto A, Gopal S, Gratten J, Green MF, Greenwood TA, Guillin O, Gülöksüz S, Gur RE, Gur RC, Gutiérrez B, Hahn E, Hakonarson H, Haroutunian V, Hartmann AM, Harvey C, Hayward C, Henskens FA, Herms S, Hoffmann P, Howrigan DP, Ikeda M, Iyegbe C, Joa I, Julià A, Kähler AK, Kam-Thong T, Kamatani Y, Karachanak-Yankova S, Kebir O, Keller MC, Kelly BJ, Khrunin A, Kim SW, Klovins J, Kondratiev N, Konte B, Kraft J, Kubo M, Kučinskas V, Kučinskiene ZA, Kusumawardhani A, Kuzelova-Ptackova H, Landi S, Lazzeroni LC, Lee PH, Legge SE, Lehrer DS, Lencer R, Lerer B, Li M, Lieberman J, Light GA, Limborska S, Liu CM, Lönnqvist J, Loughland CM, Lubinski J, Luykx JJ, Lynham A, Macek M Jr, Mackinnon A, Magnusson PKE, Maher BS, Maier W, Malaspina D, Mallet J, Marder SR, Marsal S, Martin AR, Martorell L, Mattheisen M, McCarley RW, McDonald C, McGrath JJ, Medeiros H, Meier S, Melegh B, Melle I, Mesholam-Gately RI, Metspalu A, Michie PT, Milani L, Milanova V, Mitjans M, Molden E, Molina E, Molto MD, Mondelli V, Moreno C, Morley CP, Muntané G, Murphy KC, Myin-Germeys I, Nenadić I, Nestadt G, Nikitina-Zake L, Noto C, Nuechterlein KH, O'Brien NL, O'Neill FA, Oh SY, Olincy A, Ota VK, Pantelis C, Papadimitriou GN, Parellada M, Paunio T, Pellegrino R, Periyasamy S, Perkins DO, Pfuhlmann B, Pietiläinen O, Pimm J, Porteous D, Powell J, Quattrone D, Quested D, Radant AD, Rampino A, Rapaport MH, Rautanen A, Reichenberg A, Roe C, Roffman JL, Roth J, Rothermundt M, Rutten BPF, Saker-Delye S, Salomaa V, Sanjuan J, Santoro ML, Savitz A, Schall U, Scott RJ, Seidman LJ, Sharp SI, Shi J, Siever LJ, Sigurdsson E, Sim K, Skarabis N, Slominsky P, So HC, Sobell JL, Söderman E, Stain HJ, Steen NE, Steixner-Kumar AA, Stögmann E, Stone WS, Straub RE, Streit F, Strengman E, Stroup TS, Subramaniam M, Sugar CA, Suvisaari J, Svrakic DM, Swerdlow NR, Szatkiewicz JP, Ta TMT, Takahashi A, Terao C, Thibaut F, Toncheva D, Tooney PA, Torretta S, Tosato S, Tura GB, Turetsky BI, Üçok A, Vaaler A, van Amelsvoort T, van Winkel R, Veijola J, Waddington J, Walter H, Waterreus A, Webb BT, Weiser M, Williams NM, Witt SH, Wormley BK, Wu JQ, Xu Z, Yolken R, Zai CC, Zhou W, Zhu F, Zimprich F, Atbaşoğlu EC, Ayub M, Benner C, Bertolino A, Black DW, Bray NJ, Breen G, Buccola NG, Byerley WF, Chen WJ, Cloninger CR, Crespo-

Facorro B, Donohoe G, Freedman R, Galletly C, Gandal MJ, Gennarelli M, Hougaard DM, Hwu HG, Jablensky AV, McCarroll SA, Moran JL, Mors O, Mortensen PB, Müller-Myhsok B, Neil AL, Nordentoft M, Pato MT, Petryshen TL, Pirinen M, Pulver AE, Schulze TG, Silverman JM, Smoller JW, Stahl EA, Tsuang DW, Vilella E, Wang SH, Xu S; Indonesia Schizophrenia Consortium; PsychENCODE; Psychosis Endophenotypes International Consortium; SynGO Consortium; Adolfsson R, Arango C, Baune BT, Belangero SI, Børglum AD, Braff D, Bramon E, Buxbaum JD, Campion D, Cervilla JA, Cichon S, Collier DA, Corvin A, Curtis D, Forti MD, Domenici E, Ehrenreich H, Escott-Price V, Esko T, Fanous AH, Gareeva A, Gawlik M, Gejman PV, Gill M, Glatt SJ, Golimbet V, Hong KS, Hultman CM, Hyman SE, Iwata N, Jönsson EG, Kahn RS, Kennedy JL, Khusnutdinova E, Kirov G, Knowles JA, Krebs MO, Laurent-Levinson C, Lee J, Lencz T, Levinson DF, Li QS, Liu J, Malhotra AK, Malhotra D, McIntosh A, McQuillin A, Menezes PR, Morgan VA, Morris DW, Mowry BJ, Murray RM, Nimgaonkar V, Nöthen MM, Ophoff RA, Paciga SA, Palotie A, Pato CN, Qin S, Rietschel M, Riley BP, Rivera M, Rujescu D, Saka MC, Sanders AR, Schwab SG, Serretti A, Sham PC, Shi Y, St Clair D, Stefánsson H, Stefansson K, Tsuang MT, van Os J, Vawter MP, Weinberger DR, Werge T, Wildenauer DB, Yu X, Yue W, Holmans PA, Pocklington AJ, Roussos P, Vassos E, Verhage M, Visscher PM, Yang J, Posthuma D, Andreassen OA, Kendler KS, Owen MJ, Wray NR, Daly MJ, Huang H, Neale BM, Sullivan PF, Ripke S, Walters JTR, O'Donovan MC; Schizophrenia Working Group of the Psychiatric Genomics Consortium. Mapping genomic loci implicates genes and synaptic biology in schizophrenia. *Nature* 2022;604:502–8.

281. Sullivan EM, O'Donnell P. Inhibitory Interneurons, Oxidative Stress, and Schizophrenia. *Schizophr Bull* 2012;38:373–6.
282. Do KQ, Trabesinger AH, Kirsten-Kruger M, Lauer CJ, Dydak U, Hell D, Holsboer F, Boesiger P, Cuénod M. Schizophrenia: glutathione deficit in cerebrospinal fluid and pre frontal cortex in vivo. *Eur J Neurosci*. 2000;12:3721–3728
283. Yao JK, Leonard S, Reddy R. Altered glutathione redox state in schizophrenia. *Dis Markers*. 2006;22:83–93.

284. Steullet P, Cabungcal JH, Kulak A, Kraftsik R, Chen Y, Dalton TP, Cuenod M, Do KQ. Redox dysregulation affects the ventral but not dorsal hippocampus: impairment of parvalbumin neurons, gamma oscillations, and related behaviors. *J Neurosci* 2010;30:2547–2558.
285. Lavoie S, Murray MM, Deppen P, Knyazeva MG, Berk M, Boulat O, Bovet P, Bush AI, Conus P, Copolov D, Fornari E, Meuli R, Solida A, Vianin P, Cuénod M, Buclin T, Do KQ. Glutathione Precursor, N-Acetyl-Cysteine, Improves Mismatch Negativity in Schizophrenia Patients. *Neuropsychopharmacology* 2008;33:2187–99.
286. Urban Z, Magloczky Z, Freund TF. Calretinin-containing interneurons innervate both principal cells and interneurons in the CA1 region of the human hippocampus. *Acta Biol Hungarica* 2002;53:205–20.
287. Freund TF, Magloczky Zs. Early degeneration of calretinin-containing neurons in the rat hippocampus after ischemia. *Neuroscience* 1993;56:581–96.
288. Toth K, Eross L, Vajda J, Halasz P, Freund TF, Magloczky Z. Loss and reorganization of calretinin-containing interneurons in the epileptic human hippocampus. *Brain* 2010;133:2763–77.
289. Schulmann A, Marenco S, Vawter MP, Akula N, Limon A, Mandal A, Auluck PK, Patel Y, Lipska BK, McMahon FJ. Antipsychotic drug use complicates assessment of gene expression changes associated with schizophrenia. *Transl Psychiatry* 2023;13:93.
290. Harrison PJ. Postmortem studies in schizophrenia. *Dialogues Clin Neurosci* 2000;2:349–57.
291. Wani RA, Dar MA, Margoob MA, Rather YH, Haq I, Shah MS. Diabetes mellitus and impaired glucose tolerance in patients with schizophrenia, before and after antipsychotic treatment. *JNRP* 2015;6:017–22.
292. Turkheimer FE, Selvaggi P, Mehta MA, Veronese M, Zelaya F, Dazzan P, Vernon AC. Normalizing the Abnormal: Do Antipsychotic Drugs Push the Cortex Into an Unsustainable Metabolic Envelope? *Schizophr Bull* 2020;46:484–95.
293. Perzel Mandell KA, Eagles NJ, Deep-Soboslay A, Tao R, Han S, Wilton R, Szalay AS, Hyde TM, Kleinman JE, Jaffe AE, Weinberger DR. Molecular phenotypes

associated with antipsychotic drugs in the human caudate nucleus. *Mol Psychiatry* 2022;27:2061–7.

294. Hoffman GE, Bendl J, Voloudakis G, Montgomery KS, Sloofman L, Wang YC, Shah HR, Hauberg ME, Johnson JS, Girdhar K, Song L, Fullard JF, Kramer R, Hahn CG, Gur R, Marenco S, Lipska BK, Lewis DA, Haroutunian V, Hemby S, Sullivan P, Akbarian S, Chess A, Buxbaum JD, Crawford GE, Domenici E, Devlin B, Sieberts SK, Peters MA, Roussos P. CommonMind Consortium provides transcriptomic and epigenomic data for Schizophrenia and Bipolar Disorder. *Sci Data* 2019;6:180.
295. Kerestes R, Ladouceur CD, Meda S, Nathan PJ, Blumberg HP, Maloney K, Ruf B, Saricicek A, Pearlson GD, Bhagwagar Z, Phillips ML. Abnormal prefrontal activity subserving attentional control of emotion in remitted depressed patients during a working memory task with emotional distracters. *Psychol Med* 2012;42:29–40.
296. Lin Y, Feng T. Lateralization of self-control over the dorsolateral prefrontal cortex in decision-making: a systematic review and meta-analytic evidence from noninvasive brain stimulation. *Cogn Affect Behav Neurosci* 2024;24:19–41.
297. Crow T. Schizophrenia as the price that Homo sapiens pays for language: a resolution of the central paradox in the origin of the species. *Brain Research Reviews* 2000;31:118–29.
298. Spironelli C, Angrilli A. Language lateralization in phonological, semantic and orthographic tasks: a slow evoked potential study. *Behav Brain Res* 2006;175:296-304.
299. Ho NF, Li Z, Ji F, Wang M, Kuswanto CN, Sum MY, Tng HY, Sitoh YY, Sim K, Zhou J. Hemispheric lateralization abnormalities of the white matter microstructure in patients with schizophrenia and bipolar disorder. *JPN* 2017;42:242–51.
300. Szocsics P, Papp P, Havas L, Lőke J, Magloczky Z. Interhemispheric differences of pyramidal cells in the primary motor cortices of schizophrenia patients investigated postmortem. *Cerebral Cortex* 2023;33:8179–93.

9. Bibliography of the candidate's publications

A) Directly relevant for dissertation

1. Batiuk M*, **Tyler T*,** Dragicevic K, Mei S, Rydbirk R, Petukhov V, Deviatiiarov V, Sedmak D, Frank E, Feher V, Habek N, Hu Q, Igolkina A, Roszik L, Pfisterer U, Garcia-Gonzalez D, Petanjek Z, Adorjan I, Kharchenko PV, Khodosevich K. Upper cortical layer–driven network impairment in schizophrenia. *Sci Adv* 2022*;*8, eabn8367. **these authors contributed equally* (IF: 13.6)

2. Adorjan I, Sun B, Feher V, **Tyler T**, Veres D, Chance SA, Szele FG. Evidence for decreased density of calretinin-immunopositive neurons in the caudate nucleus in patients with schizophrenia. *Front Neuroanat* 2020;14:86. (IF: 3.86)

B) Not directly relevant for dissertation

1. Kelmer P, Hoppa P, Frank E, **Tyler T**, Adorjan I. Lower density of calretinin-immunopositive neurons in the putamen of subjects with schizophrenia. *J Anat* 2024:joa.14180. (IF: 2)

2. Olar A, **Tyler T,** Hoppa P, Frank E, Csabai I, Adorjan I, Pollner P. Annotated dataset for training deep learning models to detect astrocytes in human brain tissue. *Sci Data* 2024;11:96. (IF: 9.8)

3. Menassa DA, Muntslag TAO, Martin-Estebané M, Barry-Carroll L, Chapman MA, Adorjan I, **Tyler T,** Turnbull B, Rose-Zerilli MJJ, Nicoll JAR, Krsnik Z, Kostovic I, Gomez-Nicola D. The spatiotemporal dynamics of microglia across the human lifespan. *Dev Cell* 2022;57:2127-2139.e6. (IF: 11.8)

4. Zachar G, Kemecsei RG, Papp SZM, Wéber K, Kisparti T, **Tyler T**, Gáspár G, Balazsa T, Csillag A. D-Aspartate consumption selectively promotes intermediate-term spatial memory and the expression of hippocampal NMDA receptor subunits. *Sci Rep* 2021;11:6166. (IF: 4.99)

5. Dalahmah A, Soares LC, Nicholson J, Draijer S, Mundim M, Lu VM, Sun B, **Tyler T**, Adorjan I, O'Neill E, Szele FG. Galectin-3 modulates postnatal subventricular zone gliogenesis. *Glia* 2020;68:435–50. (IF: 7.45)

6. Adorjan I, **Tyler T**, Bhaduri A, Demharter S, Finszter CK, Bako M, Sebok OM, Nowakowski TJ, Khodosevich K, Møllgård K, Kriegstein AR, Shi L, Hoerder-Suabedissen A, Ansorge O, Molnár Z. Neuroserpin expression during human brain development and in adult brain revealed by immunohistochemistry and single cell RNA sequencing. *J Anat* 2019;235:543–54. (IF: 2)

7. Nagy JGY, Zsinka B, Verebélyi V, Zorkóczy OK, Tyler T. A Vaccinium microcarpum (Turcz. ex Rupr.) Schmalh. Magyarországon. *KITAIBELIA* 2017;22:1pp.71-76. (IF: -)

10. Acknowledgements

I want to express my sincere gratitude to every person who directly or indirectly contributed in any way to my work throughout the years. I want to especially thank Dr. Lang Zsolt and Dr. Veres Dániel (biostatistics); Frank Erzsébet and Bakó Mária (assistance with histology); Kovács Tamás, Dr Mórotz Gábor and Dr. Varga V. Zoltán (RNAscope training and equipment); Dr. Dobolyi Árpád and Dr. Zdravko Petanjek (support, education, and partial funding of collaborative projects); Dr. Dóra Fanni (support and training); and Dr. Mykhailo Batiuk (single cell RNA sequencing training and support). Furthermore, I want to thank my supervisor, Dr. Adorján István, for his trust, support, and flexibility. I am grateful to the undergraduate students working with me over longer periods of time for their hard work (Somogyi Eszter, Örvényesi-Petik Sára, Muskan Awashti). I also want to thank the colleagues of the Workgroup for Science Management (Semmelweis University) for providing valuable guidance about writing the dissertation. I thank my colleagues at the Neuropsychiatry Workgroup for their support, encouragement, and friendship. I am also extremely grateful to my family and friends, for everything.

I also wish to pay tribute to late Dr. Benedek István, whose writings deeply inspired me and opened my eyes.

Finally, I want to express my deepest gratitude and respect to the individuals and families whose generous contributions through brain tissue donation make human brain research possible.